INFORMATION TO USERS

This manuscript has been reproduced from the microfilm master. UMI films the text directly from the original or copy submitted. Thus, some thesis and dissertation copies are in typewriter face, while others may be from any type of computer printer.

The quality of this reproduction is dependent upon the quality of the copy submitted. Broken or indistinct print, colored or poor quality illustrations and photographs, print bleedthrough, substandard margins, and improper alignment can adversely affect reproduction.

In the unlikely event that the author did not send UMI a complete manuscript and there are missing pages, these will be noted. Also, if unauthorized copyright material had to be removed, a note will indicate the deletion.

Oversize materials (e.g., maps, drawings, charts) are reproduced by sectioning the original, beginning at the upper left-hand corner and continuing from left to right in equal sections with small overlaps.

ProQuest Information and Learning
300 North Zeeb Road, Ann Arbor, MI 48106-1346 USA
800-521-0600

SOME PHENOMENOLOGICAL ASPECTS OF JET INDUCED TURBULENCE

by

G. A. Campbell

A thesis submitted to the
Department of Chemical Engineering
of
The University of Ottawa
in partial fulfilment of the requirements
for the degree of M.Sc.

Thesis Author

Research Director

Supported under DRB Grant No. 9550-14

TABLE OF CONTENTS

LIST OF TABLES

LIST OF FIGURES

LIST OF FIGURES (continued)

I - ABSTRACT

Turbulence, induced by transverse and inclined air jets, in an air stream flowing in a four inch square duct at 138 - 250 feet per second, was studied. Flow patterns were constructed from four hundred velocity profiles measured at various distances from the injector wall and at numerous positions upstream and downstream from the injector under different experimental conditions.

The pattern indicates a steady widening of the jet, a curving motion, with the lower portion forming a vortex in the wake. The upper part of the jet widens out, slows down and reaches mainstream velocity farther down the duct.

A method for predicting the shape of the upper bounding streamline was developed from two-dimensional potential flow theory and a penetration correlation with exponents deduced from the results in this study. The shape of the lower bounding streamline and the vortex can be predicted by a logarithmic elliptical spiral using constants determined in this investigation.

The analogy between the patterns in the wake of a jet and a solid rod was checked in a six inch round duct and found to be of doubtful validity.

II - INTRODUCTION

One of the most important problems in the design of ram-jets, turbo-jets and afterburners is the stabilization of the flame.

In the early days of jet-powered flight, unexpected "flame outs" were common.

A flame can only travel through a combustible gas mixture at a finite velocity. This velocity is low, falls in the range of one to seven feet per second and cannot be exceeded or the flame will be extinguished (1). But no practical machine could generate the thrust necessary for flight and have gases passing through it at this rate. Thus the designer is faced with a problem, whose solution hinges on the creation of a region within the flow, where the conditions necessary for combustion are present.

The science of fluid dynamics has shown that an eddy region, having but a fraction of the energy of the main flow, exists behind certain shapes such as a cylinder, sphere, cone, flat plate, etc., in a fast moving fluid. Early designers grasped this knowledge and placed these metallic shapes in the main stream. The flame was successfully stabilized in the wake of these "bluff bodies" but certain difficulties soon became apparent. It was

noticed that the flame would not spread through the whole flow (2) but only part of it. Therefore the number of objects had to be increased. Worse still, the higher the velocity, the larger the metallic objects had to be, bringing the designers up against the bane of bluff body stabilization-drag, a loss of energy in the main flow undesirable in all engines, but particularly bad in unlit afterburners.

Another means of creating a stagnant zone but without increasing drag is to use transverse jets of fuel air mixture, having but a fraction of the momentum and energy of the main flow. Ease of control, simplicity and easily constructed apparatus are features of this method. If not in use, there is no loss in energy. Their number can easily be increased to let the flame spread through the whole duct and there is no metal surface to erode away or break off. Although it was known that a flame could be stabilized in this way, the mechanism was not well understood.

It was decided, therefore, to investigate the configuration of the flow in the wake of inclined injectors placed in the wall of a four by four inch duct at angles of incidence of thirty, forty-five and ninety degrees. Even though the process with combustion would differ somewhat from the situation under study, the

patterns would give some indication of the actual system, would help to settle the question of whether the injector is acting as a fluid baffle, and would help in the prediction of the location and size of the eddy region.

Some idea of gas mixing which might be of value in industrial applications can be found in this study.

III - LITERATURE SURVEY

Workers in the field of fluid dynamics (3) have long noted an eddy region in the wake of certain blunt shapes such as a cylinder, cone, sphere, flat plate, etc., placed in a fast moving stream of fluid. The flow pattern outside the boundary layer becomes markedly changed after the onset of separation, particularly on the downstream side. In the first instant after starting the flow of fluid the potential flow pattern does exist. Then separation begins at the downstream stagnation point and moves a considerable distance upstream. The streamline through the point of separation encloses a region where the flow velocities are very small. The vorticity is largest outside this streamline; it forms a vortex sheet which curls up as the pattern continues to develop and forms two concentrated vortices. In the free stream behind these vortices it is possible to discern the existence of a stagnation point which coincides with the junction of two streamlines through the point of separation. The vortices continue to grow. They become unstable with the course of time and are carried away from the body by external flow. In the steady state the motion oscillates and the pressure distribution around the body differs considerably from that stipulated by potential flow theory. It is, however, necessary to remark here that the resemblance to a pattern

with two such vortices is only transitory (4).

When these blunt objects were placed in the stream, the flame was successfully stabilized behind them. Barrère and Mestre (5) and Longwell (6) have described the mechanism of flame stabilization in the wake of bluff bodies. In the structure of the flame one can distinguish two regions. The first, downstream from the obstacle, held there for a length three or four times the size of the body. The shape of the flame front and the conditions of stabilization are related to the nature of the flow present in this region and hence to the turbulence created by the object.

The principal role of the obstacle is to create behind it a stationary nucleus formed of hot combustion products and live active centres. The initiation of combustion results from the transfer of heat and active centres between this turbulent region and fresh mixture. This transfer takes place by molecular diffusion and turbulence in the wake only.

The second region makes up the section of greatest importance in the flame front. It is characterized by sharp velocity gradients between fresh and burned gas. This region spreads out as the velocity increases. It is then controlled by a complex and unstable process of turbulent combustion.

The nature of the flow in the wake of a flame stabilizer is also illustrated by the work of Nicholson and Field (7). Small particles of sodium acetate were placed in the air stream. When one of these particles entered the flame zone, the resulting sodium vapour emitted light, which was recorded by high speed motion pictures. This allowed one to follow the path of small volumes of gas in the zone behind the baffle. With a 3/4 inch baffle immersed in a 200 feet per second gas stream, a record of 40 particles showed that 24 travelled upstream in the direction of the baffle at a velocity as high as 65 feet per second, establishing that recirculation exists in the wake of the baffle. Of these 24, 9 went up the centre of the wake, and 15 travelled up the edges. If all the particles travelled up the centre and down the edges, one would conclude that a stable pair of eddies existed in the wake of the baffle; however, since particles travelled upstream on either side of the wake, it would appear that large eddies of varying direction of rotation existed in this case and that eddy shedding probably occurs although the effect of combustion on the frequency of eddy shedding was not established.

Scurlock (8) has shown that with smaller flame stabilizers operating at lower velocities, a pair of stable eddies are found in the wake of the baffle. This trend might be expected

since, in the absence of combustion, as Reynold's number is reduced below a value of approximately 30, the alternately shedding eddy flow changes to a pair of stable eddies. The existence of a flame in the eddy zone seems to have a tendency to stabilize the eddies, this effect being overcome at high Reynold's numbers.

DeZubay (9) has correlated the effect of baffle diameter, pressure and mixture velocity using propane as fuel. The fuel air ratio at blow out is plotted as a function of the dimensional group $\frac{V}{P^{0.95}D^{0.85}}$ where D is the diameter of the circular flat discs used to stabilize the flame. If the baffle is a cylinder, cone or V shaped gutter, Longwell, Chenevey, Clark and Frost (40) recommend the correlating group $\frac{U}{D^{0.45}}$ and Haddock (41) recommends $\frac{U}{D^{0.5}}$.

Wilkerson and Fenn (10) studied the effect of flame-holder geometry on combustion efficiency in ducted burners. A number $K = \frac{q}{4\pi XT}$, with the dimensions of conductivity and in effect the diffusivity of the stream, where q is the rate of heat input in BTU/sec., X is the distance in inches along the burner axis downstream from the igniter and T is the temperature at distance X in °F, was associated with each configuration. The nature of the correlation led to a simple theory of the burner mechanism. Combustion efficiency for baffle type burners has been predicted by Bahn (11).

Williams, Woo and Shipman (12) found that the role of the boundary layer in the stabilization of the flame by bluff objects seems to be twofold. First, it determines the aerodynamic character of the zone in contact with the burned gas in the immediate wake of the stabilizer and the unburned gas coming into the zone of initial combustion have been preheated. That the boundary layer moves relatively slowly seems to be of little importance except as it influences the character of the zone of contact (laminar or turbulent) between burned and unburned gas.

Wong (13) studied the combined effect of bluff body and gaseous jet stabilization.

Grover, Kesler and Scurlock (14) tried a rotating flame stabilizer and found increased release of heat. The stabilizer was a small metal cylinder which was rotated longitudinally in a gas stream. The flame followed a helical pattern and the efficiency increased with increased rate of rotation. The power required was less than the losses due to axial drag but unfortunately the stability limits were narrowed.

Huellmantel, Ziemer and Cambel (15) stabilized the flame by placing recessed ducts in the wall of the tube to create an ignition nucleus. This scheme was most successful in smaller tubes but has the disadvantage of creating high temperatures at the wall.

Jenson and Shipman (16) tested a coaxial pilot flame for its effect on stabilization. It was found that there was no advantage in increasing the pilot diameter over a certain limit.

A flame can also be stabilized by purely aerodynamic means. A recirculation zone, formed by recirculating part of the flow to create an eddy region with the required axial velocity and mixing characteristics, can be used in the combustor. Clarke (17) has given a discussion on high intensity combustion by this means.

Spalding (18) has suggested that this recirculation can be created by directing a jet normally into the main stream where a torroidal eddy is formed by the interaction of the two. This system is simple, easy to control and needs no solid baffle. Air or combustible mixture can be injected, permitting temperature and composition control in the stagnant zone, independent of the main stream.

Shepherd (19) injected a thin sheet of fluid radially outwards from a centered tube into an annular duct containing the main stream. The stabilizer is in effect a fluid baffle. This system can be regulated according to the duty required, offers no obstruction to the fluid stream when not in use and avoids undesirable drag or pressure loss under normal conditions.

Another variation of the fluid baffle idea was tried out by Dutta, Martin and Moore (20) who injected a sheet of fluid

radially inwards into the main stream and attempted to establish a relation between some characteristic of the eddy region and flame stability. A characteristic dimension of the eddy region was established from experimental measurements of the axial velocity profile across a diameter downstream of the stabilizing jet in the absence of combustion. Using two Peclet[+] numbers, one dependent on blow-out velocity and the other based on flame speed, Spalding and Tall's (42) correlation was extended to these results.

Shaffer and Cambel (21) stabilized the flame by injecting a jet directly into the flow or in other words by an opposing jet. When the jet supply pressure was varied the performance of the burner was altered. A low pressure increased the blow off velocity.

Duclos, Shaffer and Cambel (22) studied the effect of two jets directed into the flow at small angles of incidence, in a two-inch diameter combustion chamber. Results of their tests using a single 0.055 inch inside diameter jet at angles of from 0 to 15 degrees were reported. It was found that the flame stability decreased as the angle of incidence increased from zero but it was not known why. Possibly it may be due to a breakup of the initial zone, or a

---

+ 1) $\frac{V_{B.O.}(D-d')}{\alpha}$ 2) $\frac{S_u(D-d')}{\alpha}$

change in the rate of mixing or recirculation. The effect of larger jet diameters was not investigated.

Bertin and Salmon (23) studied tranverse air jets as flame stabilizers. The process was applied, with satisfactory results at sea level and altitude to a turbo-jet engine afterburner, in the form of a fluid baffle rather than a simple jet. Flow streamlines, total and static pressures and values of velocity at numerous upstream and downstream positions were measured for the case of a fluid baffle contained in a duct. A very complete set of pressure probes mounted on a movable board measured the total and static pressure in the flow stream.

The literature contains a number of theoretical and experimental investigations on gas mixing and the dynamics of jets entering the main stream at an angle.

Chilton and Genereaux (24) injected smoke as a side-stream and traced the resultant mixing visually. It was concluded that an ordinary T configuration gave good mixing and that the mass velocity ratio of the two gas streams was the controlling variable.

Callaghan and Ruggeri (25) determined the depth of penetration of a circular jet directed perpendicularly to an air stream and developed the following equation

$$\left(\frac{\ell}{D_j}\right)^{1.65} = 2.91 \frac{\rho_j V_j}{\rho_o V_o} \sqrt{\frac{s}{D_j}} \qquad (1)$$

This correlation gives the penetration for any point downstream from the injector. It is unable to give any information upstream penetrations because it is not possible to take the logarithm of a negative number. An adjustable rake fitted with twenty-four thermocouples each spaced 1/4 inch apart, measured the penetration at four positions downstream from the jet entrance. Stream velocities of 260 to 360 feet per second were used. Numerous articles were published later in this series of studies (26, 27, 28, 29, 30).

Chelko (31) investigated the penetration characteristics of water jets directed approximately perpendicular to a high velocity air stream (742 feet per second) and developed equation 2 for correlating the results.

$$\left(\frac{\ell}{D_j}\right) = 0.450 \left(\frac{V_j}{V_o}\right)^{0.95} \left(\frac{\rho_j}{\rho_o}\right)^{0.74} \left(\frac{s}{D_j}\right)^{0.22} \qquad (2)$$

The penetration lengths and the mixing distances were determined from photographs taken through transparent tunnel walls. If the angle of incidence were changed the usual procedure was to determine new exponents for the groups.

Beauregard (32) has measured the penetration of a cold jet in a hot high velocity gas stream using a temperature rake placed at different stations and has drawn many curves of actual penetrations.

Chakko (33) has studied the mixing of hot subsonic jets with cold air streams and has correlated his results using the equation

$$\left(\frac{H_c}{d_j}\right) = 0.945 \left(\frac{N_{ji}}{N_{oi}}\right)^{0.306} \left(\frac{T_{oi}}{T_{ji}}\right)^{0.172} \left(\frac{s}{d_j}\right)^{0.265}$$

Ehrich (34) analysed the dynamics of jets entering into a general stream at an oblique angle from slots and orifices, based on simplified two-dimensional potential flow theory. This study agreed qualitatively with Callaghan and Ruggeri's (29) penetration data.

Frazer (35) made a complementary three-dimensional potential flow analysis of a round jet penetrating into a main stream at right angles and also obtained qualitative agreement with Callaghan and Ruggeri (29).

The penetration and mixing of a jet of cold air through a hole in the wall of a three-inch square duct carrying hot air was studied by Hawthorne, Rogers and Zaczek (36). Measurements were made with a temperature rake and some complimentary shadowgraph and schlieren photographs. A correlation of the distance to which the jet penetrated the stream was obtained with the factor $\frac{R_m R_v}{(1 + R_v)^2}$. Turbulence in the hot stream reduced the penetration, while penetration was increased if another jet or rod was placed immediately upstream. A jet emerging from a square hole penetrated as far into

the duct as a jet from a circular hole of equal area. A jet emerging from a rectangular hole of the same area penetrated farther into the duct when placed with its long side in the direction of the stream and less when placed at right angles to the stream.

Miller, Foster, Ross and Wohl (37) also studied gas mixing in square ducts of 1" by 1", 2" by 2" and 3" by 3" using shadow photography and chemical sampling techniques and obtained a semiquantitative picture of gas mixing which may have industrial applications. An equation for correlation was presented.

$$\frac{P}{D} = K_p \left(\frac{V_D \rho_D}{u \rho_d}\right)^{a-b} \left(\frac{V_D D^2}{\frac{u\pi d^2}{4}}\right)^{b} \left(\frac{\rho_D}{\rho_d}\right)^{c-a+b}$$

or

$$\frac{P}{D} = K_p \frac{\left(\frac{\rho_D}{\rho_d}\right)^{\gamma}}{R_m^{\alpha} R_v^{\beta}}$$

In all these references there is no quantitative method for estimating the exact location of the stagnant zone formed using auxiliary jets. Also the flow characteristics were not well understood. The validity of using rakes is doubtful since the pattern could be changed by the rake if there is reverse flow. It is desirable to probe further into the induced turbulence in a square duct.

IV - THEORETICAL PRINCIPLES

The purpose of employing and developing theory is to enable one to predict the shape and penetration of the flow knowing only the velocity and density of the main stream and the velocity, density, diameter and angle of incidence of the side stream.

The Dimensional Analysis Approach

The variables that may be expected to affect the penetration length ℓ for the case of a round jet entering an air stream are: the diameter of the jet D_j, the density of the jet ρ_j, the velocity of the jet V_j, the viscosity of the jet μ_j, the main stream velocity V_o, the main stream density ρ_o, the main stream viscosity μ_o, the mixing distance s, and the width of the duct w.

The penetration " ℓ " can be written as

$$\ell = f(D_j, \rho_j, V_j, \mu_j, V_o, \rho_o, \mu_o, s, w).$$

$$\ell = k\, D_j^{a} \cdot \rho_j^{b} \cdot V_j^{c} \cdot \mu_j^{d} \cdot V_o^{e} \cdot \rho_o^{f} \cdot \mu_o^{g} \cdot s^{h} \cdot w^{j}$$

$$L = k\,(L)^{a} \left(\frac{M}{L^3}\right)^{b} \left(\frac{L}{T}\right)^{c} \left(\frac{M}{LT}\right)^{d} \left(\frac{L}{T}\right)^{e} \left(\frac{M}{L^3}\right)^{f} \left(\frac{M}{LT}\right)^{g} (L)^{h} (L)^{j}$$

$$\text{L:} \quad a - 3b + c - d + e - 3f - g + h + j = 1$$

$$\text{M:} \quad b + d + f + g = 0$$

$$\text{T:} \quad -c - d - e - g = 0$$

$$\frac{\ell}{D_j} = K \left(\frac{\rho_o V_j D_j}{\mu_j}\right) \left(\frac{V_j}{V_o}\right) \left(\frac{\rho_j}{\rho_o}\right) \left(\frac{\mu_j}{\mu_o}\right) \left(\frac{s}{D_j}\right) \left(\frac{w}{D_j}\right)$$

$$\frac{\ell}{D_j} = K \left(\frac{\rho_j}{\rho_o}\right)^{0.52} \left(\frac{V_j}{V_o}\right)^{0.59} \left(\frac{s}{D_j}\right)^{0.26} \qquad (3)$$

Since in effect the jet is entering a flow as a point from a flat plate, (w/D_j) can be eliminated, and since the temperatures are fairly constant (μ_j/μ_o) can be dropped. Similarly, all the parameters except the ratios (V_j/V_o), (ρ_j/ρ_o), (s/D_j) and $(\rho_j V_j D_j/\mu_j)$ were eliminated. Experimentally it was found that the effect of Reynolds number was small (in the range 60,000 to 500,000) and therefore the final correlation in Callaghan and Ruggeri's work is

$$\frac{\ell}{D_j} = K \left(\frac{V_j}{V_o}\right)^{\alpha} \left(\frac{\rho_j}{\rho_o}\right)^{\beta} \left(\frac{s}{D_j}\right)^{\gamma} \qquad (3a)$$

Another equation which fits the data reasonably well is

$$\left(\frac{\ell}{D_j}\right)^{1.65} = 2.91 \frac{\rho_j V_j}{\rho_o V_o} \sqrt{\frac{s}{D_j}} \qquad (4)$$

When the static pressure ratio over an orifice exceeded that necessary for sound flow, the equation $V_j = \sqrt{\gamma RT}$ may be used. The jet density at the choked condition is found from the local temperature and total pressure by using (5)

$$\rho_j = \left(\frac{\gamma+1}{2}\right)^{1/1-\gamma} 0.041218 \frac{P_j}{T_j} = 0.0261 \frac{P_j}{T_j} \qquad (6)$$

If the fluids under study are liquids dimensional analysis again leads to

$$\frac{\ell}{D_j} = K \left(\frac{\rho_j V_j D_j}{\mu_j}\right)^a \left(\frac{V_j}{V_o}\right)^b \left(\frac{\rho_j}{\rho_o}\right)^c \left(\frac{\mu_j}{\mu_o}\right)^f \left(\frac{s}{D_j}\right)^e \left(\frac{w}{D_j}\right)^f \left(\frac{h}{D_j}\right)^g \qquad (7)$$

where h is the depth of the test section.

Experimental work has again shown that the terms $\left(\frac{\rho_j V_j D_j}{\mu_j}\right)^a$, $\left(\frac{\mu_j}{\mu_o}\right)^d$, $\left(\frac{w}{D_j}\right)^f$ and $\left(\frac{h}{D_j}\right)^g$ are relatively constant and the final equation is

$$\frac{\ell}{D_j} = K \left(\frac{V_j}{V_o}\right)^b \left(\frac{\rho_j}{\rho_o}\right)^c \left(\frac{s}{D_j}\right)^e \qquad (8a)$$

Chelko gives the completed equation as

$$\frac{\ell}{D_j} = 0.450 \left(\frac{V_j}{V_o}\right)^{0.95} \left(\frac{\rho_j}{\rho_o}\right)^{0.75} \left(\frac{s}{D_j}\right)^{0.22} \qquad (8)$$

Wohl (37) considers that a qualitative consideration of the mixing problem predicts that mixing is determined by the size of the duct and the side port and by the velocities and densities of the mainstream and side stream jet. The viscosity has been neglected here.

$$\ell = f(D_o, D_j, V_o, V_j, \rho_o, \rho_j)$$

$$\text{if } \frac{\ell}{D_o} = K_p \left(\frac{V_o}{V_j}\right)^a \left(\frac{D_o^2}{\pi D_j^2/4}\right)^b \left(\frac{\rho_o}{\rho_j}\right)^c$$

then

$$\frac{\ell}{D_o} = K_p \left(\frac{V_o \rho_o}{V_j \rho_o}\right)^{a-b} \left(\frac{V_o D_o^2}{V_j \pi V_j^2/4}\right)^b \left(\frac{\rho_o}{\rho_j}\right)^{c-a+b} \tag{9}$$

or

$$\frac{\ell}{D_o} = K_p \left(\frac{\rho_o}{\rho_j}\right)^2 \frac{1}{R_m^{\alpha} R_v^{\beta}} \tag{10}$$

where

$$R_m = \frac{V_j \rho_j}{V_o \rho_o} \tag{11}$$

and

$$R_v = \frac{V_j V_j^2}{V_o D_o^2/4} \tag{12}$$

The ratio $\left(\frac{D_o}{D_j}\right)$ was a dependent variable in these experiments, since R_m and R_v were varied separately; by definition

$$R_m = \frac{\rho_j}{\rho_o} \left(\frac{D^2}{\pi D_j^2/4}\right) R_v \tag{13}$$

Similarly

$$\frac{B}{D} = K_b \left(\frac{\rho_o}{\rho_j}\right)^{\delta} \frac{1}{R_m^{\epsilon} R_v^{x}} \tag{14}$$

and

$$\frac{M}{D} = K_m \left(\frac{\rho_o}{\rho_j}\right)^{r} \frac{}{R_m^{\varnothing} R_v^{i}} \tag{15}$$

If the ducts are small $\gamma = \delta = \sim = 0$ and the density ratio is taken care of by the term R_m.

If special pairs of values of ℓ and s are interpreted as D and ℓ respectively, in terms of the present definition of penetration distance the following expression results:

$$\frac{\ell}{D} = K_p \left(\frac{D_o}{D_j}\right)^{2.3} \frac{1}{R_m^2}$$

$$= K_p \left(\frac{\rho_o}{\rho_j}\right) \left(\frac{D_o}{D_j}\right)^{0.3} \frac{1}{R_m R_v} \tag{16}$$

$$\frac{\ell}{D_o} = K_p \left(\frac{D_o}{D_j}\right)^{2.3} \frac{1}{R_m^2 R_v 0.3}$$

$$= K_p \left(\frac{\rho_o}{\rho_j}\right) \left(\frac{D_o}{D_j}\right)^{0.3} \frac{1}{R_m R_v^{1.3}} \tag{17}$$

for a 1" by 1" duct M/D was independent of the density ratio. It was found that M/D data for the 1" by 1" and the 2" by 2" ducts could be correlated by

$$\frac{M}{D} = \frac{K_m}{(R_m R_v)^{0.5}} \qquad (18)$$

For the 3" by 3" duct

$$\frac{M}{D} = \frac{6.0}{R_m^{0.7} R_v^{0.2}} \qquad (19)$$

	Configuration	K_p
air	→ □	0.9
	→ ▭	0.9
	→ ○	1.1
	→ ▯	1.2

Potential Flow Analysis in Two Dimensions

In this study the purpose of introducing potential theory is to find the parametric equations of the vortex sheet and thus to predict the shape of the streamlines.

Many problems in applied mathematics and mathematical physics depend on the construction of functions U = U (x,y,z) which are solutions of the Laplace equation

$$\frac{\partial^2 u}{\partial x^2} + \frac{\partial^2 u}{\partial y^2} + \frac{\partial^2 u}{\partial z^2} = 0$$

where (x,y,z) are rectangular coordinates, satisfying certain

boundary conditions determined by the problem under study. If the problem is such that the value of the function $u(x,y,z)$ is independent of z, the equation reduces to the two-dimensional Laplace equation

$$\frac{\partial^2 u}{\partial x^2} + \frac{\partial^2 u}{\partial y^2} = 0$$

Thus u is a harmonic function in the domain.

It is assumed that the flow is stationary, nonviscous, irrotational and incompressible. An individual particle moves on a curve whose direction coincides at every point with the velocity vector.

If the potential $w = \Phi + i\Psi$, then the streamlines are characterized by Ψ = a constant. Thus these lines have the equation $z = F^{-1}(\Phi + i\Psi)$, or if the real and imaginary parts are separated, x = real part of $F^{-1}(\Phi + i\Psi)$

and y = imaginary part of $F^{-1}(\Phi + i\Psi)$

(the real parameter Φ varies from $-\infty$ to $+\infty$.

This method has been used where the boundary conditions for the solution of the Laplace equation are complex.

Ehrich (34) has used potential theory to describe the entry of a jet entering a fluid stream at an oblique angle from a slot or an orifice. The wake can be approximated by a large arc of motionless fluid separated from the jet by a vortex sheet at uniform

pressure. If the jet is separated from the main stream by a stream line, and the jet velocity is restricted to one particular value to prevent a discontinuity across the stream line, analysis using the conventional Helmholtz-Kirchoff method is possible, leading to computations of the many relationships between the geometrical and velocity parameters.

An equivalent analysis can be made for the case where the trailing edge of the jet does not separate from the downstream wall.

The flow is assumed to be steady, incompressible, two-dimensional potential flow of equal densities. Even though the shape of the vortex sheet boundary is not known in the physical plane (figure 1) it can be drawn in the hodograph plane because of the assumption of constant velocity along it. The hodograph of such a flow is simply the locus of the Γ' where $\Gamma' = \frac{dw}{dz}$. On the hodograph plane all the vortex sheets become arcs of circles and all straight boundaries transform into radial lines. Therefore the boundaries of the flow are readily drawn as shown in figure 2. The conjugate of this plane is functionally related to the physical and potential planes since

$$-\frac{dw}{dz} = q\, e^{-i\Theta} \qquad (20)$$

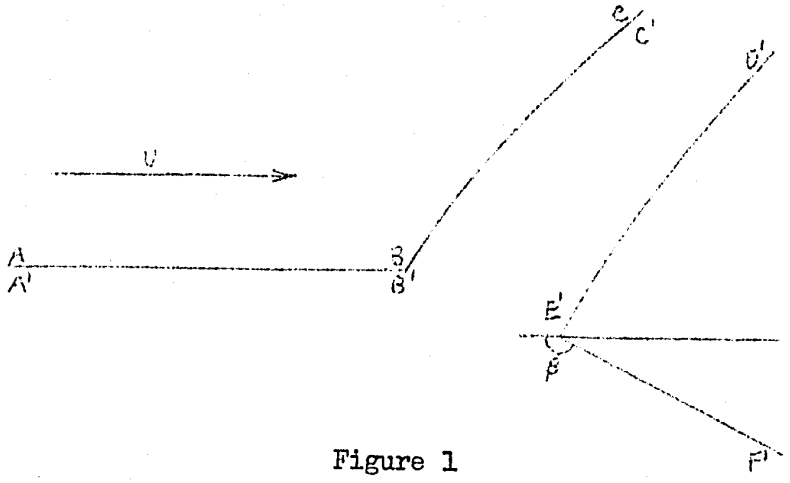

Figure 1

The physical plane showing a jet with offset boundaries entering a main stream and separating from the wall. $z = x + iy$

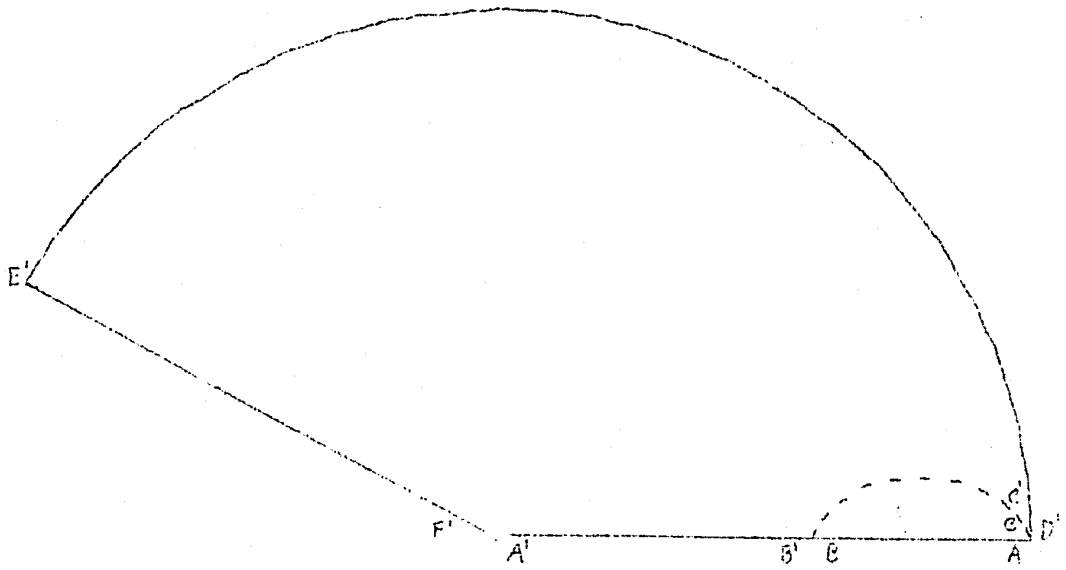

Figure 2

Figure 1 in the hodograph plane

$\Gamma = q e^{i\theta}$

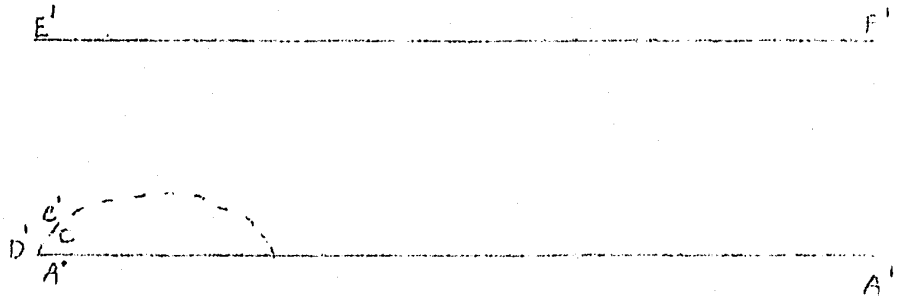

Figure 3

The logarithm of the conjugate half plane

If the logarithm of the circle sector is taken, the bound area is transformed into a degenerate rectilinear polygon (a degenerate polygon has one or more vertices at infinity) thus

$$Q = -\ln \left[\left(\frac{q}{U}\right) e^{-i\Theta} \right] \quad \text{and}$$

$$Q = \ln \frac{U}{q} + i\Theta \tag{21}$$

The boundaries of constant velocity become horizontal lines as shown in figure 3.

The Schwarz-Christoffel transformation permits this polygon to be changed into the upper half of some new plane ζ (see figure 4) having the functional relationship

$$Q = Q(\zeta) \tag{22}$$

tabulated in Table XIV and derived in detail for the various cases listed in Appendix 3. This function must be left in terms of the parameter h that indicates the relative location of the vertices of the polygon in the zeta plane and is a function of the relative orientation of the edges of the jet source in the physical plane.

The flow boundaries can be drawn in the complex potential plane w because all streamlines are horizontal lines by virtue of their constant stream functions as shown in figure 5. This plane can be transformed directly into the zeta upper half

plane by using the Schwarz-Christoffel transformation. Because of the basic similarity of the configurations under consideration, all give the same transforming function (see Appendix 3 for derivation):

$$\frac{dw}{d\zeta} = \frac{-(1+h)^2\, Uc}{\pi(\zeta + h)(\zeta - 1)^2} \qquad (23)$$

The set of transformations given by equations 20, 21, 22 and 23 completely determines the problem functionally and permits the calculation of the various parameters.

The actual shape of the vortex sheet can be determined from the assumption of constant velocity.

$$ds = |dz| = \left|\frac{dz}{dw}\right|\left|\frac{dw}{d\zeta}\right| d\zeta \Big| = \frac{1}{U}\left|\frac{dw}{d\zeta}\right| d\zeta \qquad (24)$$

and

$$dx = ds\cos\theta = [\text{real part of } e^{Q}]\, ds \qquad (25a)$$

$$dy = ds\sin\theta = [\text{imaginary part of } e^{Q}]\, ds \qquad (25b)$$

hence

$$\frac{x}{c} = -\int_{-1}^{\zeta} \frac{[\text{real part of } e^{Q}]\,(1+h)^2\, d\zeta}{\pi(\zeta + h)(\zeta - 1)^2} \qquad (26a)$$

$$\frac{y}{c} = -\int_{-1}^{\zeta} \frac{[\text{imaginary part of } e^{Q}]\,(1+h)^2\, d\zeta}{\pi(\zeta + h)(\zeta - 1)^2} \qquad (26b)$$

The solutions of 25a and 25b give two parametric equations in zeta which determine the shape of the vortex sheet in terms of h and may be seen in Table XV and developed in detail in Appendix 3 for different geometries.

A somewhat similar procedure, modified to some extent, is useful in finding the relative orientation of the orifice edges in terms of h. An integration of the physical plane from edges B' to E' is equivalent to an integration from B' to E' in the zeta plane. But an integration in the zeta plane along the real axis must avoid the pole at the point A'F'. This is most readily done by the path shown on figure 6 where the integration is carried out along the real axis to a distance $(-h-\epsilon)$. Then the integration is calculated along a semicircle of radius ϵ from $(-h-\epsilon)$ to $(-h+\epsilon)$ from which point the integration can be carried out along the real axis.

Thus

$$\int_{B'}^{E'} \frac{dz}{c} = \int_{-\infty}^{-1} \left(\frac{dz}{dw}\right)\left(\frac{dw}{d\zeta}\right) d\zeta$$

$$= \int_{-\infty}^{-1} \frac{e^{Q}\,(1+h)^2\, d\zeta}{\pi\,(\zeta+h)\,(\zeta-1)^2} \qquad (27a)$$

$$\int_{B'}^{E'} \frac{dz}{c} = \lim_{\epsilon \to 0} \left[\int_{-\infty}^{-h-\epsilon} F(\zeta)d\zeta + \int_{\pi}^{0} F(\epsilon e^{i\theta} - h)d(\epsilon e^{i\theta}) + \right.$$

$$\left. \int_{-h+\epsilon}^{-1} F(\zeta)\, d\zeta \right] \qquad (27b)$$

The real part gives the contraction ratio a/c tabulated in Table XVI and developed in Appendix 3. When the equations are solved for the case of a jet entering the main stream at ninety degrees the equation

$$\frac{y}{D_j} = 1.91 \left[\frac{x + \frac{a}{2}}{a} \right]^{0.303}$$

results from the parametric equations given in section 4 in Table XV. This equation agrees qualitatively with the penetration data of Callaghan and Ruggeri (29).

Potential Flow Analysis in Three Dimensions

If the analysis, using potential theory is extended to the three-dimensional case as was done by Fraser (35) the velocity potential within the jet must satisfy the equation

$$\phi_{xx} + \frac{1}{r}(r\phi_r)\, r + \frac{1}{r^2}\, \phi_{\theta\theta} = 0 \qquad (28)$$

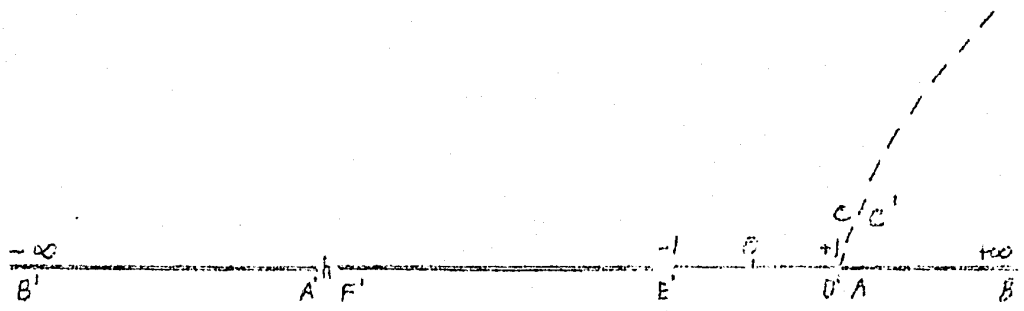

Figure 4

The ζ or mapping half plane

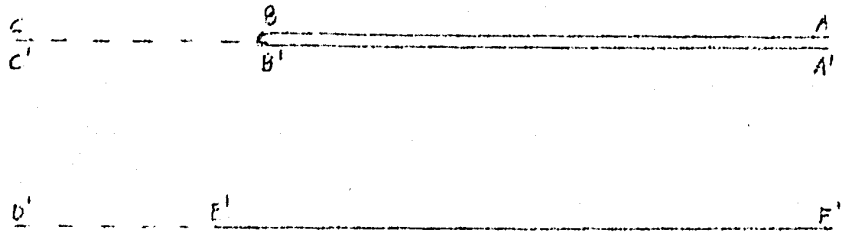

Figure 5

The complex potential plane $w = \Phi + i\Psi$

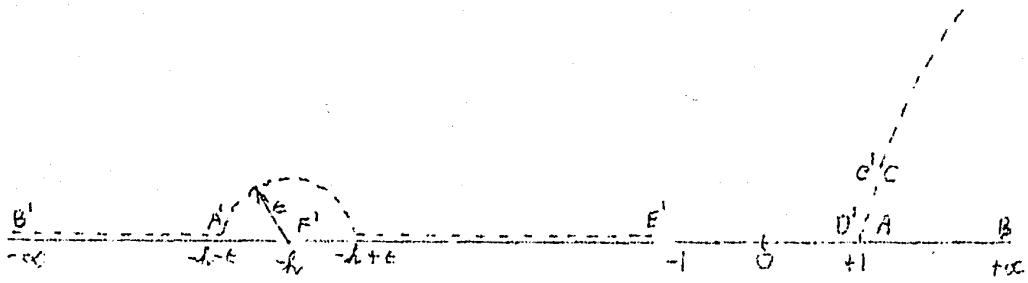

Figure 6

Integration from B' to E' in the zeta plane

since the velocity potential within the jet was assumed in the form

$$\phi = \sum_{m=1}^{\infty} \sum_{n=0}^{\infty} a_m{}^n (r)\, x^m \cos n\theta + Ux \qquad (29)$$

To satisfy equation (28), $A_m{}^n(r)$ takes the form

$$A_m{}^n(r) \sim C_m{}^n r^n \qquad (30)$$

where C_m r are constants. The pressure around an infinitely long cylinder was assumed to be the same as the pressure around a cylinder of gas of the same diameter and at the same Reynold's number. The pressure at the boundary was represented by the series

$$\bar{P} = A_0 + A_1 \cos\theta + A_2 \cos 2\theta + A_3 \cos 3\theta + A_4 \cos 4\theta \qquad (31)$$

whose constants were determined for the streamlines on figure 7.

1. Assuming that cross velocity components in the jet are negligible at the entrance plane and linearization is possible

$$\bar{P} = \frac{2\,U_1}{U}$$

and

$$\bar{P} = \frac{2}{U} \frac{\partial \phi}{\partial x}\bigg|_{x=0} \qquad (32)$$

If n is limited to 4 and m to 2 in equation (29), an approximate solution for the potential function can be found. The constants C_1^0, C_1^1, ... C_1^4 and $C_2^0 = C_2^1 = C_2^4 = 0$ can be determined from equations (31) and (32) at the five streamlines mentioned. The results can be written as

$$\phi_{n=4} = f(x,r,\theta) \qquad (33)$$

$$m = 2$$

From equation (33) radial and tangential curvatures of jet surface streamlines were calculated for x = 0 and used in the prediction of approximate values of θ, r, u_1, u_2, and u_3 at x = d/2 for surface streamlines.

The boundary pressure distribution at x = D/2 was based on the assumption that the pressure along a streamline would remain constant for this short distance. The assumption seems justified at x = 0 and in the wake. It allows for a spreading pressure region on the upstream side qualitatively consistent with the flattening of the jet front which takes place.

The flow solution from equation (33) was dropped at this point and the more elaborate expression

$$\phi_{n=4} = g(x,r,\theta) \qquad (34)$$

$$m = 3$$

satisfying equations (28) and (29) and involving ten constants to be determined, was adopted.

The number of unknowns was cut in half by matching static pressures at the same five streamlines as before at $x = 0$. Instead of matching the static pressure at more positions at this station, the remaining five constants were determined by matching the total pressures at the same five streamlines at $x = D/2$, assuming uniform total head throughout the jet. To perform this calculation it was found convenient to use approximate values of θ, r, u_1, u_2, and u_3 at $x = D/2$ obtained above and to assume the true velocity components to be only slightly different from the approximate ones, i.e. to make a linear perturbation calculation. This is simply a short cut and does not affect the method in principle; the main point is that the ten coefficients of equation (34) were determined by matching these conditions.

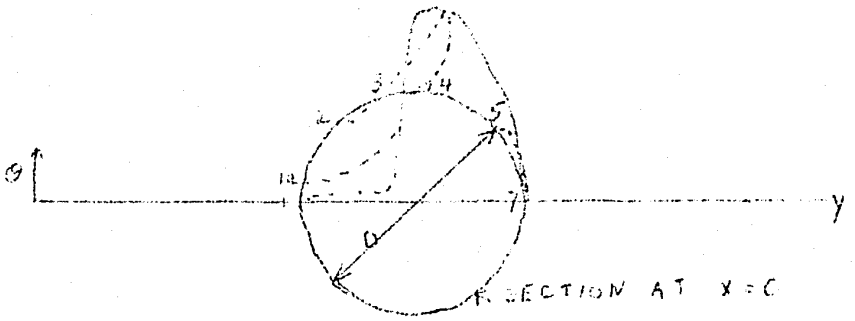

Figure 7

The distortion of a jet cross section in the first diameter of travel

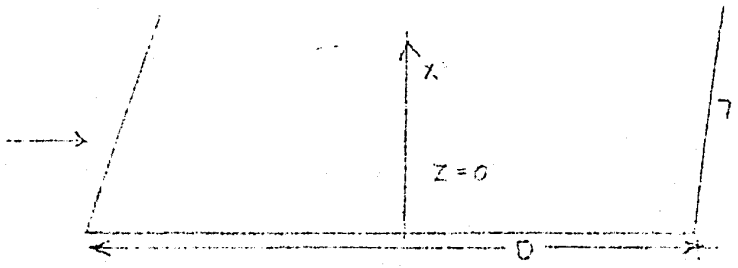

Figure 8

The deflection of a jet at the plane symmetry

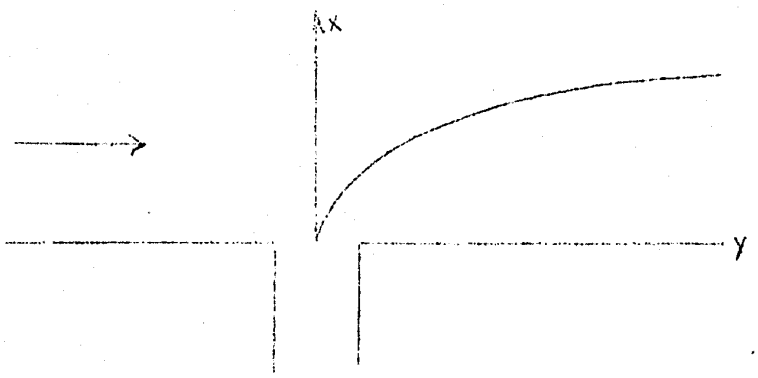

Figure 9

The experimental curve of Callaghan and Ruggeri (Reference 29, figure 6)

Figures 7, 8 and 9 represent the jet flow corresponding to equation (34). The conclusions were based on the assumption that pressure forces limit jet penetration by accomplishing the sharp turning after entering followed by a further slow penetration by jet mixing. This agrees with Hawthorne, Rogers and Zaczek (36), who found better penetration if a round hole were elongated in the stream direction and if another hole or rod were placed immediately downstream.

The agreement between Fraser (35), the results of Ehrich (34) and Callaghan and Ruggeri (29) can be explained thus:

(1) The rapid flattening of a round jet as in figure 7 making a two-dimensional treatment quickly applicable.

(2) The filling of the narrow (3 diameters) cross section used by Callaghan and Ruggeri (29) due to flattening and venturi action between the jet passage side walls. This action is believed capable of contributing to two-dimensional test data.

V - EXPERIMENTAL DETAILS

(1) EQUIPMENT

A - The main duct - Experimental work was carried out in a four inch square duct constructed from steel plates 1/4 inch thick. One wall was drilled with tiny holes, each of which was reamed with a ten degree tapered reamer and closed with a tapered pin. This avoided threading the holes and permitted a large increase in the number of measuring points since each could now be set much closer together. The wall of the tube was in effect closed since only one pin was withdrawn at a time to insert the probe.

A si inch diameter round duct was used to check the analogy between the patterns in the wake of a rod and a jet.

B - The probe - To measure the configuration of the flow in the eddy region, a tiny probe was constructed out of a fifteen B.D. hypodermic needle. A hole was drilled on the upstream side at the tip. The probe was soldered to a brass tube which was connected through rubber and copper tubing to the recorders.

C - The probe carriage - The probe was placed on a moveable carriage to reach any upstream or downstream position above or below the injector with ease. It could be locked in place to prevent vibration from the blower from shaking it loose and could easily be removed to permit changes in the arrangement.

To attain a suitable withdrawal rate, a 1 R.P.M. synchronous motor, chosen because of its constant speed, was connected through rack and pinion gearing to the probe. The gear ratios were such that the probe moved one inch in five minutes.

D - The injector - The injector was a tiny round hole drilled in a flat, round, 1/4 inch thick piece of steel plate. It had a diameter of one inch, was threaded on the edge and had a lip and a gasket, which prevented it from being screwed too far into the hole in the top of the duct. Thus it was always flush with the wall. A three inch piece of 3/8 inch steel pipe was welded to the top of the piece and the pipe was connected by a flexible metal hose to the air supply.

If an angled injector was desired, the hole through the metal disc was simply drilled at the required angle of incidence and a mark was stamped on the upstream side to be certain that the jet pointed in the right direction. This method of replacing discs whenever the injector was to be changed avoided drilling and plugging more than one hole in the main duct.

E - The blower - A Buffalo high pressure blower rated at forty-five inches of water and a thousand cubic feet per minute supplied high velocity air for the main stream. It was controlled by a vane type inlet damper.

F - Compressors - Two compressors, one a Gardiner Denver and the other an Ingersol Rand, supplied air to the regulating system at 125 psig. Their combined capacity was fifty-seven standard cubic feet per minute.

G - The regulator - Since the pressure of the air from the compressors was not constant, a Moore Regulating Company constant pressure valve model number 42H100 was installed in the air line to keep the pressure steady.

H - The recording system - The pressure line from the probe led through two solenoid valves to a Brown pressure recorder model number Y702X23-C38-11-111-(64)-SK999 with two pens. One pen (0-20 psi) was deliberately set high to record negative readings, and the other (0-10 psi) was not changed.

I - U tube manometer - Since the probe measured the total pressure i.e. static pressure plus velocity pressure, it was necessary to measure the static pressure separately. This was done by measuring the pressure at the wall with a U tube manometer.

J - Smoothing section - Since a main duct four feet long has insufficient length to ensure fully developed turbulent flow, a smoothing section was added in front of the duct. A galvanized pipe four inches square and having enough length to ensure at least twenty diameters of undisturbed flow upstream from the measuring station, was installed.

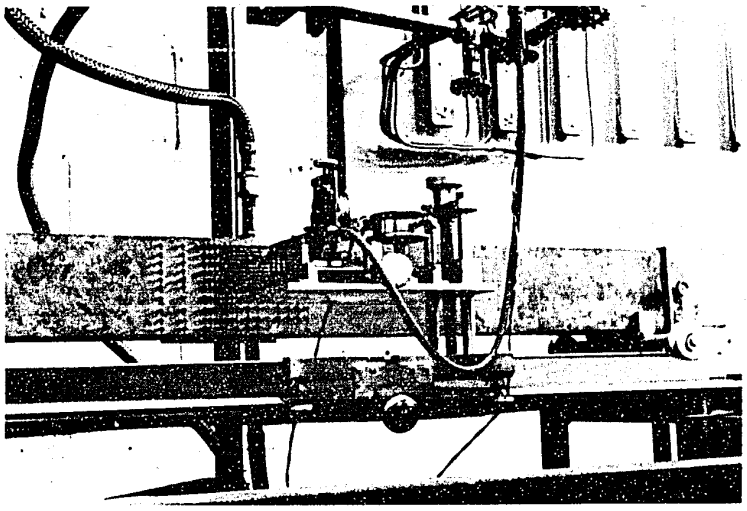

A photograph of the four-inch square duct showing the working section, the pressure measuring probe and air injectors

Fig. 10

Figure 11

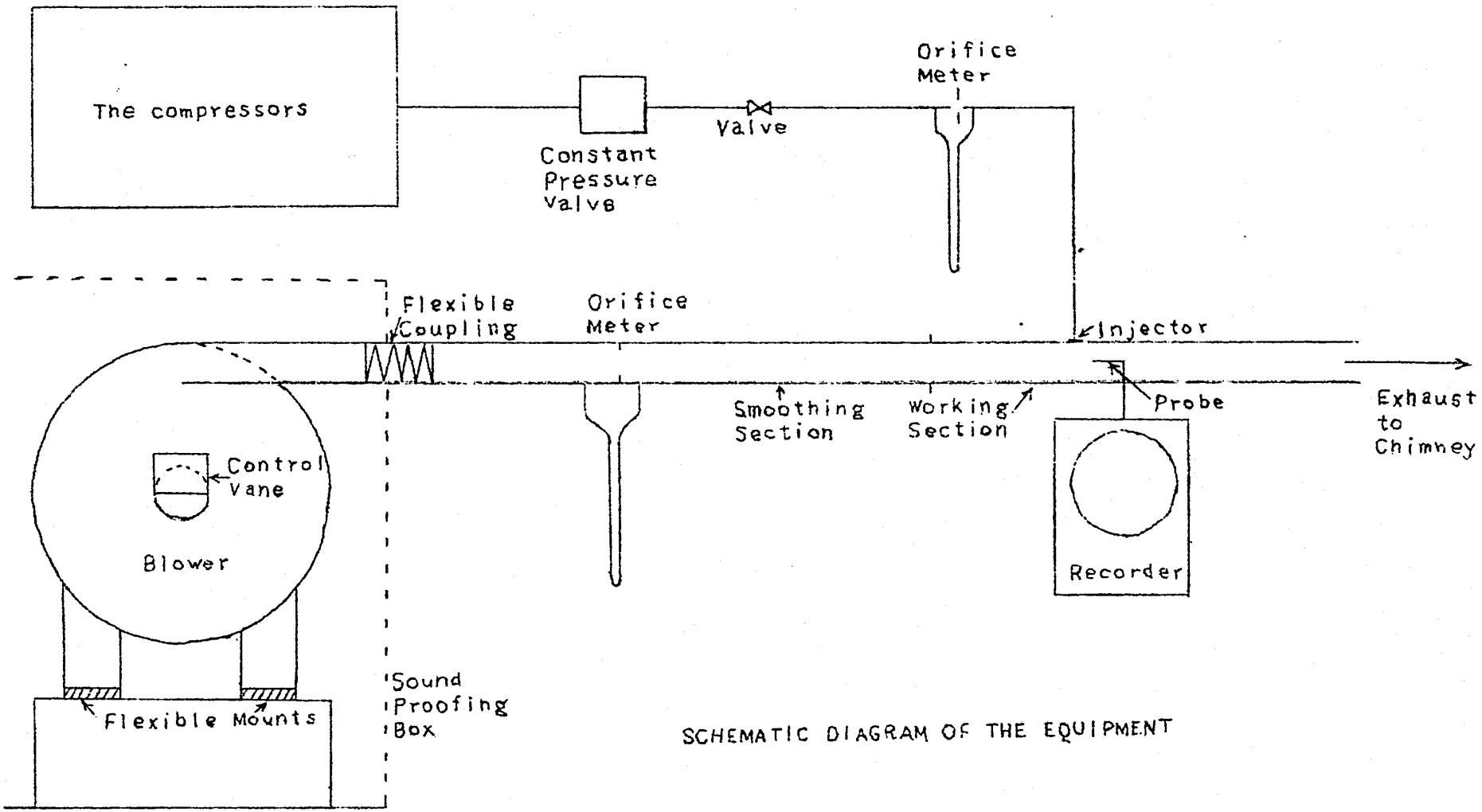

SCHEMATIC DIAGRAM OF THE EQUIPMENT

K - Flow meters - All flows were measured by sharp edged orifices constructed according to the directions given in the Chemical Engineers Handbook. Each orifice was fitted with radius taps connected to water filled manometers.

L - Exhaust air - Exhaust air was removed from the experimental section by joining the rear of the duct to an old chimney.

M - Sound proofing - The blower, which supplied the air, had to be sound proofed to keep the noise level low. This was accomplished by placing a 6' x 6' by 6' fiber board box over the blower, leading the incoming air through a vertical four inch wide duct along one side and placing a flexible rubber coupling on the outlet of the blower to reduce vibration. The blower itself was mounted on a concrete block and four vibration damping mounts were placed under its feet.

(2) PHOTOGRAPHS AND DIAGRAMS OF THE EQUIPMENT

Figure 10 is a photograph of the four inch square duct showing the working section, the pressure measuring probe and air injectors.

Figure 11 is a schematic diagram of the overall arrangement of the equipment.

(3) PROCEDURE

The working fluid, air, was forced through the duct at 130 to 250 feet per second by the blower, whose inlet vane was adjusted to give the required velocity. The eddy was then created by the injection of air at angles of incidence of thirty, forty-five and ninety degrees. Point velocities were measured with a probe connected to a Brown Pressure Recorder. Velocity traverses were taken above and below the injector and profiles were calculated from them. The probe was inserted through one of the tapered holes in the duct. It had to be withdrawn slowly because time was necessary for the pressure in the line to the recorder to be in equilibrium with the pressure at the tip in the flow. If it were withdrawn too quickly, the pressure recorded on the chart and the actual pressure at the measuring point would be different and erroneous results would be obtained. This also helped to spread the reading on the chart over a larger area. The twenty-four motor was removed from the recorder and replaced by a two-hour motor. This helped to spread the reading out even more and permitted the use of twenty-four hour charts on which each large division was equivalent to five minutes rather than one hour.

All flow rates were measured by sharp edged orifice meters and water filled manometers. The orifices were checked by a "Precision" wet test meter.

VI - PRESENTATION AND DISCUSSION OF RESULTS

Point velocities along the direction of the main stream were calculated from the measured pressure traverses by means of the usual expression

$$V_x = \sqrt{2 g \Delta h} \qquad (35)$$

The flow patterns were plotted on the three planes as indicated in figure 12. Typical examples of flow patterns are shown in figures 13 - 15. In figure 13, 2" down and a 1/2" downstream refers to the position which is 2" below the top wall and a 1/2" downstream of the injector. The profiles a-b-c-d as shown in figure 15 were taken from the semi-traverses at the same distance from the wall and a mirror image was drawn to complete the picture. On the plane A-B-C-D, in line of the air injector as shown in figure 15, the velocity near the top wall was observed to be positive. Slightly away from the top wall, strong negative velocity readings were observed. Below this region, a stagnant zone was located in which the velocity was less than one third of the main stream velocity. Further away from the top wall, very strong positive readings were observed. In some cases, the positive velocity readings obtained in this region were somewhat higher than the main stream velocity. The recirculation of the flow indicated the formation of elliptically shaped spirals. In figure 15, the flow patterns in the form of

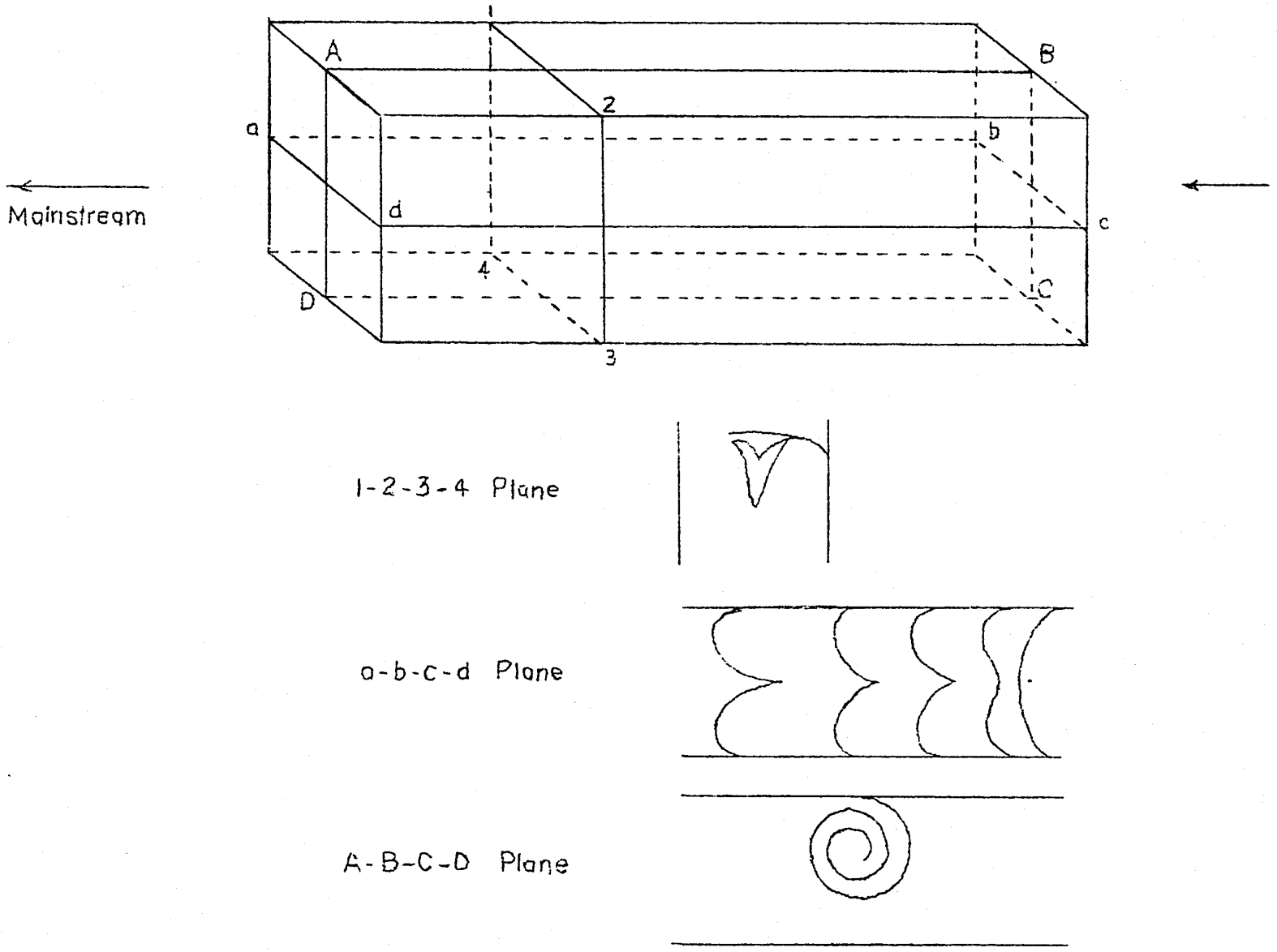

Fig.12 Flow Patterns in Various Planes

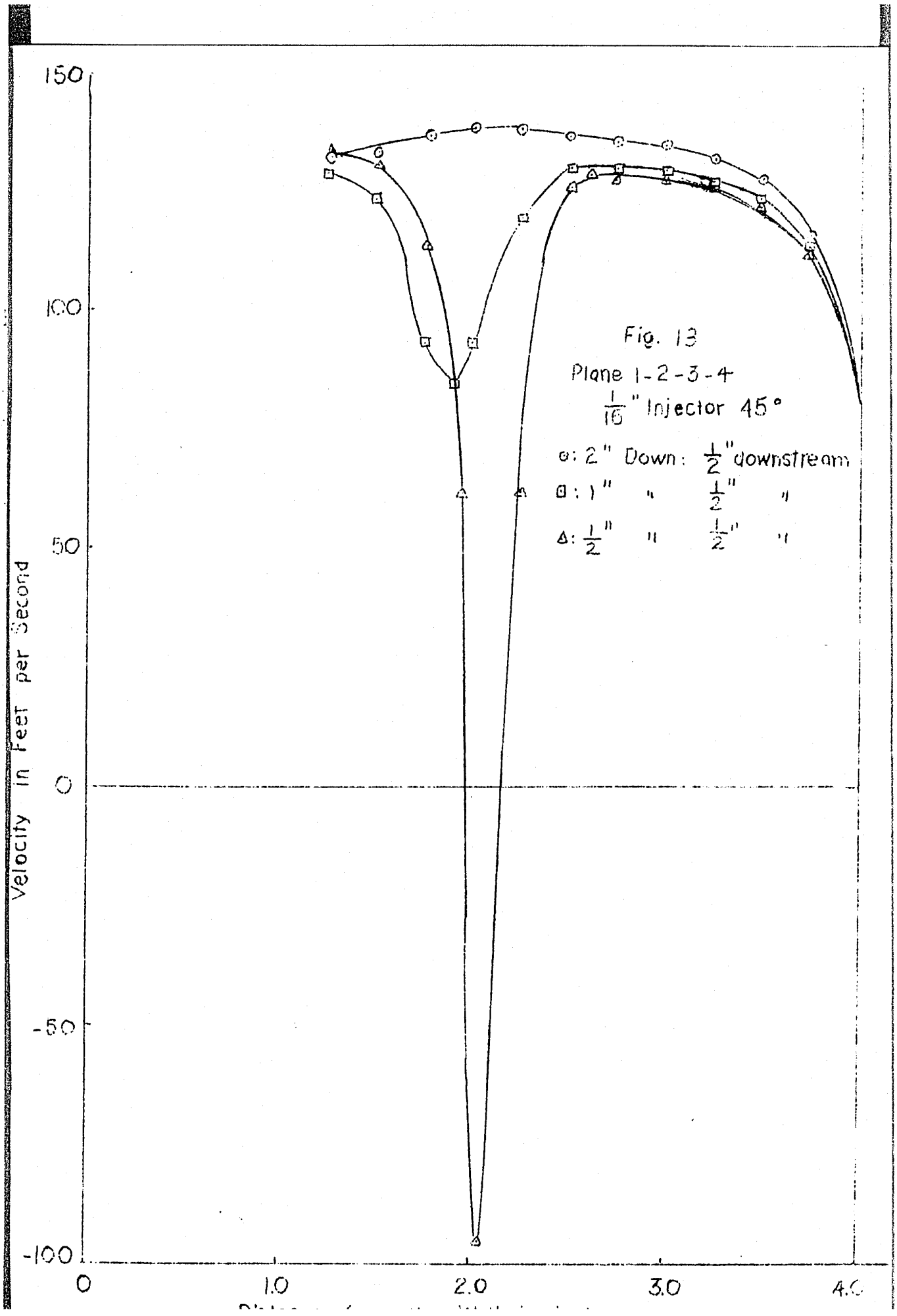
150
100
50
0
-50
-100
Velocity in Feet per Second
0
1.0
2.0
3.0
4.0
Fig. 13
Plane 1-2-3-4
1/16" Injector 45°
o: 2" Down: 1/2" downstream
□: 1" " 1/2" "
Δ: 1/2" " 1/2" "

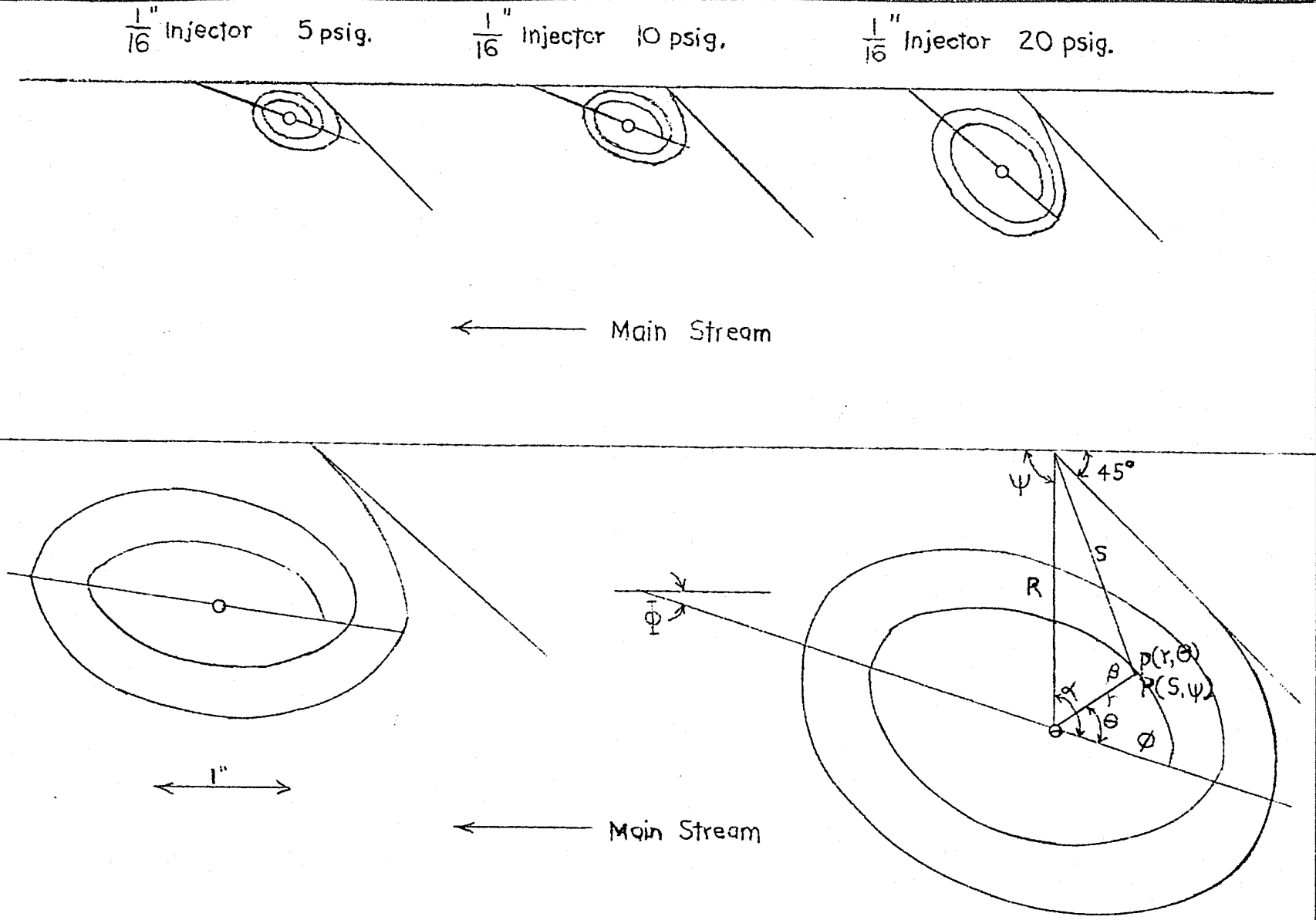

Fig. 14 Flow Patterns in Plane A-B-C-D
Incidence Angle = 45°

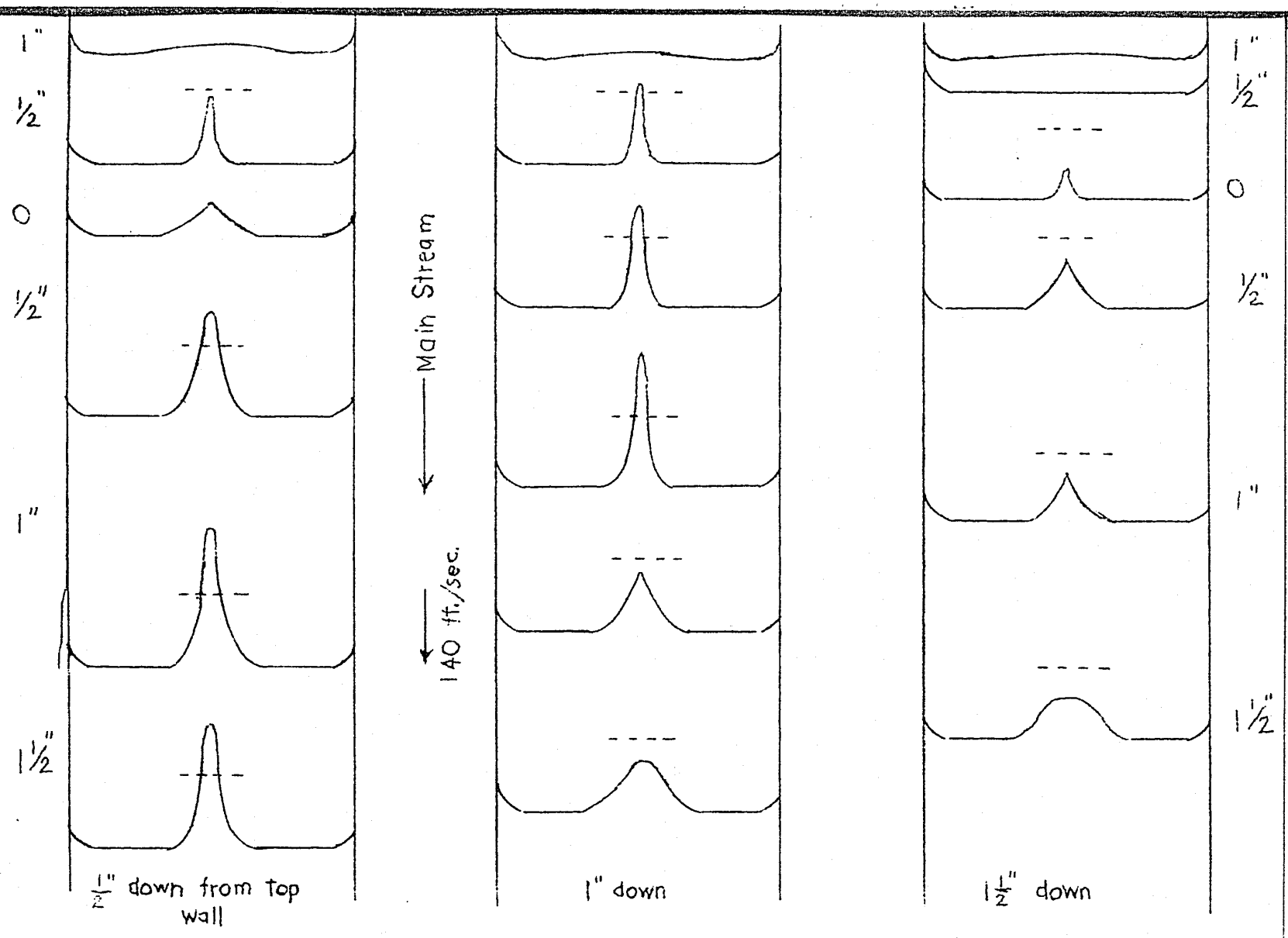

Fig.15 Flow Patterns in Plane a-b-c-d
Injector size: $\frac{1}{16}$". Jet Pressure: 40psig., ence Angle: 45°.

spirals were shown in actual sizes for incidence angle equals 45° cases. The area enclosed within the first revolution (the inner one) of the spiral was considered as the stagnant zone. It was observed that the larger the size of the injector, the larger would be the stagnant zone, and similarly, the higher the mass velocity of the air injected, the larger the stagnant zone. These spiral diagrams were constructed from the best line drawn on the vector diagram. Letting the spiral revolve twice to give the best picture of the centre zone and the recirculation region about a quarter turn more to be tangent to the injector wall. This general movement is a qualitative description of the motion necessary to produce a diagram of the type actually found.

Figure 16 gives the velocity profiles in the plane a-b-c-d in the wake of a 1/4" metal rod and a 1/4" jet in a six inch round duct. The jet configuration is totally different from the one found in the wake of the metal rod. Yet many investigators (35,37) are continually drawing an analogy between the case of a rod and a jet penetrating the flow. The above casts considerable doubt on this analogy. Yet, after considerable reflection it will be seen that the analogy could not be true since in the case of metal the fluid velocity at the boundary is actually zero whereas in the case of a jet mainstream molecules are continually

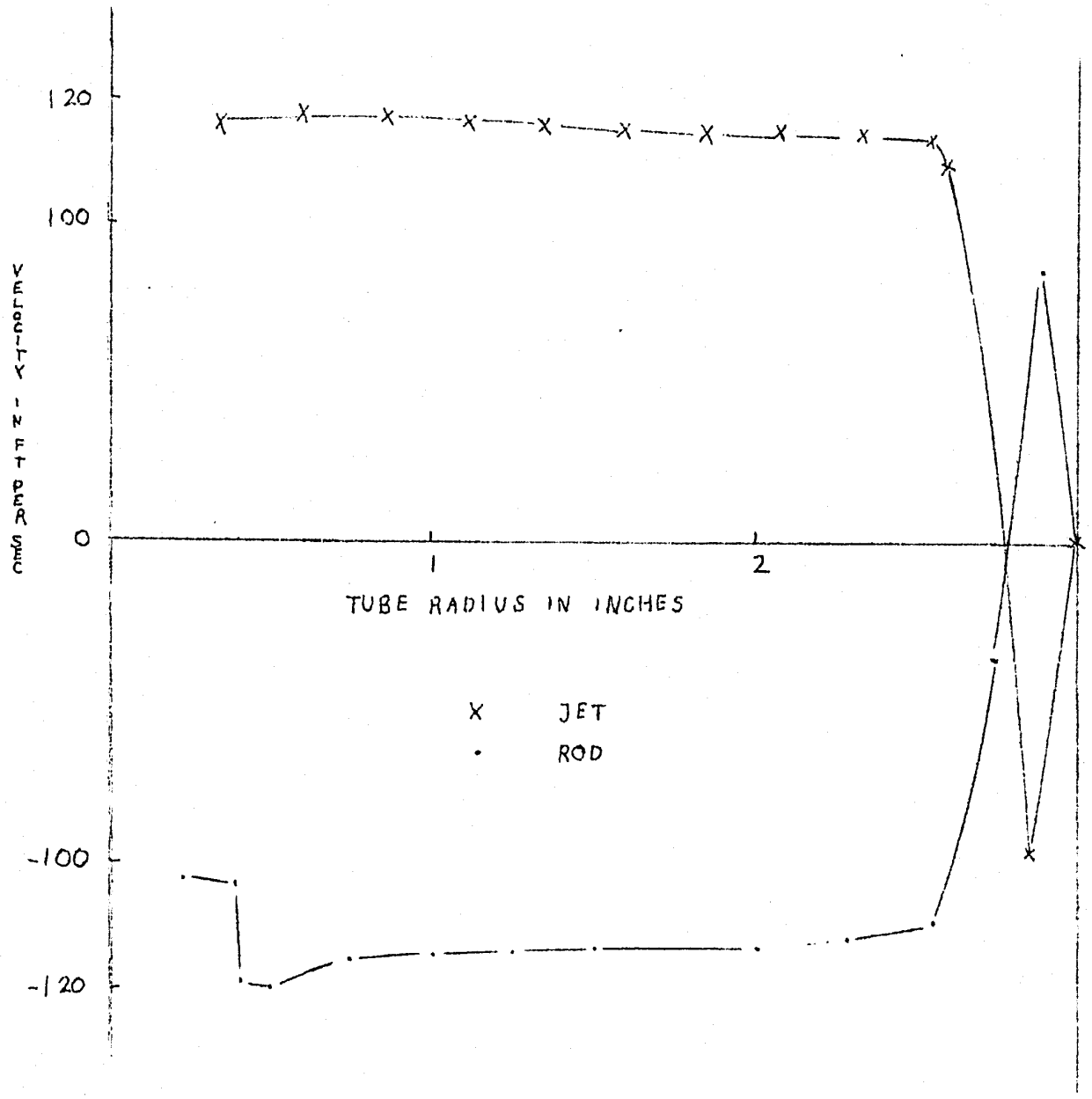

THE VERTICAL VELOCITY PROFILES FOR A $\frac{1}{4}$" ROD AND A $\frac{1}{4}$" JET TAKEN IN A SIX INCH ROUND DUCT AT A MAINSTREAM VELOCITY OF 137 FEET PER SECOND.

FIG. 16

blasting into the jet. There really is nothing to stop a mainstream molecule from doing this because a gas is mostly empty space. Only the molecules which actually collide with the jet molecules would be deflected. Therefore the mechanism at the wall of a jet is much different from the one at a metal surface. It is closer to the case of a blast of fine sand across a stream of dust particles. If the stream velocity is high, the jet will turn as a result of the collisions and start to move downstream. But there is no assurance that it will remain a smooth stream inside another, as drawn on many flow diagrams or as assumed in the potential flow analysis.

Figure 17 is a vector diagram, with streamlines added, in the plane A-B-C-D. In the wake drawn on figure 17 it is clearly seen that reverse flow is present behind the injector and in some figures shown in the work of Ghosh (43) a loop of null velocities is seen in the injector wake. Thus one type of pattern, with reverse flow and a wake seems to be emerging. The pattern may be explained by the separation of the jet from the main stream by a streamline on the upstream side and from the wake by a vortex sheet at a uniform pressure on the downstream side.

If the wake with separation is examined it will be seen that a line of null velocities could exist from the wall, up the centre of the recirculation region and down behind the injected

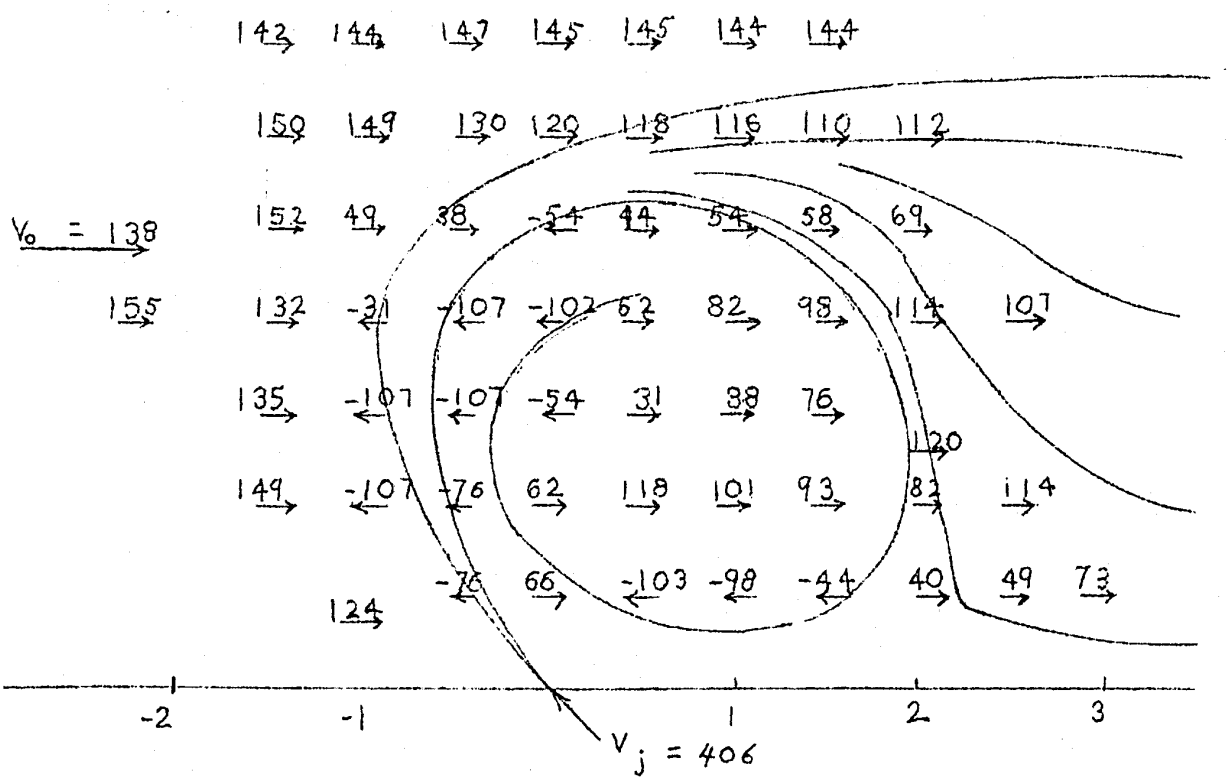

A TYPICAL POINT VELOCITY DIAGRAM WITH SUPERIMPOSED STREAMLINES.

FIG. 17.

stream. This explains the line drawn in the work of Bertin and Salmon (23) for the pattern behind the fluid baffle and also some of the results of Ghosh (43). This is probably more pronounced in these works because they are using a slot which is closer to the two-dimensional picture than the pattern behind a round jet. In the results section of this thesis, this pattern is not quite so obvious because the jet is smaller and closer to the three-dimensional case but the underlying factors are much the same.

An attempt was made previously by Campbell and Lu (38) to predict the shape of the eddy region knowing only the main stream velocity and density, and also the angle, diameter, velocity and density of the jet. This involves first a prediction of the distance of the centre of the pattern from the injector. Letting R be the distance between the centre of the spiral and the position of the injector at the wall, the following correlation was obtained using the variables D_j, ρ_j, ρ_o, V_j, V_o, λ, and λ_{90}, by dimensional analysis.

$$\frac{R}{D_j} = 2.577 \left(\frac{\rho_j}{\rho_o}\right)^{1.1723} \left(\frac{V_j}{V_o}\right)^{0.3647} \left(\frac{\lambda}{\lambda_{90}}\right)^{0.4737} \qquad (36)$$

The values of the exponents were obtained using an IBM 650 computer and the best line was found from the method of least squares. The variables are listed in Table XIV and graph is drawn in figure 18.

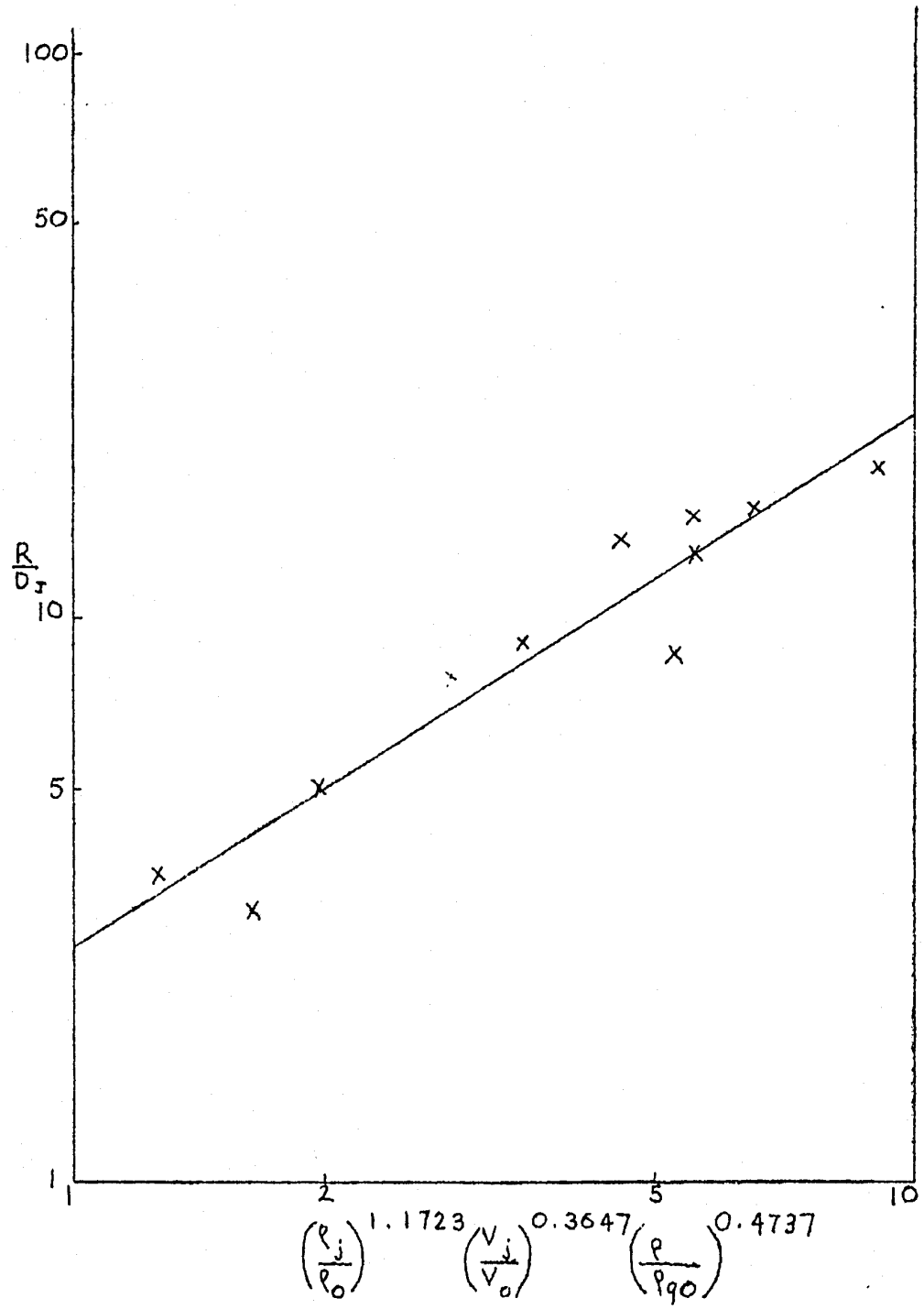

THE DISTANCE TO THE CENTRE CORRELATION

FIG. 18

Knowing R the major and minor axes of the ellipse could be determined approximately; for the forty-five degree case by means of the relationship

$$R = 2a = 3b \tag{37}$$

When $r = R$, the angle θ equals α. The angle α was found from the best value of θ to give a tangent to the injector at the wall with the proper inclination of the major axis of the ellipse. The value of k was calculated using

$$R = \frac{e^{k\alpha}}{\sqrt{\frac{\cos^2 \alpha}{a^2} + \frac{\sin^2 \alpha}{b^2}}} \tag{38}$$

TABLE I

Experimental Conditions and Penetration Results

Pattern	γ	P_j	D_j	ℓ	ρ_j	ρ_o	s	V_o	V_j
1.	45	40	0.0104	0.283	0.279	0.0748	0.0104	138	406
2.	45	40	0.00521	0.156	0.279	0.0748	0.0208	138	662
3.	45	20	0.00521	0.104	0.177	0.0748	0.0	138	468
4.	45	10	0.00521	0.052	0.126	0.0748	0.0208	138	332
5.	45	5	0.00521	0.0365	0.1005	0.0748	0.0104	138	181
6.	30	40	0.0104	0.229	0.279	0.0748	0.0	138	406
7.	30	40	0.00521	0.104	0.279	0.0748	0.208	138	662
8.	30	20	0.00521	0.0832	0.177	0.0748	0.0	138	468
9.	30	10	0.00521	0.0417	0.126	0.0748	0.0	138	332
10.	90	40	0.00521	0.146	0.279	0.0748	0.0	138	662
11.	45	40	0.00521	0.1333	0.279	0.0748	0.0208	250	662

TABLE II

Values of R, k, α and ϕ

Pattern	R	k	α	ϕ
1.	0.1615	0.074	790°	10°
2.	0.1096	0.074	790°	10°
3.	0.0468	0.074	790°	10°
4.	0.0260	0.074	790°	10°
5.	0.0182	0.074	790°	10°
6.	0.146	0.074	790°	15°
7.	0.0676	0.074	790°	15°
8.	0.0416	0.074	790°	15°
9.	0.0156	0.074	790°	15°

The values of R, k, and α for the 45 degree and 30 degree cases are listed in Table XV. If it is desired to change to coordinates based on the position of the injector, it could be done in the following way

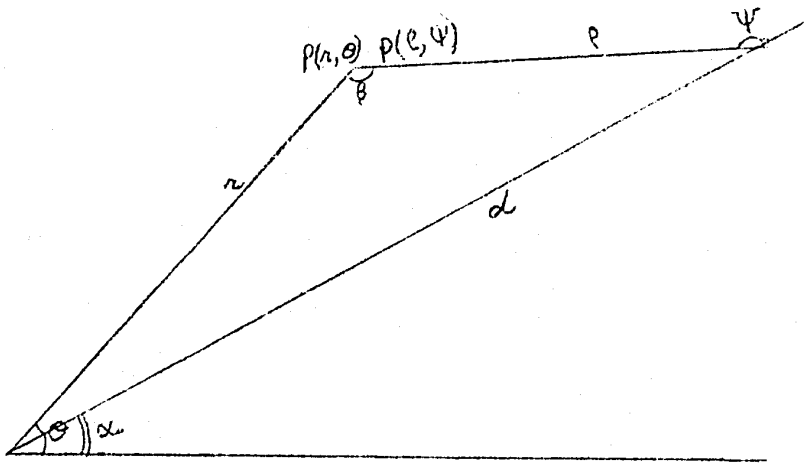

By glancing at the diagram (Fig. 19) it can be seen that

$$\frac{\rho}{d} = \frac{\sin(\theta - \alpha)}{\sin \beta} \qquad (39)$$

from the law of sines.

Also

$$\rho^2 = r^2 + d^2 - 2rd \cos(\theta - \alpha) \qquad (40)$$

and

$$\psi = (\theta - \alpha) + \beta \qquad (41)$$

By means of the relations:

$$\delta^2 = r^2 + R^2 - 2rR \cos (\alpha - \theta)$$

$$\frac{\delta}{R} = \frac{\sin (\alpha - \theta)}{\sin \beta}$$

and

$$\psi = 180 - \phi - \beta + \theta \qquad (42)$$

the point $P(\delta, \psi)$ on the spiral using the new coordinates can be found.

Most probably the theoretical analysis from potential flow theory will prove superior to this method if the mapping function is known, but this can always serve as a qualitative check to be sure that nothing has gone awry.

A penetration correlation was also deduced by the methods of Callaghan and Ruggeri, but this time an extra group was introduced to take care of different angles of incidence. The penetration was measured perpendicularly to the wall and always downstream from the injector. The actual measurement was made on a vector diagram such as figure 17, or in effect at the point where the velocity once more became equal to the main stream velocity. One could also use the spiral diagram and measure the distance to the farthest loop. The results of the penetrations are listed in Table XIV and may be correlated by the relationship

$$\left(\frac{\ell}{D_j}\right) = 5.40 \left(\frac{\rho_j}{\rho_o}\right)^{0.9438} \left(\frac{V_j}{V_o}\right)^{0.3323} \left(\frac{s}{D_j}\right)^{-0.003987} \left(\frac{\gamma}{\gamma_{90}}\right)^{0.2614} \quad (43)$$

found from dimensional analysis using the variables D_j, ρ_j, ρ_o, V_j, V_o, s, γ and γ_{90}. The angles are thought to be significant here. The graph of equation 43 is plotted on figure 20. The values of the exponents were evaluated by an IBM 650 computer. This correlation is valid inside the limits of V_o and V_j between 50 feet per second and 350 ft/sec., positive s and γ not greater than 90°.

Wohl (37) has given a correlation for the penetration dependent on R_m - the mass velocity ratio - sidestream:mainstream. This is felt to be unwise because in effect the situation is that of a jet issuing from a hole in a plate into a main stream. Thus the mass flow of the main stream is not a vital factor and its effect has nothing to do with the correlation. The vital factors are throught to be the velocity and density of the main stream and the velocity, density and angle of the jet.

Callaghan and Ruggeri (25, 26 and 29) and Chilton and Genereaux (24) have used smoke to trace the patterns in the flow. This is also thought to be doubtful since a particle of smoke has many times the mass of a gas molecule. If the flow turns, a heavy particle would be thrown outwards leaving the centre clear. Thus an investigator would see the smoke and not the configuration of

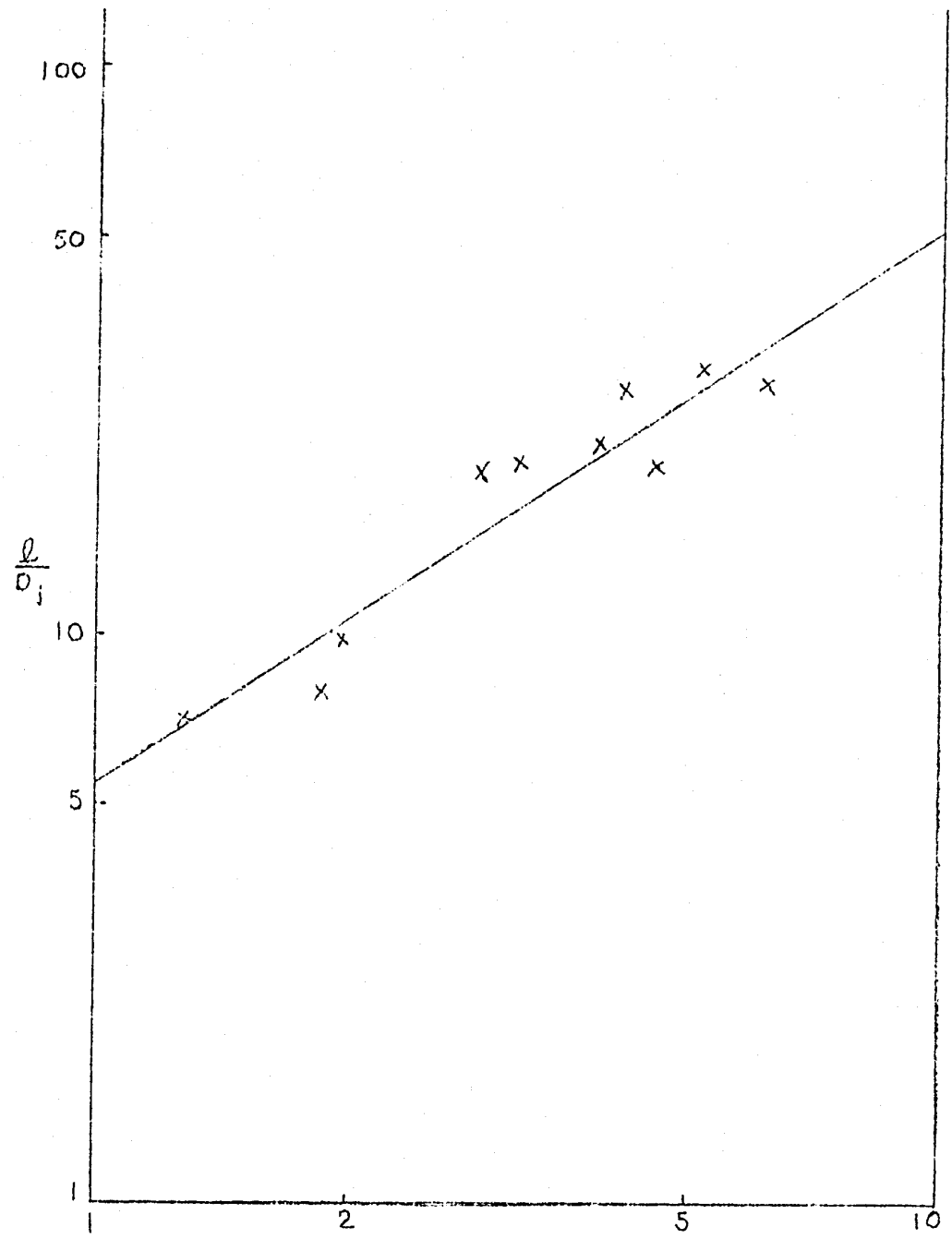

THE PENETRATION CORRELATION

FIG 20

The picture in the physical plane is

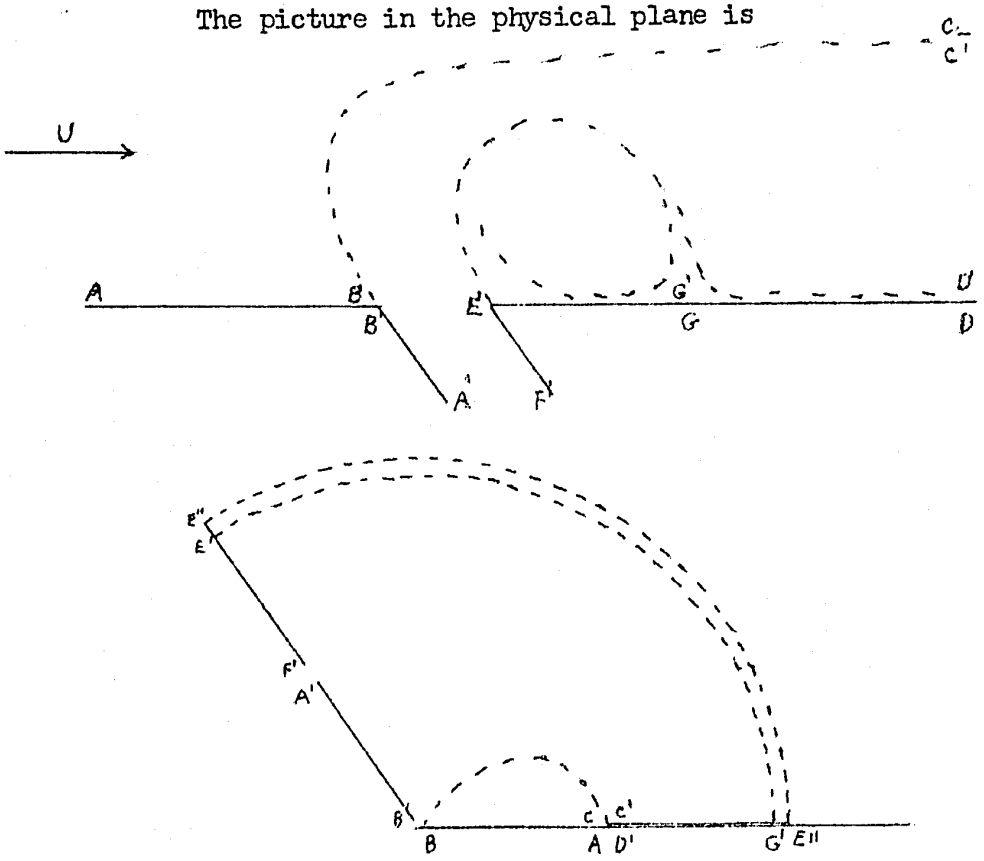

The hodograph of the flow is

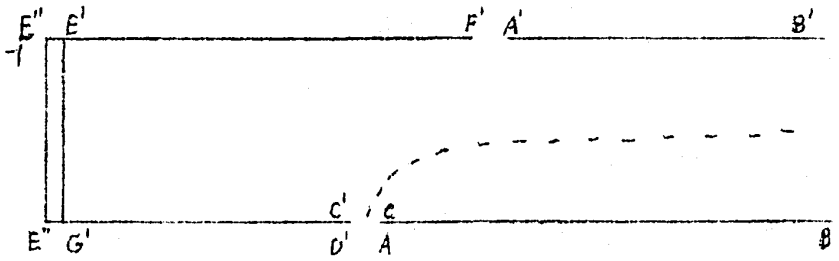

$$Q = \ln U/q + i\Theta$$

FIG 22

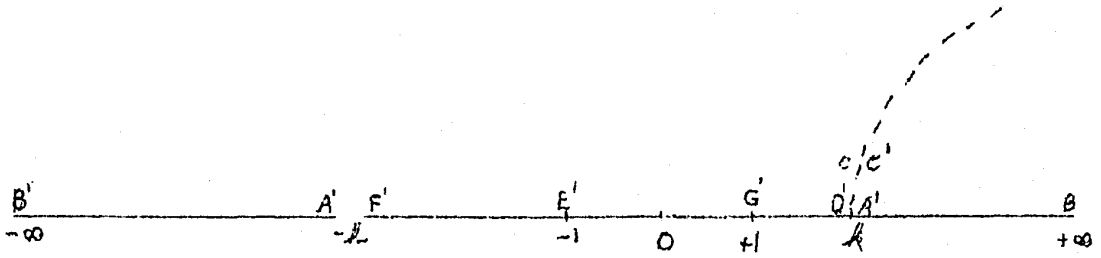

FIG. 23

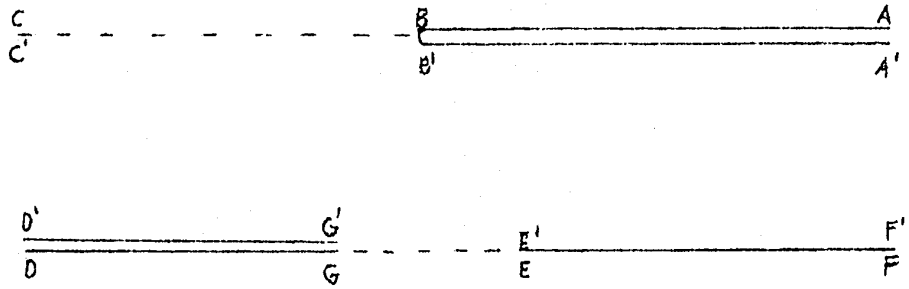

FIG 24

$$w = \Phi + i\Psi$$

of the flow.

Bertin and Salmon (23), Beauregard (32) and Chakko (33) have used rakes to measure the profiles, but this is doubtful also because a rake would interfere with reverse flow and the pattern deduced could be different from the one actually present.

The Extension of Theoretical Principles to the Present Case

The mathematical theory of ideal plane flows involves three complex quantities: the position $z = x + iy$, the complex potential $w = \phi + i\psi$, and the conjugate $\zeta = \xi + i\eta$ of the complex velocity $\zeta^* = \xi - i\eta$. Also, a vortex boundary sheet in the physical plane can be drawn in a hodograph plane if constant velocity can be assumed along it. The vortex sheets will become the arcs of circles and the straight boundaries transform into radial lines.

Ehrich's theoretical curve qualitatively predicts the shape of the upper vortex sheet but is badly astray in the prediction of the lower as determined by experiment for the case with separation. If there is no separation from the wall it does reasonably well. If it is postulated that the velocity of the jet is not constant, which is a fact, but that constant velocity is present only in the two vortex sheets bounding the jet, then it is possible to proceed.

Then the problem is to find the mapping functions. Since the arbitrary simply connected domain exists, Riemann's Theorem guarantees that a suitable mapping function exists. A formula for conformal mapping of a polygon region on the unit circle or alternatively in the upper half of a complex plane has been supplied by Schwarz and Christoffel. This formula is

$$w = A \int_{\zeta_0}^{\zeta} (\zeta' - x_1)^{-k_1} (\zeta' - x_2)^{-k_2} (\zeta' - x_3)^{-k_3} \ldots\ldots d\zeta' + B \qquad (44)$$

where πk is the exterior angle at each vertex.

$$\frac{dw}{d\zeta} = A(\zeta + h)^{-1} (\zeta - 1)^{-1} (\zeta - 1)^{-1} (\zeta + \infty)^{-k} (\zeta - \infty)^{-k} (\zeta - k)^{0} \qquad (45)$$

$$\frac{dw}{d\zeta} = \frac{A}{(\zeta + h)(\zeta - 1)^2}$$

$$w = \int \frac{A\, d\zeta}{(\zeta + h)(\zeta - 1)^2}$$

$$w = \frac{A}{(1+h)} \left[\frac{1}{(1-\zeta)} + \frac{1}{(1+h)} \ln \frac{(h+\zeta)}{(1-\zeta)} \right] + B \qquad (46)$$

Let $w = 0$ at $\zeta = -1$

$$B = \frac{A}{2(h+1)} + \frac{A}{(h+1)^2} \ln \frac{-2}{0} \tag{47}$$

At $w = -Uci$ the formula becomes

$$w = -Uci = \frac{-A}{(h+1)(\zeta - 1)} + \frac{A}{(h+1)^2} \ln \left| \frac{\zeta - 1}{\zeta + 1} \right| + \frac{A\,\pi i}{(h+1)^2} - \frac{A}{2(h+1)}$$

$$- \frac{A}{(h+1)^2} \ln \frac{-2}{0} \tag{48}$$

equating the imaginary parts

$$-Uci = \frac{A\,\pi i}{(h+1)^2}$$

$$A = \frac{-Uc(h+1)^2}{\pi}$$

when this is substituted for A the transformation in differential form is

$$\frac{dw}{d\zeta} = \frac{-Uc\,(h+1)^2}{\pi(\zeta + h)\,(\zeta - 1)^2} \tag{49}$$

To transform the logarithm of the conjugate hodograph plane into the mapping plane the Schwarz-Christoffel transformation gives

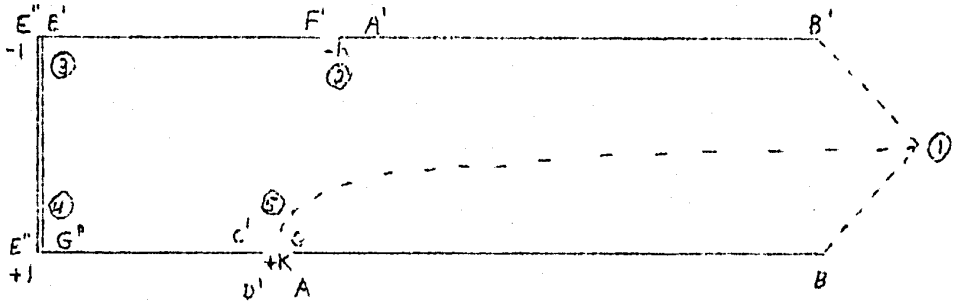

FIG 2.5

$$\pi k_1 = \pi$$
$$\pi k_2 = 0$$
$$\pi k_3 = \pi/2$$
$$\pi k_4 = \pi/2$$
$$\pi k_5 = 0$$

$$\therefore \quad k_1 = 1$$
$$k_2 = 0$$
$$k_3 = 1/2$$
$$k_4 = 1/2$$
$$k_5 = 0$$

$$\frac{dQ}{d} = A\,(\zeta - \infty)^{-1}\,(\zeta + k)^{0}\,(\zeta + 1)^{-1/2}\,(\zeta - 1)^{-1/2}\,(\zeta - k)^{0} \tag{50}$$

$$dQ = \frac{A\,d\zeta}{(\zeta+1)^{1/2}\,(\zeta-1)^{1/2}}$$

$$Q = \int \frac{A\,d\zeta}{(\zeta^2 - 1)^{1/2}}$$

$$Q = A \ln (\zeta + \sqrt{\zeta^2 - 1}) + B \tag{51}$$

at $\quad Q = 0, \quad \zeta = +1$

$$Q = A \ln (1 + \sqrt{1-1}) + B$$

$$Q = A \ln 1 + B$$

$$Q = A(0) + B$$

$$B = 0$$

and $$Q = A \ln (\zeta + \sqrt{\zeta^2 - 1}) \qquad (52)$$

at $$Q = \beta_i, \quad \zeta = -1$$

$$\beta_i = A \ln (-1 + \sqrt{1-1})$$

$$\beta_i = A \ln |-1| + A\pi i$$

equating the imaginary parts

$$\beta_i = A\pi i$$

$$A = \beta/\pi$$

and $$Q = \beta/\pi \ln (\zeta + \sqrt{\zeta^2 - 1}) \qquad (53)$$

since $$ds = |dz|$$

$$= \left| \frac{dz}{dw} \right| \left| \frac{dw}{d\zeta} \right| d\zeta \Big|$$

$$= \frac{1}{U} \left| \frac{dw}{d\zeta} \right| d\zeta$$

and $dx = ds \cos\theta$

$= [\text{real part of } e^{Q}]\, ds$

$dy = ds \sin\theta$

$= [\text{imaginary part of } e^{Q}]\, ds$

$$Q = \ln\left(\zeta + i\sqrt{1-\zeta^2}\right)^{\beta/\pi} \qquad (54)$$

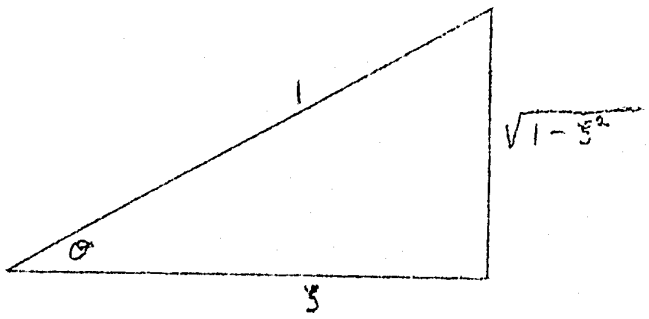

FIG 27

by a trigonometric substitution

$$\zeta/1 = \cos\theta$$

and $$(1-\zeta^2)^{\frac{1}{2}}/1 = \sin\theta$$

$$Q = \ln (\cos \theta + i \sin \theta)^{\beta/\pi}$$

$$Q = \ln e^{i \theta \beta/\pi}$$

$$Q = i \theta \beta/\pi \qquad (55)$$

for the real part of e^Q

first write $e^Q = e^{i \theta \beta/\pi}$

$$= \cos \beta/\pi \cdot \theta + i \sin \beta/\pi \cdot \theta$$

the real part is $\cos \left[\frac{\beta}{\pi} \cos^{-1} \zeta \right]$ (56)

thus $dx = \dfrac{\cos [\beta/\pi \cdot \cos^{-1} \zeta] \cdot 1 \, (-1)(1+h)^2 \, Uc \cdot d\zeta}{U \pi (\zeta + h)(\zeta - 1)^2}$ (57)

$$x/c = \frac{(h+1)^2}{\pi} \int_{-1}^{\zeta} \frac{\cos [\beta/\pi \cos^{-1} \zeta] \, d\zeta}{(\zeta + h)(\zeta - 1)^2} \qquad (58)$$

the imaginary part of e^Q is $\sin [\beta/\pi \cos^{-1} \zeta]$ (59)

hence $dy = \dfrac{\sin [\beta/\pi \cos^{-1} \zeta] \cdot (-1)(h+1)^2 \, Uc \cdot d\zeta}{U \pi (\zeta + h)(\zeta - 1)^2}$ (60)

$$y/c = \frac{(h+1)^2}{\pi} \int \frac{\sin [\beta/\pi \cos^{-1} \zeta] \, d\zeta}{(\zeta + h)(\zeta - 1)^2} \qquad (61)$$

The contraction ratio a/c may be found from

$$a/c = U/U_1 \qquad (h > 1) \tag{62}$$

and h is determined from

$$a/c = \left[h + \sqrt{(h^2-1)} \right]^{\beta/\pi} \tag{63}$$

The two parametric equations can be solved by graphical integration noting that $(h > 1)$ and $-1 < \zeta < +1$.

The shape of the curve will agree qualitatively with experimental results if the above equations are used, but to make them agree more closely the value of c must be redefined. If c is taken as the penetration from the dimensionless analysis formula at a small value of x, the agreement is better. This formula is

$$\left(\frac{\ell}{D_j}\right) = 5.813 \left(\frac{\rho}{\rho_o}\right)^{0.9438} \left(\frac{V_j}{V_o}\right)^{0.3323} \left(\frac{s}{D_j}\right)^{-0.003987} \left(\frac{\theta}{\theta_{90}}\right)^{0.2614}$$

It must be noted however that the original value of c is used right down to the end of the calculation and the new value is used only in the parametric equations.

The lower streamline of the pattern may be approximated by a flow defined by

$$\Gamma = \zeta^{-i\beta} \tag{64}$$

and

$$\zeta = w \qquad (\beta > 0)$$

The flow pattern is a spiral

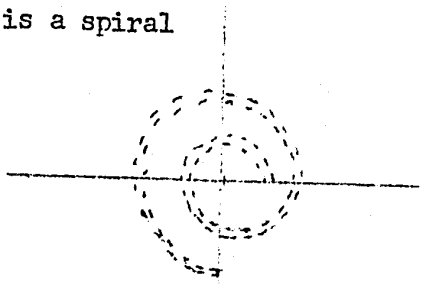

FIG 28

$z = x + iy$

The hodograph of the flow is

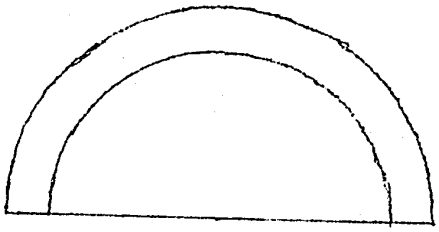

FIG 29

$\zeta = \xi + i\eta$

The potential plane is

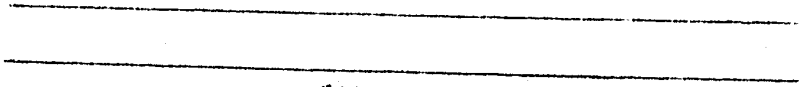

FIG 30

$w = \Phi + i\Psi$

This gives a flow between two equiangular spirals, the first being a free streamline of velocity 1, and the second one with a velocity $e^{\beta\pi}$. Conversely, it may be shown that this is the only way two free streamlines of different velocities can meet locally. (Zarantonello (39).

The mapping half plane is

Fig. 31

$$\Delta : \operatorname{Im}[\tilde{T}] \geq 0$$

$$\tilde{T} = -\frac{1}{2}(t + t^{-1}) \qquad (65)$$

The results for equation 65 were tabulated by Kaplan (44).

The shape of the potential theory curve is still not quite right as can be seen by glancing at figure 34. Since more work needs to be done on the theory before it can be used with complete confidence, the values of h have not been tabulated in Table I.

VII - CONCLUSIONS

1. A large vortex is present in the wake of the injector which is suitable for flame stabilization. This vortex is fed from the jet and therefore is being constantly replenished with combustible gas. Its velocity is much smaller than the mainstream velocity and so a flame could easily exist in it.

2. A penetration correlation taking into account the angle of incidence of the injector has been worked out. It gives good agreement with experiment from the injection point and downstream.

3. A complete two dimensional flow pattern has been presented for the case of a jet entering a main stream. The pattern indicates a steady widening of the jet, a curving motion, with the lower portion coming back almost to the wall and then turning upstream behind the jet and forming a vortex in the wake. The upper part of the jet widens out, slows down and reaches main stream velocity farther down the duct.

4. The shape of the upper bounding streamline can be predicted from two dimensional potential flow theory and the penetration correlation. The lower bounding streamline can also be predicted qualitatively using potential flow theory.

5. An elliptical shaped spiral with constants determined in this investigation is also presented to predict the flow pattern of a particle on one side of the jet. This spiral gives a good rough picture of the flow of fluid particles which form the vortex.

VIII - RECOMMENDATIONS

An attempt should be made to find an equation to describe the path of all the fluid particles in the jet entering the main stream. This might be approached from potential flow theory and the transformation planes. If a way around the difficulty of a polygon with too many vertices could be found then this would be a practical approach. On the other hand, the problem might be attacked empirically by simply finding a family of equations with the right shape and relating these to the velocities, densities and angles of the flow.

IX - ACKNOWLEDGEMENT

The author wishes to thank the many people who through their advice, guidance and technical help made this thesis possible.

Mr. L. A. Madonna for initiating the project and getting the work started.

For the direction of this research program, for providing invaluable advice and for his readiness to discuss technical problems, I wish to express great appreciation to Dr. Benjamin C.-Y. lu, with whom I have had the privilege to work.

Mr. A. Malek, a graduate student in the Department, freely gave his time and helpful advice.

Much is owed to Mr. Giacobbi for constructing the equipment and to Miss Boshko for programming the IBM 650 computer.

The Defence Research Board assumed the financial support, through grant # 9550-08, for this research.

X - APPENDIX

(1) Data

The point velocities are presented in Tables III to XI.

A few six-inch round duct values are presented in Table XIII and a traverse for the rod is given in Table XII.

The complete set of velocity profiles are too voluminous to be included here. They have been compiled into a second book which is available on request at the departmental office.

TABLE III

Experimental data for the 1/16 inch diameter, ninety degree injector (Vel. = 662 feet per second) in a flow travelling at 138 feet per second in a four inch square duct

Position		
Distance down from the top in inches	Distance from the injector in inches	Point velocity in feet per second
1/8	3/8 upstream	94
1/4	"	116
3/8	"	116
3/8	3/16 upstream	116
1/8	1/8 "	95
3/8	1/8 "	109
3/4	1/8 "	128
1/8	in line	- 31
1/4	in line	- 64
3/8	in line	-100
3/4	in line	66
7/8	in line	- 38
2	in line	136
1/8	1/8 downstream	66
1/4	"	0
7/8	1/4 "	31
1/2	3/8 "	69
1/2	1/2 "	- 69
1	1/2 "	- 96
1-1/4	1/2 "	153
1-1/2	1/2 "	136
2	1/2 "	137
1/2	1 "	96
1	1 "	88
1-1/4	1 "	110

TABLE IV

Experimental data for the 1/16 inch injector (Vel. = 662 feet per second) set at a 45° angle of incidence into a flow travelling at 138 feet per second in a four inch square duct

Position		
Distance down from the top in inches	Distance from the injector in inches	Point velocity in feet per second
1-1/4	1-1/2 upstream	139
1/8	1 "	95
3/8	1 "	115
3/4	1 "	127
1-1/4	1 "	142
1/4	1/2 "	-107
3/4	1/2 "	69
1-1/4	1/2 "	- 31
2	1/2 "	140
1/2	1/4 "	-101
3/4	1/4 "	-114
1/4	in line	116
7/8	in line	86
1-1/2	in line	- 49
1-1/2	in line	90
1-7/8	in line	131
1/2	1/2 downstream	- 96
1/8	1/2 "	68
1	1/2 "	- 73
1-1/2	1/2 "	76
2	1/2 "	139
1/8	1 "	69
1/2	1 "	- 69
7/8	1 "	22

....cont.

TABLE IV (continued)

Position		
Distance down from the top in inches	Distance from the injector in inches	Point velocity in feet per second
1-1/2	1 downstream	82
2	1 "	137
1/8	1-1/2 "	73
1/2	1-1/2 "	- 41
1-1/4	1-1/2 "	71
1-1/2	1-1/2 "	88
2	1-1/2 "	133
1-1/4	1-7/8 "	79
1/8	2 "	76
1/2	2 "	62
1	2 "	103
1-1/4	2 "	79
1-1/2	2 "	101
1-1/4	2-1/4 "	85
1	2-1/2 "	105
1-1/4	2-1/2 "	89
1-1/4	2-3/4 "	90
1-1/4	3 "	90
1	4 "	85
1	5 "	90
2	5 "	128

.... cont.

TABLE IV (continued)

Velocity = 468 feet per second

Position		
Distance down from the top in inches	Distance from the injector in inches	Point velocity in feet per second
3/8	1/2 upstream	-100
1/2	1/2 "	116
3/8	1/4 "	- 73
1/2	1/4 "	101
1/8	1/4 "	-100
3/8	1/4 "	88
1/8	in line	22
3/8	in line	82
1/8	1/4 upstream	0
3/8	1/4 "	105
1/8	in line	38
3/8	in line	110
0.15	1/2 downstream	69
0.35	1/2 "	- 38
0.55	1/2 "	- 76
0.75	1/2 "	58
0.95	1/2 "	- 62

Velocity = 711 feet per second

0.95	1/2 downstream	- 54

Velocity = 662 feet per second

1.1	1/2 downstream	62
1.25	1/2 "	31
1.5	1/2 "	62
1.7	1/2 "	106
1.9	1/2 "	126

..... cont.

TABLE IV (continued)

Velocity = 662 feet per second

Position		
Distance down from the top in inches	Distance from the injector in inches	Point velocity in feet per second
2	1/2 downstream	133
0.75	1-1/4 upstream	135
0.95	1-1/4 "	140
1.1	1-1/4 "	143
1.3	1-1/4 "	144
0.75	1 "	126
1.0	1 "	107
1.1	1 "	60
1.3	1 "	101
1.5	1 "	131
1.7	1 "	142
1.85	1 "	142
0.4	3/4 "	120
0.55	3/4 "	- 65
0.8	3/4 "	crossing injector
0.95	3/4 "	"
1.1	3/4 "	"
1.3	3/4 "	"
1.5	3/4 "	58
1.65	3/4 "	112
1.85	3/4 "	138
0.2	1/2 "	69
0.35	1/2 "	-131
0.55	1/2 "	-121
0.75	1/2 "	-121
0.95	1/2 "	-121
1.1	1/2 "	-121
1.3	1/2 "	- 76
1.5	1/2 "	71
1.65	1/2 "	105
1.9	1/2 "	131
2.0	1/2 "	140

.... cont.

TABLE IV (continued)

Position		
Distance down from the top in inches	Distance from the injector in inches	Point velocity in feet per second
0.2	1/4 upstream	- 76
0.35	1/4 "	62
0.55	1/4 "	- 64
0.75	1/4 "	- 72
0.9	1/4 "	29
1.1	1/4 "	- 76
1.3	1/4 "	- 76
1.5	1/4 "	42
1.7	1/4 "	101
1.9	1/4 "	127
2.0	1/4 "	137
0.2	in line	58
0.3	in line	83
0.5	in line	84
0.7	in line	- 55
0.9	in line	66
0.15	0.35 downstream	66
0.4	0.35 "	54
0.55	0.35 "	110
0.75	0.35 "	58
0.95	0.35 "	68
1.15	0.35 "	84
1.3	0.35 "	- 42
1.5	0.35 "	54
1.7	0.35 "	86
1.8	0.35 "	111
2.05	0.35 "	133
0.15	0.65 "	73
0.4	0.65 "	66
0.55	0.65 "	112
0.75	0.65 "	82
1.00	0.65 "	66
1.1	0.65 "	90
1.3	0.65 "	71
1.5	0.65 "	62

.... cont.

TABLE IV (continued)

Position		
Distance down from the top in inches	Distance from the injector in inches	Point velocity in feet per second
1.7	0.65 downstream	85
1.85	0.65 "	109
2.0	0.65 "	128
0.2	0.85 "	73
0.4	0.85 "	73
0.55	0.85 "	107
0.75	0.85 "	96
0.95	0.85 "	76
1.1	0.85 "	90
1.3	0.85 "	73
1.45	0.85 "	73
1.65	0.85 "	89
1.9	0.85 "	110
2.0	0.85 "	127
0.2	1.15 "	81
0.35	1.15 "	79
0.60	1.15 "	106
0.75	1.15 "	104
1.00	1.15 "	82
1.1	1.15 "	93
1.3	1.15 "	88
1.55	1.15 "	79
1.7	1.15 "	93
1.85	1.15 "	110
2.0	1.15 "	126

TABLE V

Experimental data for the 1/16 inch injector (Vel. = 662 feet per second) set at a 45° angle of incidence into a flow travelling at 250 feet per second in a four inch square duct

Position		
Distance down from the top in inches	Distance from the injector in inches	Point velocity in feet per second
0.4	3/4 upstream	209
0.6	3/4 "	236
0.75	3/4 "	246
0.95	3/4 "	248
1.1	3/4 "	245
1.3	3/4 "	247
1.5	3/4 "	250
0.2	1/2 "	134
0.35	1/2 "	- 38
0.55	1/2 "	- 38
0.75	1/2 "	- 38
0.95	1/2 "	149
1.1	1/2 "	216
1.3	1/2 "	243
1.5	1/2 "	248
1.65	1/2 "	250
0.15	1/4 "	- 66
0.35	1/4 "	- 66
0.55	1/4 "	- 66
0.75	1/4 "	- 66
0.9	1/4 "	90
1.1	1/4 "	209
1.3	1/4 "	234

..... cont.

TABLE V (continued)

Position		Point velocity in feet per second
Distance down from the top in inches	Distance from the injector in inches	
0.2	in line	71
0.35	in line	101
0.5	in line	0
0.75	in line	- 58
0.95	in line	44
1.1	in line	134
1.3	in line	229
1.5	in line	242
1.7	in line	247
0.15	1/4 downstream	110
0.4	1/4 "	137
0.6	1/4 "	97
0.75	1/4 "	90
0.95	1/4 "	101
1.15	1/4 "	181
1.35	1/4 "	222
1.7	1/4 "	248
0.15	1/2 "	96
0.4	1/2 "	150
0.6	1/2 "	132
0.95	1/2 "	114
1.15	1/2 "	173
1.35	1/2 "	212
0.15	3/4 "	101
0.35	3/4 "	159
0.55	3/4 "	146
0.75	3/4 "	129
0.95	3/4 "	133
1.15	3/4 "	168
1.3	3/4 "	219
1.5	3/4 "	242
0.35	1 "	164
0.55	1 "	156
0.75	1 "	150

TABLE VI

Experimental data for the 1/8 inch injector (Vel. = 406 feet per second) set at a 45° angle of incidence into a flow travelling at 138 feet per second in a four inch square duct

Position		
Distance down from the top in inches	Distance from the injector in inches	Point velocity in feet per second
2	2-1/4 upstream	155
1	1-1/2 "	144
1-1/2	1-1/2 "	135
2	1-1/2 "	132
2-1/2	1-1/2 "	152
3	1-1/2 "	150
3-1/2	1-1/2 "	142
0.35	1 "	124
1/2	1 "	118
1	1 "	-107
1-1/2	1 "	-107
2	1 "	- 31
2-1/2	1 "	49
3	1 "	149
3-1/2	1 "	144
0.15	1/2 "	- 76
1/2	1/2 "	- 76
1	1/2 "	- 76
1-1/2	1/2 "	-107
2	1/2 "	-107
2-1/2	1/2 "	38
3	1/2 "	130
3-1/2	1/2 "	147
1/2	in line	66
1.1	in line	62
1.5	in line	- 54
2	in line	-103
2-1/2	in line	- 54

..... cont.

TABLE VI (continued)

Position		Point velocity in feet per second
Distance down from the top in inches	Distance from the injector in inches	
3	in line	120
3-1/2	in line	145
1/2	1/2 downstream	-103
0.95	1/2 "	118
1-1/2	1/2 "	31
2	1/2 "	62
2-1/2	1/2 "	44
3	1/2 "	118
3-1/2	1/2 "	145
1/2	1 "	- 98
1	1 "	101
1-1/2	1 "	88
2	1 "	82
2-1/2	1 "	54
3	1 "	116
3-1/2	1 "	144
1/2	1-1/2 "	- 44
1	1-1/2 "	93
1-1/2	1-1/2 "	76
2	1-1/2 "	98
2-1/2	1-1/2 "	58
3	1-1/2 "	110
3-1/2	1-1/2 "	144
1/2	2 "	40
1	2 "	82
1.3	2 "	120
2	2 "	114
2-1/2	2 "	69
3	2 "	112
1/2	2-1/2 "	49
1	2-1/2 "	114
2	2-1/2 "	107
1/2	3 "	73
1/2	4 "	88
1	4 "	96
1/2	5 "	96
1	5 "	107

TABLE VII

Experimental data for the 1/16 inch injector (Vel. = 662 feet per second) set at a 30° angle of incidence into a flow travelling at 138 feet per second in a four inch square duct

Position		
Distance down from the top in inches	Distance from the injector in inches	Point velocity in feet per second
1/8	1-1/2 upstream	100
1/4	1-1/2 "	107
1/2	1-1/2 "	- 95
3/4	1-1/2 "	- 95
1-1/4	1-1/2 "	107
1/8	1 "	- 92
1/4	1 "	- 95
1/2	1 "	- 95
3/4	1 "	- 95
1-1/4	1 "	101
2	1 "	139
1/8	1/2 "	- 31
1/4	1/2 "	- 58
1/2	1/2 "	- 44
3/4	1/2 "	0
1/8	1/4 "	54
1/4	1/4 "	54
1/2	1/4 "	54
3/4	1/4 "	54
1/8	in line	62
1/4	in line	71
1/2	in line	69
3/4	in line	66
7/8	in line	71
1-1/8	in line	83
1-1/4	in line	102
1-1/2	in line	118
1-3/4	in line	128

.... cont.

TABLE VII (continued)

Position		Point velocity in feet per second
Distance down from the top in inches	Distance from the injector in inches	
2	in line	136
1/8	1/2 downstream	64
3/8	1/2 "	82
5/8	1/2 "	85
3/4	1/2 "	82
1	1/2 "	82
1-1/8	1/2 "	86
1-1/4	1/2 "	106
1-1/2	1/2 "	119
1-3/4	1/2 "	129
1/8	1 "	69
3/8	1 "	92
1/2	1 "	94
3/4	1 "	90
1	1 "	93
1-1/8	1 "	98
1-1/4	1 "	110
1-1/2	1 "	121
1-3/4	1 "	131
1-7/8	1 "	135
2	1 "	138
1/8	1-1/2 "	73
3/8	1-1/2 "	90
1/2	1-1/2 "	98
3/4	1-1/2 "	98
7/8	1-1/2 "	98
1-1/8	1-1/2 "	103
1-1/4	1-1/2 "	113
1-1/2	1-1/2 "	124
1-3/4	1-1/2 "	132
2	1-1/2 "	139
1/8	2 "	73
3/8	2 "	93
1/2	2 "	101
3/4	2 "	103
1	2 "	104

....cont.

TABLE VII (continued)

Position			Point velocity in feet per second
Distance down from the top in inches	Distance from the injector in inches		
1-1/8	2	downstream	109
1-1/4	2	"	114
1-1/2	2	"	120
1-3/4	2	"	127
1-7/8	2	"	131
2	2	"	136
1/8	3	"	78
1/2	3	"	105
7/8	3	"	112
1-3/8	3	"	120
1-3/4	3	"	128
1/8	4	"	85
1/2	4	"	107
7/8	4	"	115
1-1/4	4	"	120
1-3/4	4	"	128
1/8	5	"	92
1/2	5	"	110
7/8	5	"	116
1-3/8	5	"	123
2	5	"	127

TABLE VIII

Experimental data for the 1/16 inch injector (Vel. = 468 feet per second) set at a 30° angle of incidence into a flow travelling at 138 feet per second in a four inch square duct

Position		
Distance down from the top in inches	Distance from the injector in inches	Point velocity in feet per second
1/8	1-1/2 upstream	82
3/8	1-1/2 "	0
1/2	1-1/2 "	0
3/4	1-1/2 "	71
1-1/4	1-1/2 "	135
2	1-1/2 "	138
1/8	1 "	0
3/8	1 "	0
1/2	1 "	0
3/4	1 "	0
1-1/4	1 "	128
2	1 "	137
1/8	1/2 "	0
3/8	1/2 "	0
1/2	1/2 "	0
3/4	1/2 "	71
1-1/4	1/2 "	131
2	1/2 "	135
1/8	1/4 "	0
1/4	1/4 "	0
1/2	1/4 "	0
3/4	1/4 "	85
1/8	in line	0
3/8	in line	0
1/2	in line	71
3/4	in line	90
7/8	in line	106
1-1/8	in line	122

.....cont.

TABLE VIII (continued)

Position		Point velocity in feet per second
Distance down from the top in inches	Distance from the injector in inches	
1-1/4	in line	129
1/8	1/2 downstream	73
5/8	1/2 "	85
1	1/2 "	101
1-3/8	1/2 "	131
1-3/4	1/2 "	131
2	1/2 "	135
1/8	1 "	83
5/8	1 "	90
1	1 "	118
1-3/8	1 "	131
1-3/4	1 "	133
2	1 "	136
1/8	1-1/2 "	88
5/8	1-1/2 "	94
1	1-1/2 "	107
1-3/8	1-1/2 "	125
1-5/8	1-1/2 "	135
2	1-1/2 "	135
1/8	2 "	85
5/8	2 "	100
1	2 "	107
1-3/8	2 "	122
1-3/4	2 "	135
2	2 "	136
1/8	2-1/2 "	92
5/8	2-1/2 "	111
1	2-1/2 "	111
1-3/8	2-1/2 "	127
1-3/4	2-1/2 "	135
2	2-1/2 "	136
1/8	3 "	90
5/8	3 "	107
1	3 "	114
1-3/8	3 "	127

.... cont.

TABLE VIII (continued)

Position			Point velocity in feet per second
Distance down from the top in inches	Distance from the injector in inches		
1-3/4	3	downstream	134
1/8	4	"	91
5/8	4	"	117
1	4	"	118
1-3/8	4	"	126
1-5/8	4	"	131
2	4	"	120
1-3/8	5	"	125
1-3/4	5	"	130
2	5	"	134

TABLE IX

Experimental data for the 1/16 inch injector (Vel. = 332 feet per second) set at a 30° angle of incidence into a flow travelling at 138 feet per second in a four inch square duct

Position		
Distance down from the top in inches	Distance from the injector in inches	Point velocity in feet per second
1/8	1-1/2 upstream	93
3/8	1-1/2 "	112
1/2	1-1/2 "	120
3/4	1-1/2 "	125
1-1/4	1-1/2 "	132
1/8	1 "	84
3/8	1 "	111
1/2	1 "	118
3/4	1 "	123
1/8	1/2 "	0
3/8	1/2 "	0
1/2	1/2 "	76
3/4	1/2 "	110
1-1/4	1/2 "	129
1/8	1/4 "	0
3/8	1/4 "	0
1/2	1/4 "	79
3/4	1/4 "	107
1/8	in line	0
3/8	in line	71
1/2	in line	93
3/4	in line	113
7/8	in line	126
1-1/8	in line	130
1-3/8	in line	133
1-1/2	in line	134
1/8	1/8 downstream	69
1/8	1/4 "	92
1/2	1/4 "	66
7/8	1/4 "	122
1-1/4	1/4 "	131

.... cont.

TABLE IX (continued)

Position		Point velocity in feet per second
Distance down from the top in inches	Distance from the injector in inches	
1/8	1/2 downstream	79
5/8	1/2 "	123
7/8	1/2 "	119
1-1/4	1/2 "	132
1/8	3/4 "	99
3/8	3/4 "	93
5/8	3/4 "	79
7/8	3/4 "	127
1-1/4	3/4 "	130
1-1/2	3/4 "	132
1-5/8	3/4 "	133
1/8	1 "	85
3/8	1 "	82
5/8	1 "	88
3/4	1 "	96
1-1/4	1 "	133
1-3/8	1 "	130
1-1/2	1 "	133
1/8	1-1/8 "	93
5/8	1-1/8 "	88
1	1-1/8 "	127
1-1/4	1-1/8 "	131
1-1/2	1-1/8 "	132
1/8	1-1/4 "	86
3/8	1-1/4 "	85
1/2	1-1/4 "	88
3/4	1-1/4 "	103
1	1-1/4 "	120
1-1/4	1-1/4 "	131
1-3/8	1-1/4 "	132
1/8	1-1/2 "	98
3/8	1-1/2 "	85
5/8	1-1/2 "	92
3/4	1-1/2 "	101
1	1-1/2 "	117

.... cont.

TABLE IX (continued)

Position		
Distance down from the top in inches	Distance from the injector in inches	Point velocity in feet per second
1-1/4	1-1/2 downstream	132
1-3/8	1-1/2 "	132
1/8	1-3/4 "	90
1/2	1-3/4 "	102
3/4	1-3/4 "	110
1	1-3/4 "	118
1-1/4	1-3/4 "	126
1-3/8	1-3/4 "	132
1/8	1-7/8 "	83
1/2	1-7/8 "	103
7/8	1-7/8 "	115
1-1/8	1-7/8 "	125
1-3/8	1-7/8 "	129
1-5/8	1-7/8 "	133
1/8	2 "	82
3/8	2 "	96
5/8	2 "	107
3/4	2 "	112
1	2 "	120
1-1/8	2 "	127
1-3/8	2 "	132
1-1/2	2 "	133
1/8	2-1/4 "	85
5/8	2-1/4 "	105
1	2-1/4 "	122
1-3/8	2-1/4 "	132
1-3/4	2-1/4 "	133
1/8	2-1/2 "	82
5/8	2-1/2 "	105
1	2-1/2 "	120
1-3/8	2-1/2 "	132
1/8	2-3/4 "	85
5/8	2-3/4 "	110
1	2-3/4 "	121
1-3/8	2-3/4 "	132
1-3/4	2-3/4 "	133

.... cont.

TABLE IX (continued)

Position		Point velocity in feet per second
Distance down from the top in inches	Distance from the injector in inches	
1/8	3 downstream	90
5/8	3 "	112
1	3 "	122
1-3/8	3 "	132
1/8	4 "	82
5/8	4 "	116
1	4 "	125
1-3/8	4 "	131
1/8	5 "	96
5/8	5 "	117
1	5 "	126
1-3/8	5 "	130

TABLE X

Experimental data for the 1/8 inch injector (Vel. = 406 feet per second) set at a 30° angle of incidence into a flow travelling at 138 feet per second in a four inch square duct

Position		Point velocity in feet per second
Distance down from the top in inches	Distance from the injector in inches	
2	2-1/4 upstream	150
1-1/2	2 "	147
1	1-3/4 "	136
1-1/2	1-3/4 "	- 93
1/2	1-1/2 "	131
1	1-1/2 "	58
1-1/2	1-1/2 "	-124
2	1-1/2 "	- 98
2-1/2	1-1/2 "	118
1	1 "	-124
1-1/2	1 "	-124
2	1 "	- 73
2-1/2	1 "	101
1/2	1/2 "	- 98
1	1/2 "	- 98
1-1/2	1/2 "	-103
2	1/2 "	- 49
2-1/2	1/2 "	99
3	1/2 "	136
1/2	in line	76
0.95	in line	- 38
1-1/2	in line	- 31
2	in line	- 22
2-1/2	in line	93
1	3/4 downstream	79
1/2	1 "	103
1	1 "	66

..... cont.

TABLE X (continued)

Position		
Distance down from the top in inches	Distance from the injector in inches	Point velocity in feet per second
1-1/2	1 downstream	76
2	1 "	79
2-1/2	1 "	96
1/2	1-1/2 "	103
1	1-1/2 "	101
1-1/2	1-1/2 "	98
2	1-1/2 "	78
2-1/2	1-1/2 "	99
1/2	2 "	107
1	2 "	106
1/2	3 "	112
1/2	4 "	114
1	4 "	116

TABLE XI

Experimental data for the 1/16 inch diameter, ninety degree injector in a flow travelling at 138 feet per second in a four inch square duct

Position	injector velocity in feet per sec.	distance from the wall in inches	point velocity ft/sec
1/8 inch from the top, and 3/8 inches upstream	662	2.75	90.43
	662	2.50	90.43
	662	2.25	94.34
"	662	2.00	98.09
"	662	1.75	100.51
"	662	1.50	102.88
"	662	1.25	105.19
"	662	1.00	105.19
"	662	0.50	105.19
"	662	0.25	102.88
"	662	0.00	0.00
1/4 inch down from the top and 3/8 inches upstream	662	2.85	116.06
	662	2.60	116.06
	662	2.35	116.06
"	662	2.10	117.09
"	662	1.85	119.13
"	662	1.60	120.13
"	662	1.35	122.12
"	662	1.10	122.12
"	662	0.85	122.12
"	662	0.60	121.13
"	662	0.35	118.11
"	662	0.10	102.88
"	662	0.00	0.00

.....cont.

TABLE XI (continued)

3/8 inches down from	662	2.75	121
the top, and 3/16	662	2.50	120
inches upstream	662	2.15	116
"	662	1.95	127
"	662	1.75	126
"	662	0.75	126
"	662	0.50	124
"	662	0.25	118
"	662	0.00	0
1/8 inch down from the	662	2.75	94.34
top, and 1/8 inch	662	2.25	94.34
upstream	662	2.00	95.61
"	662	1.75	102.88
"	662	1.50	102.88
"	662	1.25	105.19
"	662	0.50	105.19
"	662	0.25	102.88
"	662	0.00	0.00
3/8 inches down from	662	2.75	113.97
the top, and 1/8 inch	662	2.50	112.91
upstream	662	2.25	111.84
"	662	2.15	109.67
"	662	2.00	111.84
"	662	1.90	118.11
"	662	1.50	118.11
"	662	1.25	120.13
"	662	0.75	120.13
"	662	0.50	119.13
"	662	0.25	115.02
"	662	0.00	0.00
3/4 inches down from	662	2.85	126.00
the top, and 1/8 inch	662	2.60	124.07
upstream	662	2.35	126.00
"	662	2.10	128.83
"	662	1.90	132.51
"	662	1.85	131.60
"	662	1.60	130.68
"	662	1.35	129.76

.....cont.

TABLE XI (continued)

3/4 inches down from the top, 1/8 inch upstream	662	1.10	129.76
"	662	0.85	128.83
"	662	0.60	126.00
"	662	0.35	120.13
"	662	0.10	105.10
"	662	0.00	0.00
1/8 inch down from the top, inline with the injector	662	2.75	96.85
	662	2.50	98.09
	662	2.25	100.51
"	662	2.05	102.88
"	662	2.00	- 31
"	662	1.75	96
"	662	1.50	102
"	662	1.25	103
"	662	1.00	105
"	662	0.75	105
"	662	0.50	104
"	662	0.25	100
"	662	0.00	0
1/4 inch down from the top, and inline with the injector	662	2.75	119
	662	2.50	119
	662	2.25	120
"	662	2.05	126
"	662	2.00	- 64
"	662	1.75	253
"	662	1.70	124
"	662	1.50	122
"	662	1.25	123
"	662	1.00	124
"	662	0.75	124
"	662	0.50	124
"	662	0.25	120
"	662	0.00	0
3/8 inches down from the top, and inline with the injector	662	2.75	122.12
	662	2.15	122.12
	662	2.00	-100.00
"	662	1.75	144

.....cont.

TABLE XI (continued)

3/8 inches down from	662	1.65	129.76
the top, and inline	662	1.50	126.95
with the injector	662	1.00	126.95
"	662	0.75	126.00
"	662	0.50	124.07
"	662	0.25	116.06
"	662	0.00	0.00
3/4 inches down from	662	2.90	126.00
the top, and inline	662	2.65	124.07
with the injector	662	2.40	118.11
"	662	2.15	65.80
"	662	1.90	134.31
"	662	1.65	132.51
"	662	1.40	131.60
"	662	1.15	130.68
"	662	0.90	127.89
"	662	0.65	126.00
"	662	0.40	[illegible]
"	662	0.15	[illegible]
"	662	0.00	62.04
7/8 inches down from	662	2.90	129.76
the top, and inline	662	2.65	129.76
with the injector	662	2.40	126.00
"	662	2.15	- 38
"	662	1.90	136.97
"	662	1.65	133.42
"	662	1.40	132.51
"	662	1.15	131.60
"	662	0.90	129.76
"	662	0.65	126.00
"	662	0.40	120.13
"	662	0.15	105.19
"	662	0.00	0.00
2 inches down from	662	2.75	136.09
the top, and inline	662	2.50	136.97
with the injector	662	1.50	136.97
"	662	1.25	136.97
"	662	1.00	133.42
"	662	0.75	131.60
"	662	0.50	127.89
"	662	0.25	120.13
"	662	0.00	0.00

.....cont.

TABLE XI (continued)

1/8 inch down from the top, and 1/8 inch downstream	662	2.55	100.51
	662	2.30	104.04
	662	2.05	87.73
"	662	2.00	65.80
"	662	1.80	79.08
"	662	1.55	98.09
"	662	1.30	102.88
"	662	1.05	105.19
"	662	0.55	105.19
"	662	0.30	102.88
"	662	0.05	90.43
"	662	0.00	0.00
1/4 inch down from the top, and 1/8 inch downstream	662	2.60	118.11
	662	2.35	122.12
	662	2.10	93.06
"	662	2.05	0.00
"	662	1.85	93.06
"	662	1.60	117.09
"	662	1.35	120.13
"	662	1.10	121.13
"	662	0.85	121.13
"	662	0.60	120.13
"	662	0.35	118.11
"	662	0.10	102.88
"	662	0.00	0.00
7/8 inches down from the top, and 1/4 inch downstream	662	2.75	127.89
	662	2.55	124.07
	662	2.50	126.00
"	662	2.35	151.96
"	662	2.25	65.80
"	662	2.15	31
"	662	2.00	126.00
"	662	1.90	135.21
"	662	1.50	133.42
"	662	1.25	132.51
"	662	1.00	130.68
"	662	0.75	127.89
"	662	0.50	122.12
"	662	0.25	109.67
"	662	0.00	0.00

.....cont.

TABLE XI (continued)

1/2 inch down from the	662	2.75	126.00
top, and 3/8 inches	662	2.50	127.89
downstream	662	2.25	69.36
"	662	2.05	124.07
"	662	1.95	120.13
"	662	1.80	126.00
"	662	1.50	126.00
"	662	1.25	126.00
"	662	1.00	126.00
"	662	0.75	126.00
"	662	0.50	123.10
"	662	0.25	116.06
"	662	0.00	0.00
1/2 inch down from the	662	2.55	128.83
top, and 1/2 inch	662	2.30	151.96
downstream	662	2.20	156.64
"	662	2.00	- 69
"	662	1.80	116.06
"	662	1.65	135.21
"	662	1.30	133.42
"	662	1.05	132.51
"	662	0.80	130.68
"	662	0.55	127.89
"	662	0.30	118.11
"	662	0.05	98.09
"	662	0.00	0.00
1 inch down from the	662	2.75	127.89
top, and 1/2 inch	662	2.55	143.83
downstream	662	2.30	135.21
"	662	2.15	- 96
"	662	1.90	103
"	662	1.65	139
"	662	1.40	137
"	662	1.15	135
"	662	1.00	137
"	662	0.75	133
"	662	0.50	130
"	662	0.25	116
"	662	0.00	0

.....cont.

TABLE XI (continued)

1-1/4 inches down from	662	2.75	126.00
the top, and 1/2 inch	662	2.60	122.12
downstream	662	2.50	129.76
"	662	2.25	153.53
"	662	2.00	138.72
"	662	1.75	136.09
"	662	1.50	135.21
"	662	1.25	133.42
"	662	1.00	130.68
"	662	0.75	126.95
"	662	0.50	122.12
"	662	0.25	109.67
"	662	0.00	0.00
1-1/2 inches down from	662	2.60	131.60
the top, and 1/2 inch	662	2.35	126.00
downstream	662	2.10	135.21
"	662	2.05	136.97
"	662	1.60	136.97
"	662	1.35	136.09
"	662	1.10	133.42
"	662	0.85	131.60
"	662	0.60	127.89
"	662	0.35	122.12
"	662	0.10	109.67
"	662	0.00	0.00
2 inches down from the	662	2.60	136.97
top, and 1/2 inch	662	1.35	136.97
downstream	662	1.10	136.09
"	662	0.85	133.42
"	662	0.60	131.60
"	662	0.35	126.00
"	662	0.10	111.84
"	662	0.00	62.04
1/2 inch down from the	662	2.75	126.00
top, and 1 inch downs-	662	2.50	127.89
tream	662	2.35	127.89
"	662	2.25	122.12
"	662	2.00	95.61
"	662	1.75	105.19

.....cont.

TABLE XI (continued)

1/2 inch down from the	662	1.50	124.07
top, and 1 inch	662	1.25	126.00
downstream	662	1.00	126.00
"	662	0.75	125.04
"	662	0.50	122.12
"	662	0.25	113.97
"	662	0.00	0.00
1 inch down from the	662	2.80	131.60
top, and 1 inch	662	2.55	138.72
downstream	662	2.30	113.97
"	662	2.05	87.73
"	662	1.80	124.07
"	662	1.60	133.42
"	662	1.55	133.42
"	662	1.30	131.60
"	662	1.05	129.75
"	662	0.80	127.89
"	662	0.55	122.71
"	662	0.30	116.00
"	662	0.05	84.95
"	662	0.00	0.00
1-1/4 inches down from	662	2.75	132.51
the top, and 1 inch	662	2.60	140.44
downstream	662	2.50	135.21
"	662	2.25	113.97
"	662	2.00	109.67
"	662	1.75	135.21
"	662	1.50	133.42
"	662	1.25	132.51
"	662	1.00	129.76
"	662	0.75	126.00
"	662	0.50	120.13
"	662	0.25	107.45
"	662	0.00	0.00

TABLE XII

Experimental data for the 1/4 inch rod placed in a flow travelling at 137 feet per second in a six inch round duct

position	radius in inches	point velocity
1/2 inch downstream	0.25	-105
"	0.40	-107
"	0.42	-137
"	0.50	-140
"	0.75	-132
"	1.00	-130
"	1.25	-130
"	1.50	-128
"	1.75	-128
"	2.00	-128
"	2.25	-126
"	2.55	-121
"	2.75	- 38
"	2.90	84
"	3.00	0
7/8 inches downstream	0.25	105
"	0.40	138
"	0.50	132
"	0.75	- 49
"	1.00	- 79
"	1.25	- 90
"	1.50	- 93
"	1.75	- 91
"	2.00	- 85
"	2.25	- 66
"	2.50	- 22
"	2.75	96
"	2.90	105
"	3.00	0

.....cont.

TABLE XII (continued)

position	radius in inches	point velocity
1-1/4 inches downstream	0.35	110
"	0.50	124
"	0.60	118
"	0.85	69
"	1.10	35
"	1.35	- 22
"	1.60	- 41
"	1.85	- 35
"	2.10	22
"	2.35	62
"	2.60	98
"	2.80	107
"	2.85	103
"	3.00	0
2 inches downstream	0.10	103
"	0.35	118
"	0.60	123
"	0.85	125
"	1.10	127
"	1.35	128
"	1.60	128
"	1.85	129
"	2.10	130
"	2.35	130
"	2.60	132
"	2.85	132
"	3.10	133
"	3.35	133
"	3.60	126
"	3.85	101
"	4.10	76
"	4.35	62
"	4.60	56
"	4.85	62
"	5.10	79
"	5.35	101
"	5.60	111
"	5.85	82
"	6.00	0

TABLE XIII

Experimental data for the 1/4 inch diameter, ninety degree injector in a flow travelling at 137 feet per second in a six inch round duct

position	injector velocity in ft. per sec.	radius in inches	point velocity
1/2 inch downstream	96	0.35	134
"	96	0.60	135
"	96	0.85	135
"	96	1.10	134
"	96	1.35	133
"	96	1.60	133
"	96	1.85	133
"	96	2.10	133
"	96	2.35	129
"	96	2.55	126
"	96	2.60	118
"	96	2.85	- 98
"	96	3.00	0
7/8 inches downstream	96	0.35	132
"	96	0.60	133
"	96	0.85	133
"	96	1.10	133
"	96	1.35	133
"	96	1.60	133
"	96	1.85	133
"	96	2.10	134
"	96	2.35	130
"	96	2.50	126
"	96	2.60	105
"	96	2.85	- 38
"	96	3.00	0

.....cont.

TABLE XIII (continued)

position	injector velocity in ft. per sec.	radius in inches	point velocity
1-1/4 inches downstream	96	0.35	133
"	96	0.60	133
"	96	0.85	133
"	96	1.10	133
"	96	1.35	133
"	96	1.60	133
"	96	1.85	133
"	96	2.10	133
"	96	2.35	130
"	96	2.60	107
"	96	2.80	76
"	96	2.90	79
"	96	3.00	0
1/2 inch downstream	191.5	0.30	135
"	191.5	0.65	135
"	191.5	0.90	135
"	191.5	1.15	135
"	191.5	1.40	135
"	191.5	1.65	134
"	191.5	1.80	133
"	191.5	2.05	130
"	191.5	2.30	144
"	191.5	2.55	- 90
"	191.5	2.80	-133
"	191.5	3.00	0
7/8 inches downstream	191.5	0.40	133
"	191.5	0.65	133
"	191.5	0.90	133
"	191.5	1.15	133
"	191.5	1.40	133
"	191.5	1.65	133
"	191.5	1.90	132
"	191.5	2.15	139
"	191.5	2.20	140
"	191.5	2.40	82
"	191.5	2.65	- 85
"	191.5	2.90	- 69
"	191.5	3.00	0

.....cont.

TABLE XIII (continued)

position	injector velocity in ft. per sec.	radius in inches	point velocity
1-1/4 inches downstream	191.5	0.35	135
"	191.5	0.60	135
"	191.5	0.85	135
"	191.5	1.10	135
"	191.5	1.35	134
"	191.5	1.60	134
"	191.5	1.85	133
"	191.5	2.00	133
"	191.5	2.10	136
"	191.5	2.15	137
"	191.5	2.35	112
"	191.5	2.60	0
"	191.5	2.65	- 22
"	191.5	2.85	49
"	191.5	2.95	58
"	191.5	3.00	0
1/2 inch downstream	271	0.30	135
"	271	0.55	136
"	271	0.80	136
"	271	1.05	136
"	271	1.30	136
"	271	1.65	135
"	271	1.95	132
"	271	2.15	157
"	271	2.30	58
"	271	2.55	-139
"	271	2.80	-114
"	271	2.90	-105
"	271	3.00	0
7/8 inches downstream	271	0.35	133
"	271	0.60	133
"	271	0.85	133
"	271	1.10	133
"	271	1.35	133
"	271	1.60	133
"	271	1.90	149
"	271	2.10	98

.....cont.

TABLE XIII (continued)

position	injector velocity in ft. per sec.	radius in inches	point velocity
7/8 inches downstream	271	2.35	- 88
"	271	2.45	- 98
"	271	2.60	- 88
"	271	2.80	0
"	271	3.00	0
1-1/4 inches downstream	271	0.35	134
"	271	0.60	134
"	271	0.85	134
"	271	1.10	134
"	271	1.35	133
"	271	1.60	137
"	271	1.80	144
"	271	1.85	142
"	271	2.10	66
"	271	2.35	- 58
"	271	2.60	0
"	271	2.85	73
"	271	3.00	0
1/2 inch downstream	383	0.30	136
"	383	0.55	137
"	383	0.80	137
"	383	1.05	136
"	383	1.30	133
"	383	1.55	149
"	383	1.75	170
"	383	1.80	160
"	383	2.05	-114
"	383	2.15	-209
"	383	2.30	-166
"	383	2.55	-122
"	383	2.80	-101
"	383	3.00	0

.....cont.

TABLE XIII (continued)

position	injector velocity in ft. per sec.	radius in inches	point velocity
7/8 inches downstream	383	0.30	134
"	383	0.55	134
"	383	0.80	133
"	383	0.90	132
"	383	1.05	150
"	383	1.30	154
"	383	1.40	157
"	383	1.55	126
"	383	1.80	- 82
"	383	2.05	-137
"	383	2.30	-114
"	383	2.55	- 22
"	383	2.80	22
"	383	3.00	0
1-1/4 inches downstream	383	0.35	133
"	383	0.60	133
"	383	0.85	133
"	383	1.10	145
"	383	1.25	152
"	383	1.35	144
"	383	1.60	49
"	383	1.85	- 85
"	383	1.95	- 90
"	383	2.10	- 82
"	383	2.35	22
"	383	2.60	76
"	383	2.70	79
"	383	2.85	62
"	383	3.00	0
1/2 inch downstream	468	0.35	139
"	468	0.60	135
"	468	0.85	133
"	468	1.10	150
"	468	1.30	167
"	468	1.35	164
"	468	1.60	- 69
"	468	1.85	-267
"	468	2.10	-144
"	468	2.35	-126

.....cont.

TABLE XIII (continued)

position	injector velocity in feet per sec.	radius in inches	point velocity
1/2 inch downstream	468	2.60	-103
"	468	2.85	- 66
"	468	3.00	0
7/8 inches downstream	468	0.35	137
"	468	0.60	140
"	468	0.85	161
"	468	1.00	166
"	468	1.10	144
"	468	1.35	- 73
"	468	1.60	-166
"	468	1.85	-130
"	468	2.10	- 90
"	468	2.35	38
"	468	2.60	69
"	468	2.85	38
"	468	3.00	0
1-1/4 inches downstream	468	0.30	150
"	468	0.55	158
"	468	0.80	126
"	468	1.05	- 49
"	468	1.35	-144
"	468	1.55	-120
"	468	1.80	- 98
"	468	2.05	44
"	468	2.30	85
"	468	2.55	90
"	468	2.80	73
"	468	3.00	0
1/2 inch downstream	541	0.30	122
"	541	0.55	130
"	541	0.80	147
"	541	0.95	152
"	541	1.05	137
"	541	1.30	-114
"	541	1.55	-290

.....cont.

TABLE XIII (continued)

position	injector velocity in feet per sec.	radius in inches	point velocity
1/2 inch downstream	541	1.80	-166
"	541	2.05	-140
"	541	2.30	-116
"	541	2.55	-116
"	541	2.80	- 85
"	541	3.00	0
7/8 inches downstream	541	0.15	124
"	541	0.40	150
"	541	0.55	155
"	541	0.65	145
"	541	0.90	44
"	541	1.15	-209
"	541	1.90	-166
"	541	2.15	-150
"	541	2.40	- 66
"	541	2.65	0
"	541	2.85	38
"	541	2.90	22
"	541	3.00	0
1-1/4 inches downstream	541	0.30	114
"	541	0.55	49
"	541	0.80	-114
"	541	0.85	-166
"	541	1.05	-163
"	541	1.30	-147
"	541	1.55	-114
"	541	1.80	- 44
"	541	2.05	58
"	541	2.30	76
"	541	2.55	82
"	541	2.80	69
"	541	3.00	0

.....cont.

TABLE XIII (continued)

position	injector velocity	diameter	point velocity
2 inches downstream	541	0.15	116
"	541	0.40	118
"	541	0.65	128
"	541	0.90	132
"	541	1.15	133
"	541	1.40	133
"	541	1.65	133
"	541	1.90	132
"	541	2.15	133
"	541	2.40	142
"	541	2.65	154
"	541	2.90	140
"	541	3.15	90
"	541	3.40	- 44
"	541	3.65	-105
"	541	3.80	-116
"	541	3.90	-114
"	541	4.15	- 85
"	541	4.40	31
"	541	4.65	90
"	541	4.90	88
"	541	5.15	90
"	541	5.40	92
"	541	5.60	94
"	541	5.65	93
"	541	5.90	49
"	541	6.00	0

position	injector velocity	radius	point velocity
7/8 inches downstream	585	0.35	114
"	585	0.60	- 38
"	585	0.85	-215
"	585	1.10	-166
"	585	1.35	-144
"	585	1.60	-114

.....cont.

TABLE XIII (continued)

position	injector velocity	radius	point velocity
7/8 inches downstream	585	1.85	- 93
"	585	2.10	- 38
"	585	2.35	49
"	585	2.60	73
"	585	2.85	38
"	585	3.00	0
1-1/4 inches downstream	585	0.35	- 96
"	585	0.60	-180
"	585	0.85	-166
"	585	1.10	-140
"	585	1.35	-114
"	585	1.60	- 76
"	585	1.85	31
"	585	2.10	69
"	585	2.35	82
"	585	2.60	88
"	585	2.85	66
"	585	3.00	0

(2) Sample Calculation

For the injector velocity:

The formula for a sharp edged orifice is

$$V_o = c\sqrt{\frac{2g\ \Delta H}{1-(\frac{D_o}{D_1})^4}} \qquad (66)$$

or $$V_o = c_1\sqrt{2g\ \Delta h} \text{ if Re} > 30,000$$

to finc c_1 take $$\frac{D_o}{D_1} = \frac{0.5}{0.824} = 0.61$$

thus $c_1 \equiv 0.67$ as can be seen by glancing at the graph on pages 63 in the Principles of Chemical Engineering by Walker, Lewis, McAdams and Gilliland.

the formula is $V_o = 0.67\sqrt{2g\ \Delta h}$

The density of air at 40 psig and room temperature is

$$\rho = \frac{PM}{RT} \qquad (67)$$

$$= \frac{(54.7)(144)(29)}{(1543)(530)}$$

$$= 0.279 \text{ lbs. per cubic foot}$$

if the reading on a water tube manometer is 0.2 inches

$$\text{then} \qquad V_o = 0.67\sqrt{\frac{2 \times 32.2 \times 0.2 \times 62.4}{12 \times 0.279}}$$

$$V_o = 10.38 \text{ feet per second}$$

The velocity at the jet is

$$V_j = \frac{A_o V_o}{A_j}$$

$$= \frac{\frac{\pi D_o^2}{4}}{\frac{\pi D_j^2}{4}} V_o$$

$$= \frac{D_o^2}{D_j^2} V_o$$

For a 1/16 inch jet

$$V_j = \frac{0.5^2 \times 10.38}{0.0625^2}$$

$$= 662 \text{ feet per second}$$

For the point velocity:

Taking a chart reading of 3.2 inches of water and a static pressure reading of -0.8 inches of water and an air temperature of about 42 degrees Centigrade. Since the static pressure

reading is small, atmospheric pressure will be assumed for calculation. Therefore the air density is $\frac{PM}{RT} = \frac{2118 \times 29}{1543 \times 567.6} = 0.07$ lbs. per cubic foot

Δh = reading of total pressure - static pressure

= 3.2 - (-0.8)

= 4.0 inches of water

$$V_x = \sqrt{2gh}$$

$$= \sqrt{\frac{2 \times 64.4 \times 4.0 \times 62.4}{12 \times 0.07}}$$

$$V_x = \sqrt{19,200}$$

V_x = 139 feet per second

For the shape of the upper bounding streamline:

1/8 inch injector, angle of incidence 45°, mainstream velocity 138 and injector velocity 406 feet per second.

$$a/c = U/U_1$$

$$= (h + \sqrt{h^2-1})^{2/\pi}$$

A forty-five degree angle of incidence into the flow is equivalent to an $\alpha = \frac{3\pi}{4}$ and

$$\frac{\alpha}{\pi} = 3/4$$

now $$U/U_1 = (h + \sqrt{h^2-1})^{\alpha/\pi}$$

$$\frac{138}{406} = (h + \sqrt{h^2-1})^{3/4}$$

$$(\frac{138}{406})^{3/4} = h + \sqrt{h^2-1}$$

let $$x = (\frac{138}{406})^{4/3}$$

$$\log x = \frac{4}{3}(\log 138 - \log 406)$$

$$\log x = \frac{4}{3}(2.1399 - 2.6085)$$

$$\log x = \frac{4}{3}(-0.5686)$$

$$\log x = -0.6248$$

$$\log x = 1.3752$$

$$x = 0.2372$$

now $0.2372 = h + \sqrt{h^2-1}$

and $0.2372 - h = \sqrt{h^2-1}$

squaring both sides gives

$$0.05628 - 0.4744\,h + h^2 = h^2-1$$

rearranging $-0.4744\,h = -1 - 0.05628$

$$-0.4744\,h = -1.05628$$

$$h = \frac{-1.05628}{-0.4744}$$

$$h = 2.226$$

The check using the negative value for h

$$(-2.226 + (-2.226)^2 - 1)$$

$$(-2.226 + 4.955076 - 1)$$

$$(-2.226 + 1.989)$$

0.237 compared to 0.2372 which is good enough.

To evaluate the integral $\int_{-1} \frac{\cos[(\alpha/\pi)\cos^{-1}\xi]\,d\xi}{(\xi+h)(\xi-1)^2}$ by graphical integration, one must first choose different values of ξ and then plot with ξ as the abscissa.

Taking $\zeta = -1$

$$\cos^{-1} -1 = 180°$$

$$\frac{3}{4} \cos^{-1} -1 = \frac{3}{4} \cdot 180 = 135°$$

$$\cos 135° = - \cos (180 - 135)$$

$$= - \cos 45°$$

$$= - 0.70711$$

Placing this value in the integral and using the positive value of h as required by the theory, we have

$$\frac{-0.70711}{(-1.0 + 2.226)(-1-1)^2} = - 0.1442$$

Similarly at ζ = - 0.9 the ordinate is - 0.0908

" " - 0.8 " - 0.0645

" " - 0.7 " - 0.0428

" " - 0.5 " 0.0000

" " - 0.3 " 0.0501

" " - 0.1 " 0.1213

Similarly at ζ = 0 the ordinate is 0.1715

" " 0.2 " 0.333

" " 0.4 " 0.682

" " 0.6 " 1.695

" " 0.8 " 7.30

" " 0.9 " 10.62

" " 0.98 " 769

" " 1.0 " ∞

The graph for the evaluation of this integral is plotted in figure 32. The areas are

From ζ = -1.0 to -0.9 = -0.012

" -1.0 " -0.8 = -0.026

" -1.0 " -0.7 = -0.031

" -1.0 " -0.6 = -0.033

" -1.0 " -0.5 = -0.034

" -1.0 " -0.4 = -0.033

" -1.0 " -0.3 = -0.0295

" -1.0 " -0.2 = -0.0225

" -1.0 " -0.1 = -0.0115

" -1.0 " 0.0 = +0.003

" -1.0 " 0.1 = 0.024

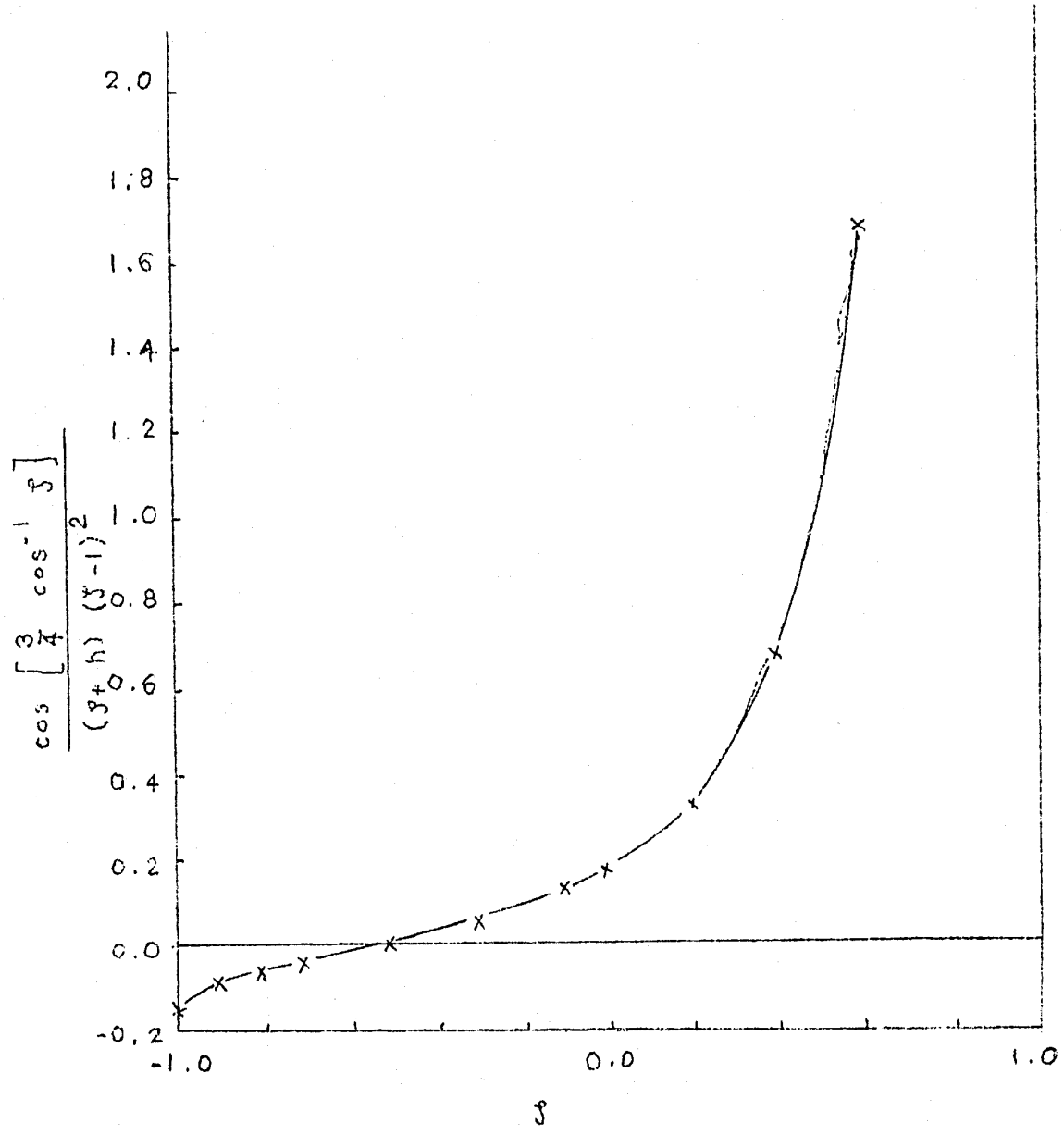

THE GRAPHICAL INTEGRATION OF THE INTEGRAL

$$\int_{-1}^{\vartheta} \frac{\cos\left[\frac{3}{4}\cdot\cos^{-1}\vartheta\right] d\vartheta}{(\vartheta+h)(\vartheta-1)^2}$$

FIG. 32

From ζ = -1.0 to 0.2 = 0.054

" -1.0 " 0.3 = 0.096

" -1.0 " 0.4 = 0.156

" -1.0 " 0.5 = 0.240

" -1.0 " 0.6 = 0.380

To evaluate the integral $\int_{-1}^{\zeta} \frac{\sin [\alpha/\pi \cos^{-1}\zeta]\, d\zeta}{(\zeta+h)(\zeta-1)^2}$ for the y component, a similar procedure is followed.

Taking ζ = -1

$$\cos^{-1} -1 = 180°$$

$$\frac{3}{4} \cdot \cos^{-1} -1 = \frac{3}{4} \cdot 180 = 135°$$

$$\sin 135 = \sin (180 - 135)$$
$$= \sin 45°$$
$$= 0.70711$$

placing this value in the integral without the derivative and using the positive value of h as required by the theory, we have

$$\frac{0.70711}{(-1.0 + 2.226)(-1-1)^2} = 0.1442$$

Similarly at	ζ =	-0.9	the ordinate is	0.1875
"	"	-0.8	"	0.2058
"	"	-0.7	"	0.222
"	"	-0.5	"	0.257
"	"	-0.3	"	0.302
"	"	-0.1	"	0.368
"	"	0.0	"	0.414
"	"	0.2	"	0.550
"	"	0.4	"	0.806
"	"	0.6	"	1.42
"	"	0.8	"	3.83
"	"	0.9	"	10.61
"	"	0.98	"	116.2
"	"	1.0	"	0.0

The graph for the evaluation of this integral is plotted in figure 33. The areas are

From	ζ =	-1.0	to	-0.9	the area is 0.017
	"			-0.8	" 0.037
	"			-0.7	" 0.059
	"			-0.6	" 0.082
	"			-0.5	" 0.106
	"			-0.4	" 0.132

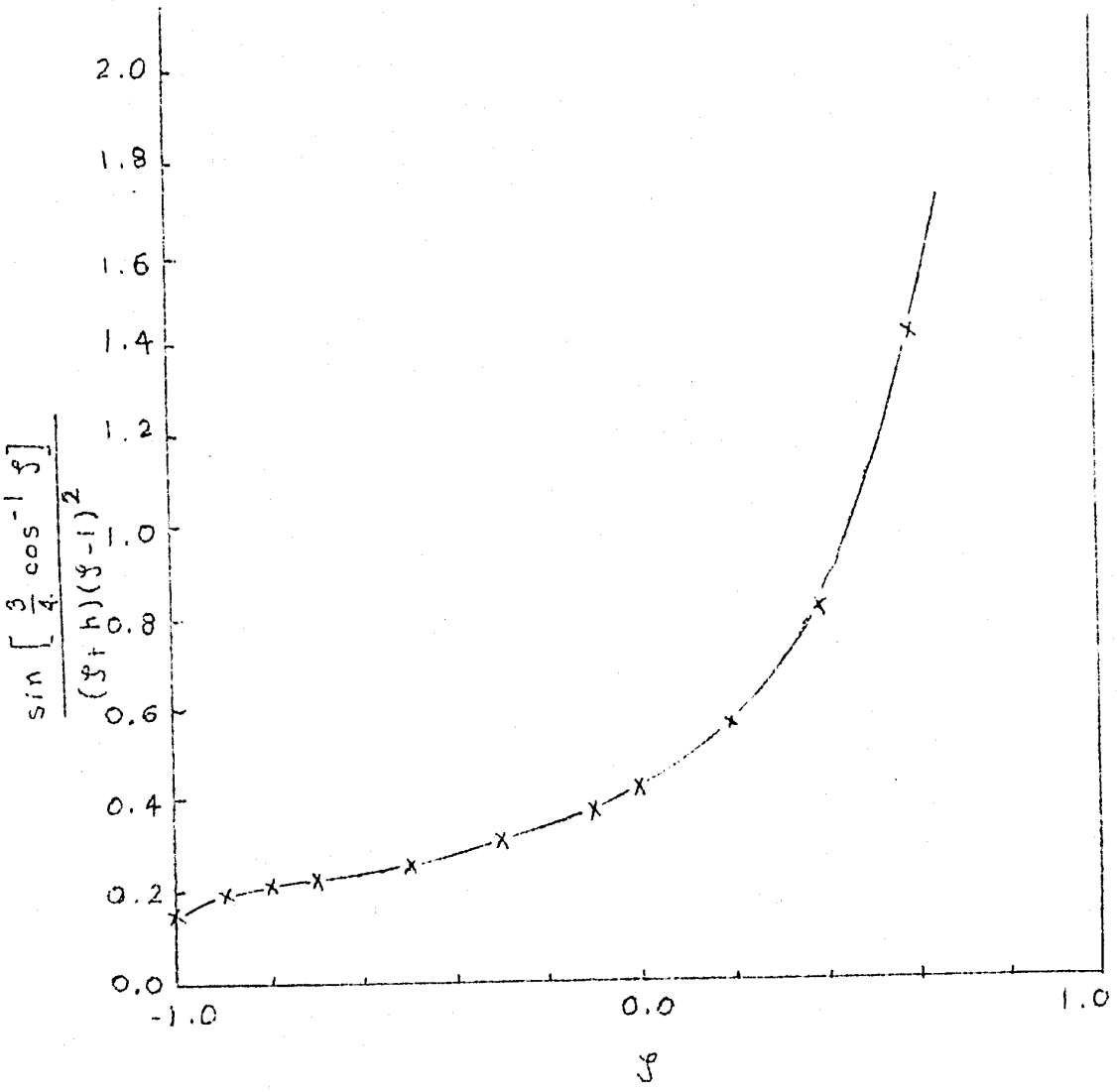

THE GRAPHICAL INTEGRATION OF THE INTEGRAL

$$\int_{-1}^{\vartheta} \frac{\sin\left[\frac{3}{4}\cdot\cos^{-1}\vartheta\right]\,d\vartheta}{(\vartheta+h)\,(\vartheta-1)^2}$$

FIG. 33

From	ξ = -1.0	to	-0.3	the area is 0.161
	"		-0.2	" 0.193
	"		-0.1	" 0.228
	"		0.0	" 0.267
	"		0.1	" 0.312
	"		0.2	" 0.363
	"		0.3	" 0.424
	"		0.4	" 0.498
	"		0.5	" 0.593
	"		0.6	" 0.720

$$x/c = \frac{(h+1)^2 \cdot \text{area}}{\pi} \qquad \text{(h must be positive)}$$

$$y/c = \frac{(h+1)^2 \cdot \text{area}}{\pi}$$

The value of c is found from the penetration correlation at a small value of s.

$$\left(\frac{\ell}{D_j}\right) = 5.40 \left(\frac{\rho_j}{\rho_o}\right)^{0.9438} \left(\frac{V_j}{V_o}\right)^{0.3323} \left(\frac{s}{D_j}\right)^{-0.003987} \left(\frac{\rho}{\rho_{90}}\right)^{0.2614}$$

$$\frac{l}{0.125} = 5.40 \left(\frac{0.279}{0.0706}\right)^{0.9438} \left(\frac{406}{138}\right)^{0.3323} \left(\frac{0.1}{0.125}\right)^{-0.003987} \left(\frac{45}{90}\right)^{0.2614}$$

$$\frac{\ell}{0.125} = 5.40 \cdot 3.95^{0.9438} \cdot 2.94^{0.3323} \cdot 0.8^{-0.003987} \cdot 0.5^{0.2614}$$

$$\frac{\ell}{0.125} = 5.40 \cdot 3.65 \cdot 1.431 \cdot 1.001 \cdot 0.833$$

$$\ell = 2.95 \text{ inches}$$

and $c = 2.95$ inches

$$x = c \frac{(h+1)^2}{\pi} \cdot \int_{-1}^{\zeta} \frac{\cos \left[\alpha/\pi \cos^{-1} \zeta \right] d\zeta}{(\zeta + h)(\zeta - 1)^2}$$

$$y = c \frac{(h+1)^2}{\pi} \cdot \int_{-1}^{\zeta} \frac{\sin \left[\alpha/\pi \cos^{-1} \zeta \right] d\zeta}{(\zeta + h)(\zeta - 1)^2}$$

At $\zeta = -1.0$ $\quad x = 2.95 \frac{(2.226 + 1)^2}{\pi} \cdot 0 = 0$

and $\quad y = 2.95 \frac{(2.226 + 1)^2}{\pi} \cdot 0 = 0$

At ζ	=	-0.9	x = 9.670 .	-0.012	=	-0.116,	y = 9.670 .	0.017 = 0.164
"		-0.8	"	-0.026	=	-0.251,	"	0.037 = 0.358
"		-0.7	"	-0.031	=	-0.300,	"	0.059 = 0.571
"		-0.6	"	-0.033	=	-0.319,	"	0.082 = 0.794
"		-0.5	"	-0.034	=	-0.329,	"	0.106 = 1.025
"		-0.4	"	-0.033	=	-0.319,	"	0.132 = 1.277

At ζ = -0.3 x = 9.670 . -0.0295 = -0.286, y = 9.670 . 0.161 = 1.558

" -0.2 " -0.0225 = -0.217, " 0.193 = 1.868

" -0.1 " -0.0115 = -0.1112, " 0.228 = 2.205

" 0.0 " +0.003 = +0.029 , " 0.267 = 2.68

" 0.1 " 0.024 = 0.232 , " 0.312 = 3.02

" 0.2 " 0.054 = 0.522 , " 0.363 = 3.51

" 0.3 " 0.096 = 0.929 , " 0.424 = 4.10

" 0.4 " 0.146 = 1.51 , " 0.498 = 4.82

" 0.5 " 0.240 = 2.32 , " 0.593 = 5.73

" 0.6 " 0.380 = 3.68 , " 0.720 = 6.96

These results are plotted in figure 34.

To find the best line for the centre distance correlation for the 45° case, the method of least squares was used. The IBM 650 gave the equation as

$$\frac{R}{D_j} = 2.430 \left(\frac{\rho_j}{\rho_j}\right)^{1.1723} \left(\frac{V_j}{V_o}\right)^{0.3647} \left(\frac{\rho}{\rho_{90}}\right)^{0.4737}$$

letting $y = \frac{R}{D_j}$ and $x = \left(\frac{\rho_j}{\rho_o}\right)^{1.1723} \left(\frac{V_j}{V_o}\right)^{0.3647} \left(\frac{\rho}{\rho_{90}}\right)^{0.4737}$

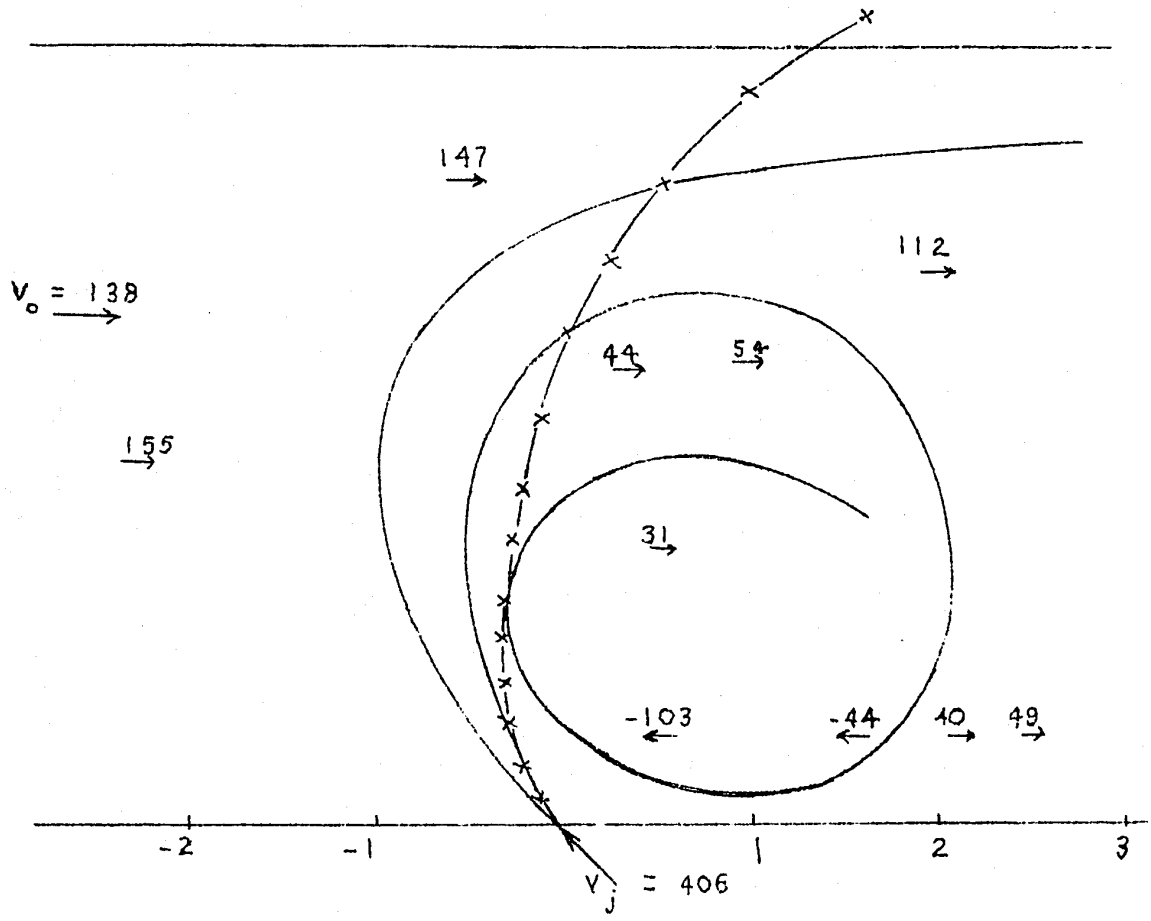

A POTENTIAL THEORY CURVE PLOTTED ON A POINT VELOCITY DIAGRAM. THE TWO BOUNDING STREAMLINES ARE ALSO SHOWN.

FIG. 34

trial	y	x	Y = Log y	X = Log x	XY	X^2
1.	15.5	5.48	1.1903	0.7288	0.8794	0.5458
2.	16.0	6.57	1.2041	0.8176	0.9845	0.6685
3.	9.0	3.403	0.9542	0.5319	0.5075	0.2829
4.	5.0	1.995	0.6990	0.3000	0.2097	0.0900
5.	3.5	1.227	0.5441	0.0888	0.0483	0.0079
6.	14.05	4.52	1.1476	0.6551	0.7518	0.4291
7.	13.00	5.42	1.1139	0.7340	0.8176	0.5388
8.	8.0	2.803	0.9031	0.4477	0.4043	0.2004
9.	3.0	1.642	0.4771	0.2153	0.1027	0.0464
10.	19.2	9.13	1.2833	0.9605	1.2326	0.9226
11.	8.79	5.26	0.9440	0.7210	0.6806	0.5198
			10.4607	6.2107	6.6190	4.2522

$$\Sigma Y = bn + m\Sigma X \quad (1)$$

$$\Sigma YX = b\Sigma X + m\Sigma X^2 \quad (2)$$

$$10.4607 = 11b + 6.2107m \quad (1)$$

$$6.6190 = 6.2107b + 4.2522m \quad (2)$$

solving 1 . (1) $10.4607 = 11b + 6.2107m$

1.7711 . (2) $11.7229 = 11b + 7.5311m$

subtracting $-1.2622 = 0 - 1.3204m$

$$m = 0.9559$$

$$\text{and } b = \frac{10.4607 - 6.2107 \cdot 0.9559}{11} = 0.4112$$

but $b = \log a$

$a = \text{antilog } 0.4112 = 2.577$

(3) The derivation of equations

The derivation of the equations in Table 1.

1. The orifice with separation of the jet from the lower wall.

Applying the schwarz-Christoffel transformation to the generate polygon in figure 35 according to the method given in Chapter 10 in Churchill (45), gives the exterior angles of the polygon as

$$\pi k_1 = \pi \qquad k_1 = 1$$
$$\pi k_2 = \pi/2 \qquad k_2 = +1/2$$
$$\pi k_3 = \pi/2 \qquad k_3 = +1/2$$
$$\pi k_4 = 0 \qquad k_4 = 0$$

(see figure 83 on page 219 in Churchill (45).

Then according to formula (7), page 221 in Churchill (45),

$$Q = A \int (\zeta+h)^{-1}(\zeta-1)^{-1/2}(\zeta-1)^{-1/2}(\zeta-\infty)^{0}\, d\zeta + B$$

$$" = A \int \frac{d\zeta}{(\zeta+h)\sqrt{\zeta^2-1}} + B$$

let $\zeta = \cosh \theta$ (using hyperbolic substitution)

$$\sqrt{\zeta^2-1} = \sinh \theta$$

$$d\zeta = \sinh \theta \, d\theta$$

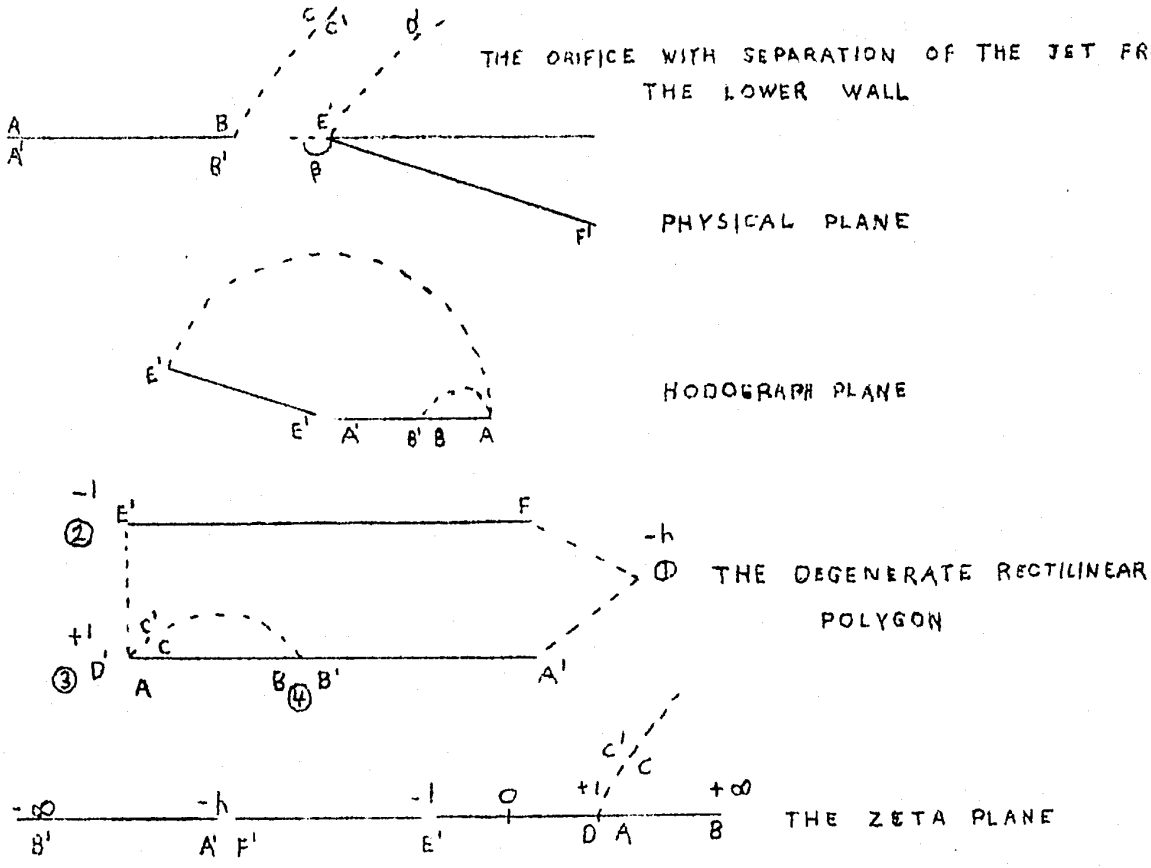
THE ORIFICE WITH SEPARATION OF THE JET FROM THE LOWER WALL
PHYSICAL PLANE
HODOGRAPH PLANE
THE DEGENERATE RECTILINEAR POLYGON
THE ZETA PLANE

FIG 35

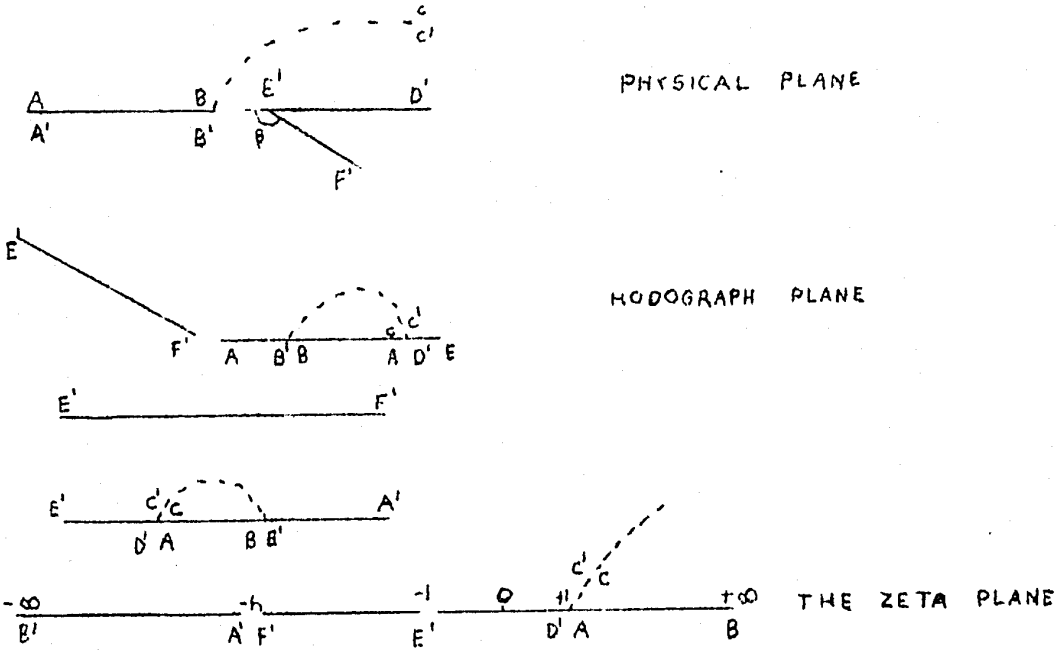
THE ORIFICE WITH NO SEPARATION OF THE JET FROM THE WALL
PHYSICAL PLANE
HODOGRAPH PLANE
THE ZETA PLANE

FIG 36

$$Q = A \int \frac{\sinh \theta \, d\theta}{(\cosh \theta + h) \sinh \theta}$$

$$Q = A \int \frac{d\theta}{(\cosh \theta + h)} + B$$

now $\cosh \theta = \cos i\theta$

$$Q = \frac{A}{i} \int \frac{d(i\theta)}{h + \cos(i\theta)} + B$$

and $$\int \frac{du}{a + b \cos u} = \frac{1}{\sqrt{b^2-a^2}} \ln \frac{b + a \cos u + \sqrt{b^2-a^2} \sin u}{a + b \cos u} + c$$

if $b^2 > a^2$

$$\therefore Q = \frac{A}{i}\left[\frac{1}{\sqrt{1-h^2}} \ln \frac{1 + h \cos i\theta + \sqrt{1-h^2}\,(+1 \sin i\theta)}{h + \cos i\theta} + c \right]$$

$$Q = A\left[\frac{1}{\sqrt{h^2-1}} \ln \frac{1 + h \cosh \theta + \sqrt{1-h^2}\,(-1/i \sinh \theta)}{h + \cosh} + c \right]$$

$$Q = A\left[\frac{1}{\sqrt{h^2-1}} \ln \frac{1 + h \cosh \theta - \sqrt{h^2-1} \sinh \theta}{h + \cosh \theta} + c \right]$$

$$Q = A\left[\frac{1}{\sqrt{h^2-1}} \ln \frac{(1 + h\zeta) - \sqrt{(h^2-1)}\sqrt{\zeta^2-1}}{(h + \zeta)} \right] + B$$

at $Q = 0$; $\zeta = 1$

$$Q = A\left[\frac{1}{\sqrt{h^2-1}} \ln \frac{(1+h) - \sqrt{(h^2-1)(1-1)}}{(h+1)}\right] + B$$

$$Q = A\left[\frac{1}{\sqrt{h^2-1}} \ln \frac{(h+1)}{(h+1)}\right] + B$$

$$Q = A\left[\frac{1}{\sqrt{h^2-1}} \ln 1\right] + B$$

$\therefore B = 0$

now at $Q = \beta i$; $\zeta = -1$

$$\beta i = A\left[\frac{1}{\sqrt{h^2-1}} \ln \frac{(1-h) - \sqrt{(h^2-1)(1-1)}}{(h-1)}\right]$$

$$\beta i = A\left[\frac{1}{\sqrt{h^2-1}} \ln -1\right]$$

the logarithm of a negative real number can be written

$$\ln x = \ln |x| + \pi i \quad \text{(page 228 in Churchill (45).}$$

$$\beta i = A \frac{1}{\sqrt{h^2-1}} \ln |-1| + \frac{A \pi i}{\sqrt{h^2-1}}$$

equating the imaginary parts gives

$$\beta i = \frac{A \pi i}{\sqrt{h^2-1}}$$

$$A = \frac{\beta \sqrt{h^2-1}}{\pi}$$

substituting A in the Q equation

$$Q = \frac{\beta\sqrt{h^2-1}}{\pi}\left[\frac{1}{\sqrt{h^2-1}}\ln\frac{(h^2\zeta+1)-\sqrt{(h^2-1)(\zeta^2-1)}}{(h+\zeta)}\right]$$

$$Q = Q(\zeta) = \frac{\beta}{\pi}\ln\frac{(h\zeta+1)-\sqrt{(h^2-1)(\zeta^2-1)}}{(h+\zeta)}$$

2. The orifice with no separation of the jet from the wall.

See figures 36 and 37

$$\pi k_1 = \pi \qquad k_1 = +1; \quad x_1 = -h$$
$$\pi k_2 = \pi \qquad k_2 = 1; \quad x_2 = 1$$
$$\pi k_3 = 0 \qquad k_3 = 0; \quad x_3 = 1$$
$$\pi k_4 = 0 \qquad k_4 = 0; \quad x_4 =$$

The Schwarz-Christoffel transformation gives

$$Q = A\int(\zeta+h)^{-1}(\zeta+1)^{-1}(\zeta-1)^{0}(\zeta-\infty)^{0}\,d\zeta + B$$

$$Q = A\int\frac{d\zeta}{(\zeta+h)(\zeta+1)} + B$$

now $$\int\frac{dx}{(a+bx)(a'+b'x)} = \frac{1}{ab'-a'b}\ln\frac{a'+b'x}{a+bx} + c$$

$$Q = A\left[\frac{1}{h-1}\ln\frac{(\zeta+1)}{(\zeta+h)}\right] + B$$

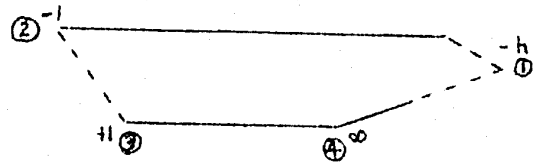

FIG. 37

THE SLOT WITH SEPARATION FROM THE WALL

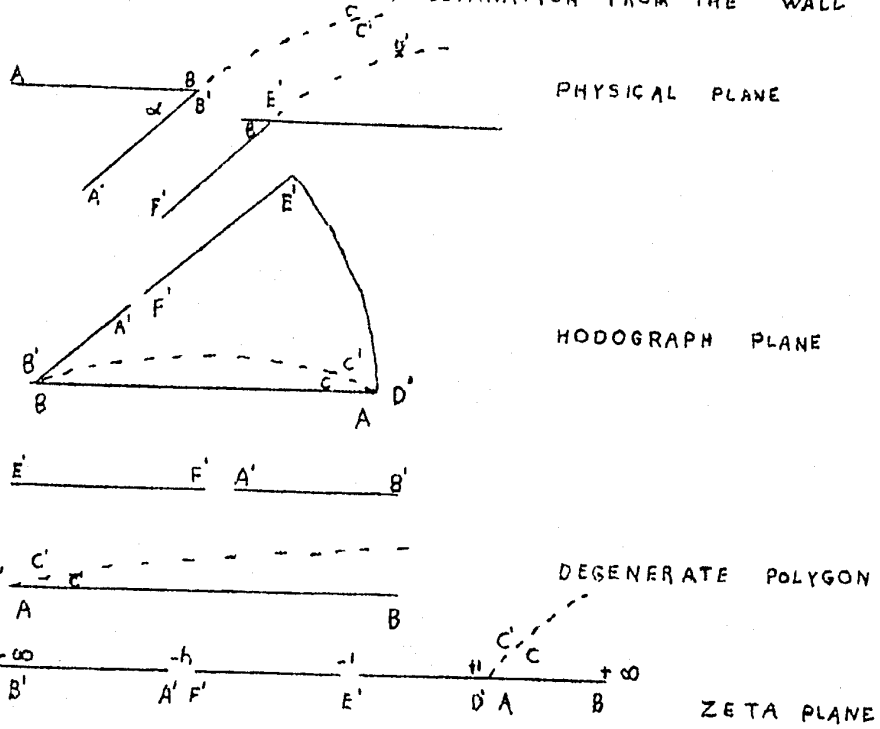

FIG 38

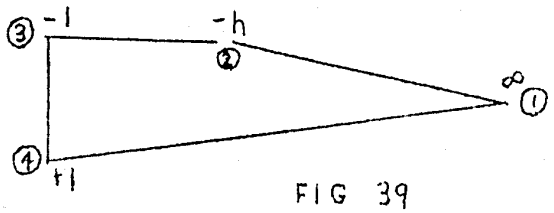

FIG 39

at $Q = 0$, $\zeta = 1$

$$Q = A\left[\frac{1}{h-1} \ln \frac{(1+1)}{(1+h)}\right] + B$$

$$B = \frac{-A}{h-1} \ln \left(\frac{2}{h+1}\right)$$

$$Q = \frac{A}{h-1} \ln \frac{(\zeta+1)(h+1)}{2(\zeta+h)}$$

at $Q = \beta i$, $\zeta = -1$

$$\beta i = \frac{A}{h-1} \ln \frac{(-1+1)(h+1)}{2(-1+h)} = \frac{A}{h-1} \ln \left| \right| + \frac{A \pi i}{h-1}$$

equating the imaginary parts

$$\beta i = \frac{A \pi i}{h-1}$$

$$A = (h-1)\,\beta/\pi$$

and " $= \beta/\pi \ln \dfrac{(\zeta+1)(h+1)}{2(\zeta+h)}$

3. The orifice with separation of the jet from the wall and $\beta = \pi$.

Taking the equation from (1)

$$Q = \beta/\pi \ln \left[\frac{(h\zeta+1) - \sqrt{(h^2-1)(\zeta^2-1)}}{(\zeta+h)}\right]$$

and setting $\beta = \pi$ we have

$$Q = \ln \frac{(h\zeta+1) - \sqrt{(h^2-1)(\zeta^2-1)}}{(\zeta+h)}$$

4. The slot with separation from the wall.

See figures 38 and 39

$$\pi k_1 = \pi \qquad k_1 = 1, \quad x_1 = \infty$$
$$\pi k_2 = 0 \qquad k_2 = 0, \quad x_2 = -h$$
$$\pi k_3 = \pi/2 \qquad k_3 = 1/2, \quad x_3 = -1$$
$$\pi k_4 = \pi/2 \qquad k_4 = 1/2, \quad x_4 = 1$$

$$Q = A \int (\zeta - \infty)^{-1} (\zeta + h)^{0} (\zeta + 1)^{-1/2} (\zeta - 1)^{-1/2} \, d\zeta + B$$

$$Q = A \int \frac{d\zeta}{\sqrt{(\zeta^2 - 1)}} + B$$

since $$\int \frac{dx}{\sqrt{x^2 - a^2}} = \ln \left(x + \sqrt{x^2 - a^2}\right) + c$$

$$Q = A \ln \left(\zeta + \sqrt{\zeta^2 - 1}\right) + B$$

at $Q = 0, \quad \zeta = 1$

$$0 = A \ln \left(1 + \sqrt{1^2 - 1}\right) + B$$
$$0 = A \ln 1 + B$$
$$0 = B$$
$$Q = A \ln \left(\zeta + \sqrt{\zeta^2 - 1}\right)$$

at $Q = \alpha i$, $\zeta = -1$

$$\alpha i = A \ln (-1 + \sqrt{-1^2-1})$$

$$\alpha i = A \ln -1$$

$$\alpha i = A \ln |-1| + A \pi i$$

equating the imaginary parts gives $\alpha i = A \pi i$

$$A = \alpha/\pi$$

$$Q = \alpha/\pi \ln (\zeta + \sqrt{\zeta^2-1})$$

5. The slot with no separation from the wall.

See figures 40 and 41.

$$\pi k_1 = \pi \qquad k_1 = 1, \quad x_1 = \infty$$

$$\pi k_2 = 0 \qquad k_2 = 0, \quad x_2 = -h$$

$$\pi k_3 = \pi \qquad k_3 = 1, \quad x_3 = -1$$

$$\pi k_4 = 0 \qquad k_4 = 0, \quad x_4 = 1$$

using the Schwarz-Christoffel transform we have

$$Q = \int A \ (\zeta-\infty)^{-1} \ (\zeta+h)^0 \ (\zeta+1)^{-1} \ (\zeta-1)^0 \ d\zeta + B$$

$$Q = A \int \frac{d\zeta}{(\zeta+1)} + B$$

$$Q = A \ln (\zeta+1) + B$$

THE SLOT WITH NO SEPARATION FROM THE WALL

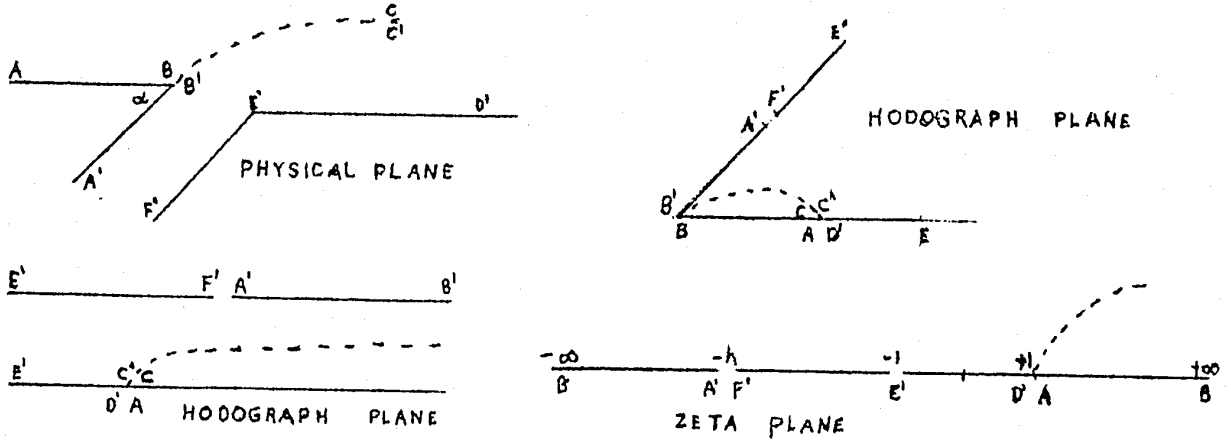

FIG 40

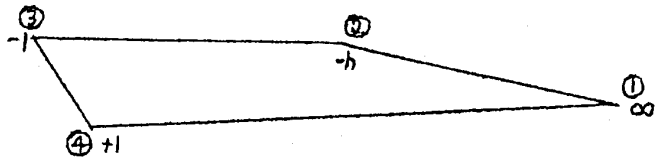

FIG 41

FOR THE DERIVATION OF THE TRANSFORMING FUNCTION FROM THE w PLANE TO THE ZETA PLANE, FOR THE CASE OF THE ORIFICE WITH SEPARATION.

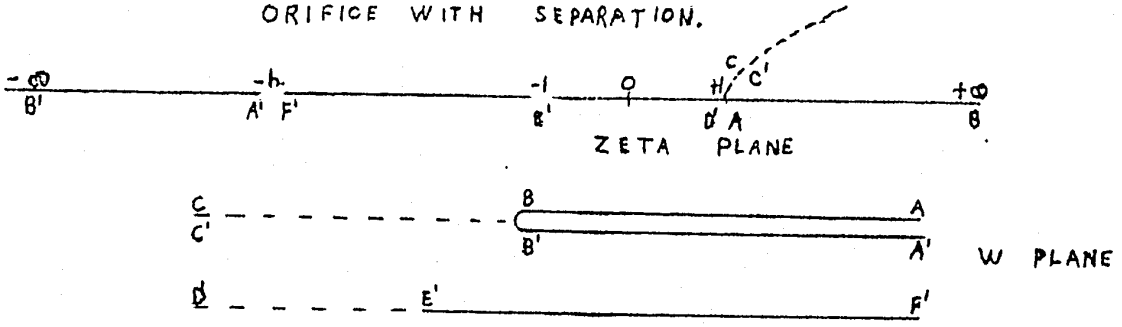

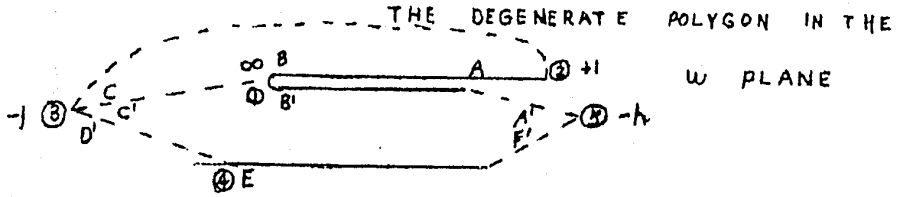

FIG 42

at $Q = 0$, $\zeta = 1$

$$0 = A \ln 2 + B$$

$$B = -A \ln 2$$

$$Q = A \ln (\zeta + 1) - A \ln 2$$

$$Q = A \ln \frac{(\zeta + 1)}{2}$$

at $Q = \alpha i$, $\zeta = -1$

$$\alpha i = A \ln \frac{(-1+1)}{2} = A \ln \frac{0}{2} = A \ln \left|\frac{0}{2}\right| + A \pi i$$

$$A = \alpha/\pi$$

$$Q = \alpha/\pi \ln \frac{(\zeta + 1)}{2}$$

6. The slot with separation from the wall and $\alpha = \pi/2$.

$$Q = \alpha/\pi \ln \left(\zeta + \sqrt{\zeta^2 - 1}\right)$$

$$Q = 1/2 \ln \left(\zeta + \sqrt{\zeta^2 - 1}\right)$$

7. The slot with no separation and $\alpha = \pi/2$.

$$Q = \alpha/\pi \ln \frac{(\zeta + 1)}{2}$$

$$Q = 1/2 \ln \frac{(\zeta + 1)}{2}$$

8. The counterflow jet with separation and $\alpha = \pi$.

$$Q = \alpha/\pi \ln \left(\zeta + \sqrt{\zeta^2 - 1} \right)$$

$$Q = \ln \left(\zeta + \sqrt{\zeta^2 - 1} \right)$$

To derive the transforming function

$$\frac{dw}{d\zeta} = \frac{-(1+h)^2 \, Uc}{\pi(\zeta+h)(\zeta-1)^2} \qquad (23)$$

See figure 42.

$$\pi k_1 = \pi \qquad k_1 = 1, \quad x_1 = \infty$$
$$\pi k_2 = \pi \qquad k_2 = 1, \quad x_2 = 1$$
$$\pi k_3 = \pi \qquad k_3 = 1, \quad x_3 = 1$$
$$\pi k_4 = 0 \qquad k_4 = 0, \quad x_4 = -1$$
$$\pi k_5 = \pi \qquad k_5 = 1, \quad x_5 = -h$$

then using the Schwarz-Christoffel transform we have

$$w = A \int (\zeta - \infty)^{-1} (\zeta-1)^{-1} (\zeta-1)^{-1} (\zeta+1)^{0} (\zeta+h)^{-1} \, d\zeta + B$$

$$w = A \int \frac{d\zeta}{(\zeta+h)(\zeta-1)^2} + B$$

$$\int \frac{dx}{(a + bx)^2(a' + b'x)} = \frac{1}{ab'-a'b} \left[\frac{1}{a + bx} + \frac{b'}{ab'-a'b} \ln \frac{(a'+b'x)}{(a + bx)} \right]$$

$a = 1,\ b = -1,\ a' = h,\ b' = 1.$

$$w = \frac{A}{(1+h)} \frac{1}{(1-)} \frac{-1\ A}{(1+h)^2} \ln \frac{(+h)}{(1-)} + B$$

at $w = 0, \quad \zeta = -1$

$$0 = \frac{A}{(1+h)(1+1)} - \frac{A}{(1+h)^2} \ln \frac{(1+h)}{(1+1)} + B$$

$$0 = \frac{A}{2(1+h)} - \frac{A}{(1+h)^2} \ln \frac{(1+h)}{2} + B$$

$$B = \frac{A}{(1+h)^2} \ln \frac{(1+h)}{2} - \frac{A}{2(1+h)}$$

$$w = \frac{A}{(1+h)(1-\zeta)} - \frac{A}{(1+h)^2} \ln \frac{(\zeta+h)}{(1-\zeta)} + \frac{A}{(1+h)^2} \ln \frac{(1+h)}{2} - \frac{A}{2(1+h)}$$

at $w = Uci, \quad = 1$

$$Uci = \frac{A}{(1+h)(0)} - \frac{A}{(1+h)^2} \ln \left| \frac{1+h}{0} \right| - \frac{A\ \pi\ i}{(1+h)^2} + \frac{A}{(1+h)^2} \ln \frac{(1+h)}{2} - \frac{A}{2(1+h)}$$

equating the imaginary parts

$$Uci = -\frac{A\pi i}{(1+h)^2}$$

$$A = -\frac{Uc\,(1+h)^2}{\pi}$$

$$\frac{dw}{d\zeta} = \frac{-Uc\,(1+h)^2\ 1}{\pi\,(\zeta+h)(\zeta-1)^2}$$

$$\frac{dw}{d\zeta} = \frac{-(1+h)^2\,Uc}{\pi\,(\zeta+h)(\zeta-1)^2}$$

The parametric equations of the vortex sheet

1. The orifice with separation of the jet from the wall. The general parametric equations are:

$$\frac{x}{c} = -\int_{-1}^{\xi} \frac{[\text{real part of } e^{Q}]\,(1+h)^2\,d\xi}{\pi\,(\xi+h)(\xi-1)^2} \qquad (26a)$$

$$\frac{y}{c} = -\int_{-1}^{\xi} \frac{[\text{imaginary part of } e^{Q}]\,(1+h)^2\,d\xi}{\pi\,(\xi+h)(\xi-1)^2} \qquad (26b)$$

by a trigonometric substitution shown on figure 43 for the Q equation

$$Q = \frac{\beta}{\pi} \ln \left[\frac{(h\mathcal{L}+1) - \sqrt{(h^2-1)(\mathcal{L}^2-1)}}{(\mathcal{L}+h)} \right]$$

$$Q = \ln \left[\frac{(h\mathcal{L}+1) - i\sqrt{(1-h^2)(\mathcal{L}^2-1)}}{(\mathcal{L}+h)} \right]^{\beta/\pi}$$

$$\frac{(h\mathcal{L}+1)}{(\mathcal{L}+h)} = \cos \phi$$

$$\frac{\sqrt{(1-h^2)(\mathcal{L}^2-1)}}{(\mathcal{L}+h)} = \sin \phi$$

$$Q = \ln (\cos \phi + i \sin \phi)^{\beta/\pi}$$

$$Q = \ln e^{i \phi \beta/\pi}$$

$$Q = \frac{i \phi \beta}{\pi}$$

for the real part of e^Q

first write $e^Q = e^{i \phi \beta/\pi}$

$$= \cos \beta/\pi \cdot \phi + i \sin \beta/\pi \cdot \phi$$

the real part is $\cos\left[\beta/\pi \cos^{-1} \frac{(h\mathcal{L}+1)}{(\mathcal{L}+h)}\right]$ and

the imaginary part is $\sin\left[\beta/\pi \cos^{-1} \frac{(h\mathcal{L}+1)}{(\mathcal{L}+h)}\right]$

thus $$\frac{x}{c} = \frac{(1+h)^2}{\pi} \int_{-1}^{\xi} \frac{\cos\left[\beta/\pi \cos^{-1} \frac{(h\xi+1)}{(\xi+h)}\right] d\xi}{(\xi+h)(\xi-1)^2}$$

and $$\frac{y}{c} = \frac{(1+h)^2}{\pi} \int_{-1}^{\zeta} \frac{\sin\left[\beta/\pi \cos^{-1} \frac{(h\zeta+1)}{(\zeta+h)}\right] d\zeta}{(\zeta+h)(\zeta-1)^2}$$

2. The orifice with separation from the wall and $\beta = \pi$.

$$\frac{x}{c} = \frac{(1+h)^2}{\pi} \int_{-1}^{\xi} \frac{\cos\left[\cos^{-1} \frac{(h\zeta+1)}{(\zeta+h)}\right] d\zeta}{(\zeta+h)(\zeta-1)^2}$$

$$\frac{x}{c} = \frac{(1+h)^2}{\pi} \int_{-1}^{\xi} \frac{(h\zeta+1)\, d\zeta}{(\zeta+h)^2 (\zeta-1)^2}$$

splitting into partial fractions

$$\frac{x}{c} = \frac{(1+h)^2}{\pi} \int_{-1}^{\xi} \left[\frac{A}{(\zeta+h)} + \frac{B}{(\zeta+h)^2} + \frac{C}{(\zeta-1)} + \frac{D}{(\zeta-1)^2}\right] d\zeta$$

it can be shown that $A = \frac{2-h}{(h+1)^2}$, $B = \frac{1-h}{h+1}$, $C = -A$, $D = \frac{1}{h+1}$

$$\frac{x}{c} = \frac{(1+h)^2}{\pi}\left[\int_{-1}^{\xi}\frac{2-h}{(h+1)^2(\xi+h)}\,d\xi - \int_{-1}^{\xi}\frac{(h-1)}{(h+1)(\xi+h)^2}\,d\xi + \int_{-1}^{\xi}\frac{h-2}{(h+1)^2(\xi-1)}\,d\xi \int_{-1}^{\xi}\frac{1}{(h+1)(\xi-1)^2}\,d\xi\right]$$

$$\frac{x}{c} = \frac{2-h}{\pi}\ln\frac{2(\xi+h)}{(h-1)(1-\xi)} + \frac{(\xi+1)(h+1)}{\pi}\left[\frac{-1}{\xi+h} + \frac{1}{2(1-\xi)}\right]$$

$$\frac{y}{c} = \frac{(h+1)^2}{\pi}\int_{-1}^{\xi}\frac{\sin\left[\sin^{-1}\frac{\sqrt{(1-h^2)(\xi^2-1)}}{(\xi+h)}\right]d\xi}{(\xi+h)(\xi-1)^2}$$

$$\frac{y}{c} = \frac{(h+1)^2}{\pi}\int_{-1}^{\xi}\frac{\sqrt{(1-h^2)(\xi^2-1)}\,d\xi}{(\xi+h)^2(\xi-1)^2}$$

whose solution is

$$\frac{y}{c} = \frac{(2-h)}{\pi}\cos^{-1}\left[\frac{-(h\xi+1)}{(\xi+h)}\right] \frac{2\sqrt{h^2-1}}{\pi}\left[\sqrt{\frac{1+\xi}{1-\xi}} - \frac{\sqrt{1-\xi^2}}{2(\xi+h)}\right]$$

3. The slot with separation from the wall

$$Q = \alpha/\pi \ \ln\left(\zeta + \sqrt{\zeta^2-1}\right)$$

$$Q = \ln\left(\zeta + \sqrt{\zeta^2-1}\right)^{\alpha/\pi}$$

$$Q = \ln\left(\xi + i\sqrt{1-\xi^2}\right)^{\alpha/\pi}$$

by a trigonometric substitution shown on figure 44

$$Q = \ln\left(\cos\theta + i \ \sin\theta\right)^{\alpha/\pi}$$

$$Q = \frac{i\,\theta\,\alpha}{\pi}$$

for the real part of e^Q

$$e^Q = e^{i\theta\alpha/\pi} = \cos\frac{\alpha}{\pi}\cdot\theta + i\sin\frac{\alpha}{\pi}\cdot\theta$$

the real part is $\cos\left[\alpha/\pi \cos^{-1}\xi\right]$ and the imaginary part is $\sin\left[\alpha/\pi \cos^{-1}\xi\right]$

thus $$\frac{x}{c} = \frac{(h+1)^2}{\pi}\int_{-1}^{\xi}\frac{\cos\left[\alpha/\pi \cos^{-1}\xi\right]\,d\xi}{(\xi+h)(\xi-1)^2}$$

and $$\frac{y}{c} = \frac{(h+1)^2}{\pi}\int_{1}^{\xi}\frac{\sin\left[\alpha/\pi \cos^{-1}\xi\right]\,d\xi}{(\xi+h)(\xi-1)^2}$$

4. The slot with separation from the wall and $\alpha = \pi/2$.

$$\frac{x}{c} = \frac{(h+1)^2}{2} \int_{-1}^{\zeta} \frac{\cos\left[1/2 \cos^{-1}\zeta\right] \, d\zeta}{(\zeta+h)(\zeta-1)^2}$$

which gives

$$\frac{x}{c} = \frac{\sqrt{2}\sqrt{h-1}}{\pi} \tan^{-1}\sqrt{\frac{1+\zeta}{h-1}} + \frac{3-h}{2\pi} \tanh^{-1}\sqrt{\frac{1+\zeta}{2}}$$

$$+ \frac{2\sqrt{2}\,(1+h)\sqrt{1+\zeta}}{2\pi(1-\zeta)}$$

$$\frac{y}{c} = \frac{(h+1)^2}{\pi} \int_{-1}^{\zeta} \frac{\sin\left[1/2 \cos^{-1}\zeta\right] \, d\zeta}{(\zeta+h)(\zeta-1)^2}$$

which gives

$$\frac{y}{c} = \frac{-\sqrt{2}\sqrt{1+h}}{\pi} \left[\tanh^{-1}\sqrt{\frac{1-\zeta}{1+h}} - \tanh^{-1}\sqrt{\frac{2}{1+h}}\right]$$

$$+ \frac{\sqrt{2}(1+h)}{\pi} \left[\frac{1}{1-\zeta} - \frac{1}{\sqrt{2}}\right]$$

5. The counterflow jet with $\alpha=\pi$.

$$Q = \ln\left(\zeta + \sqrt{\zeta^2-1}\right)$$

$$Q = \ln\left(\zeta + i\sqrt{1-\zeta^2}\right)$$

using the trigonometric substitution of figure 44, we have

$$Q = \ln(\cos\theta + i \sin\theta) = i\theta$$

$e^{Q} = \cos\theta + i \sin\theta$ and the real part is $\cos\theta = \zeta$ and the imaginary part is $\sin\theta = \sqrt{1-\zeta^2}$.

$$\frac{x}{c} = \frac{(h+1)^2}{\pi} \int_{-1}^{\zeta} \frac{\zeta \, d\zeta}{(\zeta+h)(\zeta-1)^2}$$

and

$$\frac{x}{c} = \frac{h}{\pi} \ln \frac{(h-1)(1-\zeta)}{2(h+\zeta)} + \frac{(h+1)(1+\zeta)}{2\pi(1-\zeta)}$$

$$\frac{y}{c} = \frac{(h+1)^2}{\pi} \int_{-1}^{\zeta} \frac{\sqrt{1-\zeta^2}\, d\zeta}{(\zeta+h)(\zeta-1)^2}$$

and

$$\frac{y}{c} = \frac{-\sqrt{h^2-1}}{\pi} \cos^{-1}\left[\frac{-(\zeta h+1)}{(\zeta+h)}\right] + \frac{2(h+1)}{\pi}\sqrt{\frac{1+\zeta}{1-\zeta}}$$

The contraction ratio a/c with $h > 1$.

1. The orifice with separation of the jet from the lower wall.

a/c = the real part of equation (27a)

$$e^{Q} = \left[\frac{(h\zeta+1) - \sqrt{(h^2-1)(\zeta^2-1)}}{(\zeta+h)}\right]^{\beta/\pi}$$

$$a/c = \int_{-\infty}^{-1} \left[\frac{(h\zeta+1) - \sqrt{(h^2-1)(\zeta^2-1)}}{(\zeta+h)^{\beta/\pi}} \right]^{\beta/\pi} \frac{(1+h)^2 \, d\zeta}{\pi(\zeta+h)(\zeta-1)^2}$$

$$a/c = \frac{(1+h)^2}{\pi} \int_{-1}^{+\infty} \frac{-\left[(h\zeta+1) - \sqrt{(h^2-1)(\zeta^2-1)}\right]^{\beta/\pi} d\zeta}{(\zeta+h)^{1+\beta/\pi} \, (\zeta-1)^2}$$

2. The orifice with no separation of the jet from the wall.

$$e^Q = \left[\frac{(1+h)(\zeta+1)}{2(\zeta+h)} \right]^{\beta/\pi}$$

$$a/c = \int_{-\infty}^{-1} \left[\frac{(1+h)(\zeta+1)}{2(\zeta+h)} \right]^{\beta/\pi} \frac{(1+h)^2 \, d\zeta}{\pi(\zeta+h)(\zeta-1)^2}$$

$$a/c = \frac{-(1+h)^{2+\beta/\pi}}{\pi(2)^{\beta/\pi}} \int_{-1}^{-\infty} \frac{(\zeta+1)^{\beta/\pi} \, d\zeta}{(\zeta+h)^{1+\beta/\pi} \, (\zeta-1)^2}$$

3. The orifice with separation from the wall and $\beta = \pi$.

$$e^Q = \frac{(h\zeta+1) - \sqrt{(h^2-1)(\zeta^2-1)}}{(\zeta+h)}$$

$$a/c = \int_{-\infty}^{-1} \frac{(h\zeta+1) - \sqrt{(h^2-1)(\zeta^2-1)}}{(\zeta+h)} \frac{(1+h)^2 \, d\zeta}{\pi(\zeta+h)(\zeta-1)^2}$$

$$a/c = \frac{-(2-h)}{\pi} \ln \frac{2(h + \sqrt{h^2-1})}{(h-1)} + \sqrt{\frac{h^2-1}{\pi}} + \frac{3(h+1)}{2\pi}$$

4. The orifice with no separation from the wall and $\beta = \pi$.

$$e^Q = \frac{(1+h)(\zeta+1)}{2(\zeta+h)}$$

$$a/c = \int_{-\infty}^{-1} \frac{(1+h)(\zeta+1)}{2(\zeta+h)} \frac{(1+h)^2 \, d\zeta}{\pi(\zeta+h)(\zeta-1)^2}$$

$$a/c = \frac{(h+1)}{\pi} + \frac{(3-h)}{2\pi} \ln \frac{(h-1)}{2}$$

5. The slot with separation from the wall.

$$e^Q = (\zeta + \sqrt{\zeta^2-1})^{\alpha/\pi}$$

$$a/c = \int_{-\infty}^{-1} (\zeta + \sqrt{\zeta^2-1})^{\alpha/\pi} \frac{(1+h)^2 \, d\zeta}{\pi(\zeta+h)(\zeta-1)^2}$$

$$a/c = U/U_1 = (h + \sqrt{h^2-1})^{\alpha/\pi}$$

6. The slot with no separation from the wall.

$$e^Q = \left[\frac{(\zeta+1)}{2}\right]^{\alpha/\pi}$$

$$a/c = \int_{-\infty}^{-1} \left[\frac{(\zeta+1)}{2}\right]^{\alpha/\pi} \frac{(1+h)^2\, d\zeta}{(\zeta+h)(\zeta-1)^2}$$

$$a/c = \left[\frac{(h-1)}{2}\right]^{\alpha/\pi}$$

7. The lateral jet $\alpha = \pi/2$ with separation from the wall.

$$a/c = \int_{-\infty}^{-1} (\zeta + \sqrt{\zeta^2-1})^{1/2} \frac{(1+h)^2\, d\zeta}{\pi(\zeta+h)(\zeta-1)^2}$$

$$a/c = U/U_1 = (h + \sqrt{h^2-1})^{1/2}$$

8. The lateral jet $\alpha = \pi/2$ with no separation from the wall.

$$e^Q = \left[\frac{(\zeta+1)}{2}\right]^{1/2}$$

$$a/c = \int_{-\infty}^{-1} \left[\frac{(\zeta+1)}{2}\right]^{1/2} \frac{(1+h)^2\, d\zeta}{\pi(\zeta+h)(\zeta-1)^2}$$

$$a/c = \left[\frac{h-1}{2}\right]^{1/2}$$

9. The counterflow jet $\alpha = \pi$ with separation from the wall.

$$e^{\Omega} = (\zeta + \sqrt{\zeta^2 - 1})$$

$$a/c = \int_{-\infty}^{-1} (\zeta + \sqrt{\zeta^2 - 1}) \quad \frac{(1+h)^2 \, d\zeta}{\pi(\zeta + h)(\zeta - 1)^2}$$

$$a/c = (h + \sqrt{h^2 - 1})$$

TABLE XIV

The Functional Relationship $Q = Q(\zeta)$

$h \geq 1$

1. The orifice with separation of the jet from the lower wall

$$Q = \frac{\beta}{\pi} \ln\left[\frac{(h\zeta+1) - \sqrt{(h^2-1)(\zeta^2-1)}}{(\zeta+h)}\right]$$

---

2. The orifice with no separation of the jet from the wall.

$$Q = \frac{\beta}{\pi} \ln\left[\frac{(1+h)(\zeta+1)}{2(\zeta+h)}\right]$$

---

3. The orifice with separation of the jet from the wall and $\beta = \pi$.

$$Q = \ln\left[\frac{(h\zeta+1) - \sqrt{(h^2-1)(\zeta^2-1)}}{(\zeta+h)}\right]$$

---

4. The slot with separation from the wall.

$$Q = \alpha/\pi \ln\left(\zeta + \sqrt{\zeta^2-1}\right)$$

---

5. The slot with no separation from the wall.

$$Q = \alpha/\pi \ln\frac{(\zeta+1)}{2}$$

....cont.

TABLE XIV (continued)

6. The slot with separation from the wall and $\alpha = \pi/2$.

$$Q = 1/2 \ln \left(\zeta + \sqrt{(\zeta^2 - 1)} \right)$$

---

7. The slot with no separation from the wall and $\alpha = \pi/2$.

$$Q = 1/2 \ln \frac{(\zeta + 1)}{2}$$

---

8. The counterflow jet with separation from the wall and $\alpha = \pi$.

$$Q = \ln \left(\zeta + \sqrt{(\zeta^2 - 1)} \right)$$

TABLE XV

The Parametric Equations of the Vortex Sheet ($h > 1$)

$-1 < \zeta < +1$

1. The orifice with separation of the jet from the wall.

$$x/c = \frac{(1+h)^2}{\pi} \int_{-1}^{\zeta} \frac{\cos\left[\beta/\pi \cos^{-1}(h\zeta+1)/(\zeta+h)\right] d\zeta}{(\zeta+h)(\zeta-1)^2}$$

$$y/c = \frac{(1+h)^2}{\pi} \int_{-1}^{\zeta} \frac{\sin\left[\beta/\pi \cos^{-1}(h\zeta+1)/(\zeta+h)\right] d\zeta}{(\zeta+h)(\zeta-1)^2}$$

---

2. The orifice with separation from the wall and $\beta = \pi$

$$x/c = \frac{(2-h)}{\pi} \ln \frac{2(h+\zeta)}{(h-1)(1-\zeta)} + \frac{(h+1)(\zeta+1)}{\pi}\left[\frac{1}{2(1-\zeta)} - \frac{1}{(\zeta+h)}\right]$$

$$y/c = \frac{(2-h)}{\pi} \cos^{-1}\left[\frac{-(h\zeta+1)}{(\zeta+h)}\right] \frac{2\sqrt{h^2-1}}{\pi}\left[\sqrt{\frac{1+\zeta}{1-\zeta}} - \frac{\sqrt{1-\zeta^2}}{2(\zeta+h)}\right]$$

---

3. The slot with separation from the wall.

$$x/c = \frac{(h+1)^2}{\pi} \int_{-1}^{\zeta} \frac{\cos\left[\alpha/\pi \cos^{-1}\zeta\right] d\zeta}{(\zeta+h)(\zeta-1)^2}$$

$$y/c = \frac{(h+1)^2}{\pi} \int_{-1}^{\zeta} \frac{\sin\left[\alpha/\pi \cos^{-1}\zeta\right] d\zeta}{(\zeta+h)(\zeta-1)^2}$$

.....cont.

TABLE XV (continued)

4. The slot with separation from the wall and $\alpha = \pi/2$.

$$x/c = \frac{-\sqrt{2}\sqrt{h-1}}{\pi} \tan^{-1}\sqrt{\frac{1+\zeta}{h-1}} + \frac{3-h}{2\pi} \tanh^{-1}\sqrt{\frac{1+\zeta}{2}} + \frac{2\sqrt{2}(1+h)\sqrt{1+\zeta}}{2\pi(1-\zeta)}$$

$$y/c = \frac{-\sqrt{2}\sqrt{1+h}}{\pi}\left[\tanh^{-1}\sqrt{\frac{1-\zeta}{1+h}} - \tanh^{-1}\sqrt{\frac{2}{1+h}}\right] + \frac{\sqrt{2}(1+h)}{\pi}\left[\frac{1}{\sqrt{1-\zeta}} - \frac{1}{\sqrt{2}}\right]$$

---

5. The counterflow jet with $\alpha = \pi$

$$x/c = \frac{h}{\pi} \ln\frac{(h-1)(1-\zeta)}{2(h+\zeta)} + \frac{(h+1)(1+\zeta)}{2\pi(1-\zeta)}$$

$$y/c = \frac{-\sqrt{h^2-1}}{\pi} \cos^{-1}\left[\frac{-(\zeta h+1)}{(\zeta+h)}\right] + \frac{2(h+1)}{\pi}\sqrt{\frac{1+\zeta}{1-\zeta}}$$

TABLE XVI

The Contraction Ratio a/c with $h > 1$

1. The orifice with separation of the jet from the lower wall.

$$a/c = \frac{(1+h)^2}{\pi} \int_{-1}^{\infty} \frac{-\left[\zeta h + 1) - \sqrt{(h^2-1)(\zeta^2-1)}\right]^{\beta/\pi} d\zeta}{(\zeta+h)^{1+\beta/\pi}\,(\zeta-1)^2}$$

---

2. The orifice with no separation of the jet from the wall.

$$a/c = \frac{-(1+h)^{2+\beta/\pi}}{\pi\,(2)^{\beta/\pi}} \int_{-1}^{\infty} \frac{(\zeta+1)^{\beta/\pi}\, d\zeta}{(\zeta+h)^{1+\beta/\pi}\,(\zeta-1)^2}$$

---

3. The orifice with separation of the jet from the wall and $\beta = \pi$.

$$a/c = \frac{-(2-h)}{\pi} \ln \frac{2(h+\sqrt{h^2-1})}{(h-1)} + \frac{\sqrt{h^2-1}}{\pi} + \frac{3(h+1)}{2\pi}$$

---

4. The orifice with no separation of the jet from the wall and $\beta = \pi$.

$$a/c = \frac{(h+1)}{\pi} + \frac{(3-h)}{2\pi} \ln \frac{(h-1)}{2}$$

---

5. The slot with separation from the wall.

$$a/c = U/U_1 = (h + \sqrt{h^2-1})^{\alpha/\pi}$$

.....cont.

TABLE XVI (continued)

6. The slot with no separation from the wall.

$$a/c = \left[\frac{(h-1)}{2}\right]^{\alpha/\pi}$$

---

7. The lateral jet $\alpha = \pi/2$ with separation from the wall.

$$a/c = U/U_1 = (h + \sqrt{h^2-1})^{1/2}$$

---

8. The lateral jet $\alpha = \pi/2$ with no separation from the wall.

$$a/c = \left[\frac{h-1}{2}\right]^{1/2}$$

---

9. The counterflow jet $\alpha = \pi$ with separation from the wall.

$$a/c = (h + \sqrt{h^2-1})$$

---

(4) Nomenclature for the spiral

a	-	semi mayor axis of the ellipse in feet
b	-	semi minor axis of the ellipse in feet
Δh	-	difference in head between total and static pressures in feet
ℓ	-	depth of penetration in feet
r	-	length of the radius vector in feet with the coordinate centre at the centre of the vortex
D_j	-	diameter of the jet in feet
P	-	any point on the spiral with coordinates (r, φ) or (ξ, ψ)
R	-	distance in feet between the centres of the two systems of polar coordinates
s	-	distance downstream in feet from the injector at which the depth of penetration was measured
V_o	-	mainstream velocity in feet per second
V_j	-	velocity of the jet in feet per second
V_x	-	horizontal velocity component in feet per second
α	-	angle through which the radius vector "r" revolves before it coincides with the line joining the two coordinate centres.

β - the angle between lines joining any point P to the two coordinate centres

γ - angle of incidence in degrees of the injector

θ - the angle in radians through which the radius vector "r" has revolved using polar coordinates with the centre coinciding with the centre of the vortex

ζ - length of the radius vector in feet with the coordinate centre at the injector

ρ_j - density of the jet in pounds per cubic foot

ρ_o - density of the mainstream in pounds per cubic foot

ϕ - the angle between the two zero lines of the two coordinate systems

ψ - the angle in radians through which the radius vector " " has revolved using polar coordinates with the centre at the injector

Nomenclature for the potential flow analysis

A', B', C', D', E', F'	- points in the jet
A, B, C	- points in the mainstream
a	- width of jet source
b	- offset of jet source
c	- asymptotic width of the jet in the stream
F	- a function of
h	- a distance in the plane
q	- absolute value of the velocity at a point
$Q = \ln \frac{U}{q} + i\theta$	- logarithm of the conjugate hodograph plane
s	- distance along the vortex sheet
U	- mainstream velocity
U_1	- velocity of the jet in the slot
x	- coord. of the direction of the mainstream
y	- coord. of the direction to the mainstream
$z = x + iy$	- the physical plane
α	- angular direction of the forward side of jet source
β	- angular direction of the rear side of the source
ϵ	- a small distance in the ζ plane
ζ	- the mapping half plane

θ - angular direction of the velocity at a point

Φ - the potential function

Ψ - the stream function

$w = \Phi + i\Psi$ - complex potential plane

for the three dimensional case

θ - one coord. system

ϕ - another coord.

r - the other coord.

Nomenclature for dimensional analysis

ℓ - penetration length

D_j - diameter of the jet

ρ_j - density of the jet

V_j - velocity of the jet

μ_j - viscosity of the jet

V_o - mainstream velocity

ρ_o - mainstream density

μ_o - mainstream viscosity

s - mixing distance

w - duct width

a,b,c,d,e,f,g,h,i,j - exponents

T - temperature

R - gas constant

γ - ratio of specific heats

h - depth of tost section

XI - REFERENCES

1. Gaydon and Wolfhard, Flames, pages 29-32, Chapman and Hall, London, 1953.

2. Friedman, J., Bennet, W.J. and Zwick, E.B., Fourth Symposium (International) on Combustion, p. 756, Williams and Wilkins Publ. Co., 1953.

3. Prandtl, L., Essentials of Fluid Dynamics, p. 135, Hafner Publ. Co., 1952.

4. Schlochting, H., Boundary Layer Theory, McGraw-Hill Publ. Co., 1960.

5. Barrere, M. et Mestre, A., Selected Combustion Problems, AGARD 1953, "Stabilization des Flammes par des Obstacles".

6. Longwell, J.P., et al.: Ind. Eng. Chem., 45, 1629 (1953).

7. Nicholson, H.M. and Field, J.P., Third Symposium on Combustion, Flame and Explosion Phenomena, Williams and Wilkins Publ. Co., 1949.

8. Scurlock, A.C., M.I.T. Fuel Research Laboratory, Meteor Report No. 19, 1948.

9. DeZubay, E.A., Aero Digest, 1950.

10. Wilkerson, E.C. and Fenn, J.B., Fourth Symposium (International) on Combustion p. 749, Williams and Wilkins Publ. Co., 1953.

11. Bahn, G.S., Fifth Symposium (International) on Combustion, p. 336, Reinhold, 1955.

12. Williams, G.C., Woo, P.T. and Shipman, C.W., Sixth Symposium (International) on Combustion, p. 427, Reinhold, 1956.

13. Wong, E.L., NASA Technical Note D-128, 1959.

14. Grover, J.H., Kesler, M.G. and Scurlock, A.C., Jet Propulsion 27, 386 (1959).

15. Huellmantel, L.W., Ziemer, R.W. and Cambel, A.B., Jet Propulsion, 27, 31 (1957).

16. Jensen, W.P. and Shipman, C.W., Seventh Symposium on Combustion (International), p. 674, Butterworth's Scientific Publications, 1959.

17. Clarke, J.S., Jour. Roy. Aeron. Soc., 60, 221, (1956).

18. Spalding, D.B., Aircraft Engineering, 25, 264, (1953).

19. Shepherd, D.G., "Flame Stabilization by Annular Fluid Jets", Sixth Symposium on Combustion (International), p. 472, Reinhold, 1956.

20. Dutta, B.C., Martin, D.B. and Moore, N.P.W., Sixth Symposium (International) on Combustion, p. 472, Reinhold Publ. Co., 1957.

21. Schaffer, A. and Cambel, A.B., Jet Propulsion, 25, No. 6, 284, (1956).

22. Duclos, D.P., Schaffer, A. and Cambel, A.B., Ind. Eng. Chem. 49, 2063 (1957).

23. Bertin, J. and Salmon, B., Combustion and Propulsion, 3rd AGARD Colloquium p. 555, (1958).

24. Chilton, T.H. and Genereaux, R.P., Trans. A.I.Ch.E., 25, 102 (1930).

25. Callaghan, E.E. and Ruggeri, R.S., NACA Technical Note 1615, (June 1948).

26. Ruggeri, R.S., Callaghan, E.E., and Bowden, D.T., NACA Technical Note 2019, (Feb. 1950).

27. Gordier, R.L., Technical Paper No. 28 series B, University of Minnesota, (Aug. 1959).

28. Callaghan, E.E. and Bowden, D.T., NACA Technical Note 1947, (Sept. 1949).

29. Callaghan, E.E. and Ruggeri, R.S., NACA Technical Note 2466, (1951).

30. Ruggeri, R.S., NACA Technical Note 2855, (Dec. 1952).

31. Chelko, L.J., NACA RM E 50 F 21 (1950).

32. Beauregard, J.P., "The Mixing of Cold Air Jets with a Hot Gas Stream", M.Sc. thesis, McGill University (1952).

33. Chakko, P.C., "Mixing of Hot Subsonic Jets with Cold Air Streams", M.Sc. thesis, McGill University, (1956).

34. Ehrich, F.F., Jour. Aeronaut. Sci., 20, 99 (1953).

35. Fraser, J.P., ibid 21, 59 (1954).

36. Hawthorne, W.R., Rogers, G.F.C. and Zaczek, B.Y., Roy. Aircr. Est. Tech. Not. Eng. 271 (1944).

37. Miller, E., Foster, S.P., Ross, R.W. and Wohl, K., A.I.Ch.E. Journal 3, 395 (1957).

38. Campbell, G.A. and Lu, B.C.Y., "Induced Turbulence in a Square Duct" Dept. Chem. Eng., University of Ottawa, December 1961.

39. Zarantonello, E.H., Jour. de Math. 33, 29-80 (1934).

40. Longwell, J.P., Chenevey, J.E., Clark, W.W. and Frost, E.E., Third Symposium on Combustion, Flame and Explosion Phenomena, Williams and Wilkins Publ. Co., Baltimore (1949).

41. Haddock, G.H., Cal. Tech. Jet Propulsion Lab. Report No. 3-24, May 14, 1951.

42. Spalding, D.B., and Tall, B.S., Aero Quart., 5, 195 (1954).

43. Ghosh, S.K., M.Sc. thesis, University of Ottawa, (1962).

44. Kaplan, S., NOL Memo. 10,818, June 20 (1950).

45. Churchill, R.V., "Complex Variables and Applications", McGraw-Hill Publ. Co., New York, (1960).